

Republic of Iraq
Ministry of Higher Education
and Scientific Research
Al-Nahrain University
College of Science
Department of Chemistry



Photocatalytic degradation of Orange G onto doped Au/TiO₂ and Pt/TiO₂ nano particles

A Thesis

Submitted to the College of Science / Al-Nahrain University as a partial
fulfillment of the requirements for the Degree of Master of Science in
Chemistry

By

Ala'a Razzaq Shakir

B.Sc. Chemistry / College Science / Al-Nahrain University

Supervised by

Dr. Hilal S. Wahab

(Prof.)

Jan. 2017

Jam. I 1438

بِسْمِ اللَّهِ الرَّحْمَنِ الرَّحِيمِ

بِسْمِ اللَّهِ الرَّحْمَنِ الرَّحِيمِ
بِسْمِ اللَّهِ الرَّحْمَنِ الرَّحِيمِ
بِسْمِ اللَّهِ الرَّحْمَنِ الرَّحِيمِ
بِسْمِ اللَّهِ الرَّحْمَنِ الرَّحِيمِ
بِسْمِ اللَّهِ الرَّحْمَنِ الرَّحِيمِ
بِسْمِ اللَّهِ الرَّحْمَنِ الرَّحِيمِ

صَدَقَ اللَّهُ الْعَظِيمَ

سورة العلق
بِسْمِ اللَّهِ الرَّحْمَنِ الرَّحِيمِ

الفخر

دائماً هي سطور الإهداء تكون في غابة الصعوبة عند الصياغة ربما لأنها تشعرنا دوماً بقصورها وعدم إيفائها حق من
نهديه هذه الأسطر واليوم تقف أمامي الصعوبة ذاتها

إلى من قال لي يوماً لا تكوني مثلي لا فخر بك فتعدت أن أكون مثله لا فخر بي . . إلى بطلي الأ واحد واستقامة ظهري
والدي

إلى الغيمة التي تحمل همومنا جميعاً ولا تمطرنا إلا فرحاً . . إلى من اكبر وأنا في نظرها صغيرة

والدتي

إلى من مرافقني منذ أن حملنا حقائب صغيرة ومعه سرت الدرب خطوة بخطوة . . إلى أخي ورفيق دربي في هذه الحياة ،
معك أكون أنا وبدونك أكون مثل أي شيء

إخوتي

عندما أراد الله أن يضحك قلبي أرسلها إلي . . إلى من نرالت ترافقني حتى الآن

صديقتي

إلى صاحب القاعدة التي نرتكز عليها ونراه القدوة لنا الذي تميز بشخصية قيادية متواضعة ، تعلمنا منه الحكمة والصبر .
قد تكون شهادتي فيك أستاذي مجردة لكن هنياً لنا بأستاذ مثلك

أستاذي

ACKNOWLEDGEMENT

All praise to the gracious, the greatest Almighty Allah who blessed me with the courage and made my efforts fruitful for the completion of this research to a happy ending. Without Allah's assistance, a project like this would never have come to fruition.

I would like to express my profound gratitude to everyone who has been involved in my research. First, I would like to express my sincere thanks to my supervisor, Prof. Dr. Hilal S. Wahab, for giving me the opportunity to complete a master's degree in physical chemistry. I learned a lot under his supervision, and his support and advice helped me a lot over the course of my research.

Special appreciation to Al-Nahrain University and all members of the department of chemistry in College of Science for their help during my implementation of this research work.

My gratitude to Dr. Silke Behrens / IKFT / KIT / Karlsruhe / Germany for providing working place and analytical instruments for the identification of photocatalysts and thanks also go to Christine Dietrich and Sarah Essig for their valuable assistance.

I am always eternally grateful to my father Razzaq Shaker for his unconditional love, irreplaceable moral support and spiritual guidance throughout my life. I also thank my mother and my brother for always being there to cheer me up when I needed them the most.

Finally, my wholehearted thanks is given to the love from all my friends in the university specially (Israa Nihad Esmaeel, Hussein Mohammed Hadi, Ghufraan Mohammed and Abeer Erfan) outside university (Amal Fawzi Ahmad) who were always there when I needed their warmness and a shoulder to lean on.

Summary

In this work the synthesis of Au-doped and Pt-doped TiO₂ nanoparticles employing sol-gel methodology. The doping procedures based on chemical reduction and UV photodeposition. The morphology, composition, particle size and specific surface area of these synthesized nanoparticles have been characterized using several instrumental techniques namely, Scanning Electron Microscopy (SEM), Energy Dispersive X-Ray Spectroscopy (EDXS), X-Ray Diffraction (XRD), Transmission Electron Microscopy (TEM) and N₂-adsorption Brunauer–Emmett–Teller (BET) methodology. Au impregnated (2%) nano anatase TiO₂ powder and Pt-impregnated (4%) nano anatase TiO₂ were examined in photo decolourization of Orange G as dye environmental pollutant under visible light illumination and optimum operational conditions.

The effects of some experimental variables for the photodegradation of the OG by Au-TiO₂ and Pt-TiO₂ have been investigated including, initial solution pH, initial dye concentration, Au-TiO₂ and Pt-TiO₂ loading amounts, and visible light intensity. At optimum operational conditions for OG including pH = 3, 50 mg Au-TiO₂ loading, and 10 mg/l OG, the value of the apparent rate constant, k_{app} , obtained has been 0.0123 min⁻¹ and the half life of the process, accordingly is equal to 56 min. Whereas, for Pt-TiO₂ implying pH = 3, 40 mg Pt-TiO₂ loading, and 10 mg/l OG, the value of the apparent rate constant, k_{app} , obtained has been 0.0746 min⁻¹, and the half life of the process, accordingly equals to 9 min.

The kinetic studies for the photodegradation of OG have revealed that the process follows the pseudo first order pattern regardless of reaction conditions.

The main process activation thermodynamic parameters namely, Gibbs energy, enthalpy and entropy were also deduced following the computation of photolysis activation energy employing the well known Arrhenius relation.

Employment of Au-TiO₂ revealed lower rate constant and longer half life for OG degradation, while Pt-TiO₂ exhibited higher rate constant and shorter half life, i.e; better photocatalytic activity of Pt/TiO₂ over Au/TiO₂.

Table of Contents

<i>No.</i>	<i>Subject</i>	<i>Page</i>
<i>Chapter one</i>		
<i>Introduction</i>		
1.1	Advanced oxidation processes (AOP).	1
1.2	Photocatalysis.	6
1.2.1	Heterogeneous photolysis.	6
1.2.2	Homogeneous photolysis.	9
1.3	Dyes as environmental pollutants.	10
1.4	Hydroxyl radical chemistry(\bullet OH).	13
1.5	Surface plasmon resonance (SPR).	16
1.6	Precious metal doping.	19
1.7	Photodeposition of metal ions.	23
1.8	Literature survey.	24
1.9	Scope of the project.	26
<i>Chapter two</i>		
<i>Experimental part</i>		
2.1	Chemicals.	27
2.2	Procedures.	28
2.2.1	Preparation of Potassium Trisoxalatoferrate(III) Trihydrate	28
2.2.2	Measurement of light intensity using actinometric method.	29
2.2.3	Synthesis of TiO ₂ nanoparticles catalyst.	32
2.2.4	Preparation of doped TiO ₂ with Au and Pt by UV-irradiation.	33
2.2.5	Preparation of doped TiO ₂ with Au-TiO ₂ and Pt-TiO ₂ via chemical reduction.	33

<i>No.</i>	<i>Subject</i>	<i>Page</i>
2.2.6	Effect of gold and platinum content of Au-TiO ₂ and Pt-TiO ₂ on the degradation of Orange G.	34
2.2.7	Effect of reductants (sodium borohydrate, sodium citrate and α -ketogultaric acid) and UV-irradiation on the degradation of Orange G.	35
2.2.8	Preparation of Orange G solution.	36
2.2.9	Testing of degradation of Orange G under visible light.	38
2.2.10	Testing of degradation of Orange G in the dark.	39
2.2.11	Testing of degradation of dye by visible Light in presence of TiO ₂ without O ₂ .	39
2.2.12	Testing of degradation of dye by visible Light in presence of TiO ₂ and O ₂ .	40
2.2.13	Testing of degradation of Orange G by visible light in presence of Au-TiO ₂ , O ₂ and Pt-TiO ₂ , O ₂ .	41
2.2.14	Testing of degradation of azo dye by visible light in presence of Au-TiO ₂ without O ₂ and Pt-TiO ₂ without O ₂ .	41
2.2.15	Effect of initial pH on the degradation of Orange G.	42
2.2.16	Effect of Au-TiO ₂ and Pt-TiO ₂ loading on the degradation of Orange G.	43
2.2.17	Effect of light intensity on the degradation of Orange G.	43
2.2.18	Effect of initial OG concentration on the rate of reaction.	44
2.2.19	Effect of temperature on the degradation of dye.	45
2.2.20	Determination of pH of point zero charge (pH _{pzc}).	46
2.2.21	Influence of solar irradiation.	46
2.3	Instruments.	47
2.3.1	Refrigerated circulating bath. Model (WCR-P12), wisecircu.	47
2.3.2	Nanofiltered-deionized water supply unit. model (Sm-11), Waterpia.	47
2.3.3	Centrifuge (K centrifuge PLC series.).	47
2.3.4	Muffle furnace (SX-5-12).	47

<i>No.</i>	<i>Subject</i>	<i>page</i>
2.3.5	Drying cabinet (K Hot Air Sterilizer).	47
2.3.6	Apel PD-303 single beam spectrophotometer has been used for visible light absorption measurements.	47
2.3.7	Double beam Shimadzu UV-VIS spectrophotometer. Model (1650 PC) has also been used throughout this work.	47
2.3.8	Thermostat shaker water bath JEIOTECH (BS-11).	47
2.3.9	Fourier Transform Infrared (FTIR) spectrometer.	47
2.3.10	X-ray Spectrometer.	47
2.3.11	Scanning Electron Microscopy (SEM) coupled with Energy dispersive X-ray spectroscopy (EDXS).	48
2.3.12	Chemisorption Analyzer Brunauer, Emmett and Teller (BET).	49
2.3.13	Transmission Electron Microscopy (TEM).	49
2.2.14	Inductively Coupled Plasma - Atomic Emission Spectrometry (ICP- AES).	50
2.3.15	Photoreactor system.	51
<i>Chapter three</i>		
<i>Discussion</i>		
3.1	UV-Visible spectroscopic aspects of Orange G dye.	53
3.2	Characterization of Au / Pt doped anatase TiO ₂ .	55
3.2.1	Surface morphology and composition aspects.	55
3.2.2	Porosity and surface area analysis.	60
3.2.3	Phase and crystalline size features.	62
3.2.4	Quantification of doped precious metals.	65
3.3	Control experiments.	71
3.4	Experimental optimization of photocatalysis parameters.	73
3.4.1	Effect of initial pH.	74

<i>No.</i>	<i>Subject</i>	<i>Page</i>
3.4.2	Effect of catalyst loading.	81
3.4.3	Effect of initial concentration of OG.	84
3.4.4	Effect of dopants abundance on photocatalytic activity.	86
3.4.5	Effect of radiation dose on the degradation of OG.	90
3.5	Kinetic study.	93
3.5.1	Influence of irradiation time on the reaction kinetics.	93
3.5.2	Kinetics model.	99
3.6	Influence of some experimental variables on apparent quantum yield.	101
3.7	Effect of temperature and thermodynamic parameters.	107
3.8	FTIR characterization of Orange G / Pt-TiO ₂ system.	111
3.9	photocatalytic activity of Au-TiO ₂ and Pt-TiO ₂ catalysts under solar light irradiation.	113
3.10	Comparison of reductive methodologies for Au and Pt onto nano TiO ₂ slurry particles.	115
3.11	Predicted mechanism for Orange G degradation.	117
3.12	Comparison and evaluation of photocatalytic degradation of OG azo dye using Au-TiO ₂ and Pt-TiO ₂ .	119
3.13	Conclusions and Suggestions.	120
3.13.1	Concluding remarks.	120
3.13.2	Suggestions.	122

List of Figures

<i>No.</i>	<i>Figures caption</i>	<i>Page</i>
1-1	Mineralization of Methanol by AOP.	3
1-2	Photo-excitation of a semiconducting metal oxide particle (a) and the de-excitation events; (b) electron-hole recombination within the semiconductor bulk, (c) oxidation of surface adsorbed electron donors, (d) reduction of surface adsorbed electron acceptors and (e) electron-hole recombination at the semiconductor surface.	8
1-3	The molecular structures of (a) mono azo dye Orange G (b) di azo dye Reactive black 5 (c) tri azo dye direct blue 71.	12
1-4	Features of hydroxyl radical.	14
1-5	Essential advanced oxidation processes.	15
1-6	Photocatalytic production of hydroxyl radicals.	16
1-7	Schematic diagram illustrating a surface plasmon resonance.	17
1-8	The extinction cross-section and corresponding resonant wavelength for isolated metallic nanoparticle with 10 nm in size.	18
1-9	The whole mechanism for LSPR affects the photocatalytic.	19
1-10	Mechanism of photocatalytic action of Pt-TiO ₂ nanoparticles under visible light irradiation.	22
1-11	Schematic overview of both reductive and oxidative photodeposition.	23
2-1	Calibration curve for Fe ⁺² .	31
2-2	(a) Irradiative doping of TiO ₂ ; (b) Chemical reductive doping of TiO ₂ .	34
2-3	Calibration curve for orange G together with the inset which presents the absorbance at relevant concentration.	37
2-4	UV-VIS spectrum of OG at various concentrations.	38
2-5	Panalytical Philips diffractometer (Karlsruhe Institute of Technology, Germany).	48
2-6	LEO 982 SEM coupled with EDX (Karlsruhe Institute of Technology, Germany).	48
2-7	Micromeritics AutoChem HP Chemisorption Analyzer (BET) (Karlsruhe Institute of Technology, Germany).	49

<i>No.</i>	<i>Figures caption</i>	<i>Page</i>
2-8	Philips Technai TEM (Karlsruhe Institute of Technology, Germany).	50
2-9	Inductively Coupled Plasma - Atomic Emission Spectrometry (Karlsruhe Institute of Technology, Germany).	51
2-10	Photolysis unit of visible light source.	52
3-1	Molecular structure of Orange G dye.	53
3-2	UV-Vis absorption spectrum of OG.	53
3-3	Standard scan of Orange G at different pH values.	54
3-4	Scanning Electron Microscope (SEM) micrographs for Au-doped anatase TiO ₂ with different magnifications.	55
3-5	Scanning Electron Microscope (SEM) micrographs for Pt-doped anatase TiO ₂ with different magnifications.	56
3-6	Transmission Electron Microscope (TEM) micrograph for Au-doped nano TiO ₂ powder and EDXS composition.	57
3-7	Transmission Electron Microscope (TEM) micrograph for Pt-doped nano TiO ₂ powder and EDXS composition.	58
3-8	Energy Dispersive X-ray Spectroscopy (EDXS) image of Au-doped nano TiO ₂ powder.	59
3-9	Energy Dispersive X-ray Spectroscopy (EDXS) image of Pt-doped nano TiO ₂ powder.	59
3-10	Pore size measurements for ;(a) Synthesized nano anatase TiO ₂ ; (b) Au-doped nano anatase TiO ₂ ; (c) Pt-doped nano anatase TiO ₂ ; insets represent adsorption-desorption isotherms.	61
3-11	X-ray Diffraction Spectroscopy (XRD) patterns of Au doped anatase TiO ₂ ; arrows present gold positions.	63
3-12	X-ray Diffraction Spectroscopy (XRD) patterns of Pt doped anatase TiO ₂ ; arrows present platinum positions.	64
3-13	SEM micrograph and EDXS composition for Au-doped anatase TiO ₂ using 2-Oxoglutaric acid as a reductant.	67
3-14	SEM micrograph and EDXS composition for Au-doped anatase TiO ₂ using; (a) NaBH ₄ as a reductant and (b) sodium citrate as a reductant.	68
3-15	SEM micrograph and EDXS composition for Pt-doped anatase TiO ₂ using sodium tetrahydroborate as a reductant.	69

<i>No.</i>	<i>subject</i>	<i>page</i>
3-16	SEM micrograph and EDXS composition for Pt-doped anatase TiO ₂ using; (a) 2-Oxoglutaric acid as a reductant and (b) sodium citrate as a reductant.	70
3-17	The relative decrease in absorption intensity of Orange G as a function of irradiation time (a) VIS+OG in absence of Au-TiO ₂ ; (b) Au-TiO ₂ + OG in dark; (c) VIS+TiO ₂ +OG in absence of O ₂ gas;(d) VIS+TiO ₂ +OG+ O ₂ ; (e) VIS+Au-TiO ₂ +OG in absence of O ₂ gas;(f)) VIS+Au-TiO ₂ +OG+ O ₂	72
3-18	The relative decrease in absorption intensity of Orange G as a function of irradiation time: (a) VIS +OG in absence of Pt-TiO ₂ ; (b) Pt-TiO ₂ + OG in dark; (c) VIS+TiO ₂ +OG in absence of O ₂ gas; (d) VIS+TiO ₂ +OG+ O ₂ ; (e) VIS+Pt-TiO ₂ +OG in absence of O ₂ gas; (f)) VIS+Pt-TiO ₂ +OG+ O ₂ .	73
3-19	Zero point charge pH of 2% Au-TiO ₂ .	74
3-20	Zero point charge pH of 4% pt-TiO ₂ .	75
3-21	Impact of initial pH on the percent of OG photo-degradation using 2% Au-TiO ₂ .	76
3-22	Impact of initial pH on the percent of OG photo-degradation using 4% Pt-TiO ₂ .	77
3-23	Influence of initial pH on photobleaching rate of OG using Au-TiO ₂ .	77
3-24	Influence of initial pH on photobleaching rate of OG using Pt-TiO ₂ .	78
3-25	Virtual adsorption geometry of OG onto doped TiO ₂ particle via sulphonate anchoring groups .	80
3-26	Virtual adsorption geometry of OG onto doped TiO ₂ particle via azo nitrogen and hydroxyl oxygen groups.	80
3-27	Effect of Au-TiO ₂ loading on the removal of OG.	81
3-28	Effect of Pt-TiO ₂ dosage on the degradation of OG.	82
3-29	Effect of Au-TiO ₂ catalyst loading on the degradation yield of Orange G after 270 minutes of visible light illumination; red columns represent % degradation and blue columns represent Au-TiO ₂ dosage.	82
3-30	Effect of Pt-TiO ₂ dosage on the degradation% of OG at pH = 3 and initial OG conc. 10 ppm: (a) 20; (b) 30; (c) 40; (d) 50 and (e) 60 mg.	83

<i>No.</i>	<i>Figures caption</i>	<i>page</i>
3-31	Plot of $\ln(C_0/C_t)$ vs. reaction time at different initial concentrations of OG; (2% Au-TiO ₂ = 40 mg; pH = 3.0).	85
3-32	Plot of $\ln(C_0/C_t)$ vs. reaction time at different initial concentrations of OG; (% Pt=TiO ₂ = 50 mg/L; pH = 3.0).	86
3-33	Impact of Au doping percent on the rate of photodegradation of OG under visible illumination.	88
3-34	Impact of Pt doping percent on the rate of photodegradation of OG under visible illumination.	88
3-35	Effect of Au doping percent on the degradation percent of OG under visible illumination. Inset represents variation of process rate constant (k) of photodegradation of OG with Au doping percent.	89
3-36	Effect of Pt doping percent on the photodegradation percent of OG under visible illumination. Inset represents variation of process rate constant (k) with Pt doping percent.	89
3-37	Variations of the a) initial rate and b) degradation yield of OG as a function of visible light source intensity.	92
3-38	Correlation of OG concentration with irradiation time in the presence of Au-TiO ₂ .	94
3-39	Correlation of OG concentration with irradiation time in the case of Pt-TiO ₂ .	95
3-40	(a) first and (b) second pseudo order of Orange G photodegradation at optimum experimental conditions; (A _t : Absorbance at time t and 478 nm) for Au-TiO ₂ .	97
3-41	(a) first and (b) second pseudo order of Orange G photodegradation at optimum experimental conditions; (A _t : Absorbance at time t and 478 nm) for Pt-TiO ₂ .	98
3-42	Degradation rate of OG at optimum conditions; (Au-TiO ₂ =40 mg/L; pH = 3.0 ; OG=10 ppm).	100
3-43	Degradation rate of OG at optimum conditions; (Pt-TiO ₂ =50 mg/L; pH = 3.0 ; OG=10 ppm).	100
3-44	Effect of (a) gold percent; (b) OG initial concentration ; (c) Au-TiO ₂ loading and (d) pH on the quantum yield of photocatalytic reaction.	104
3-45	Effect of (a) platinum percent; (b) OG initial concentration; (c) Pt-TiO ₂ loading and (d) pH on the quantum yield of photocatalytic reaction.	106

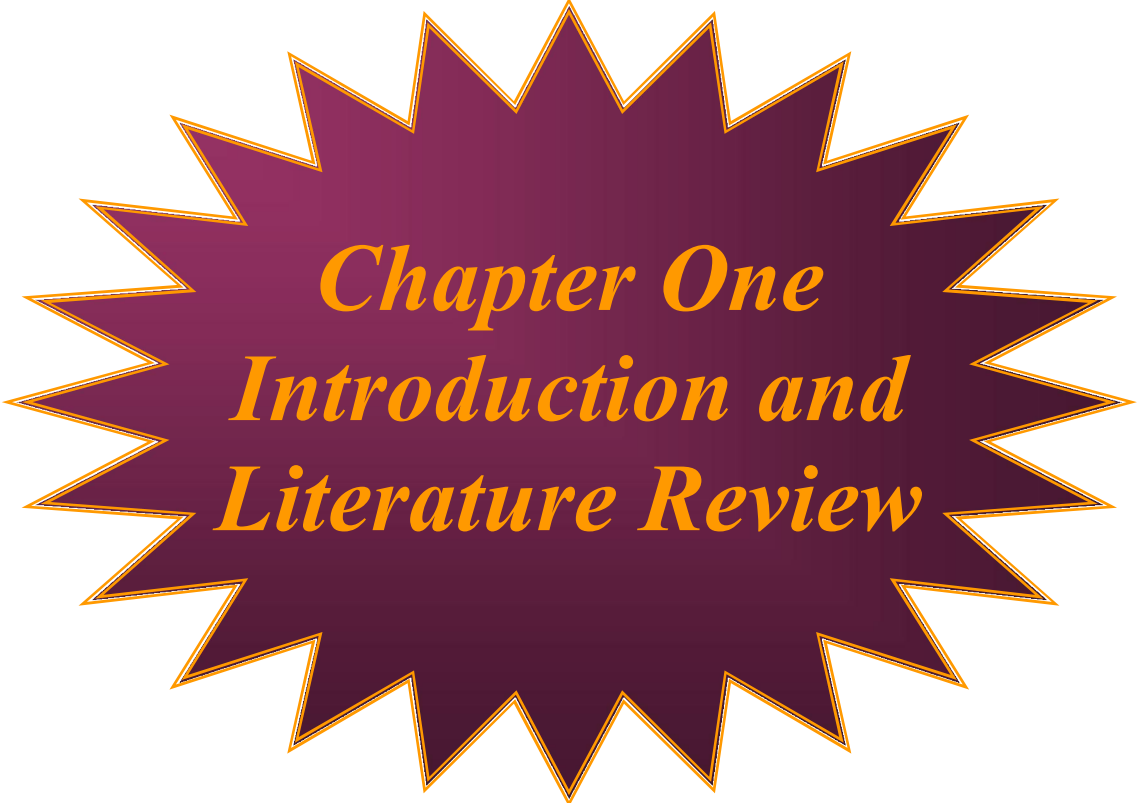
<i>No.</i>	<i>Figures caption</i>	<i>Page</i>
3-46	Arrhenius plot of rate constant versus reciprocal of reaction temperature for degradation of OG using Au-TiO ₂ .	109
3-47	Arrhenius plot of rate constant versus reciprocal of reaction temperature for degradation of OG using Pt-TiO ₂ .	110
3-48	FTIR spectra for OG: (a) reference; (b) before and (c) after Pt/TiO ₂ photocatalytic degradation.	112
3-49	Rate of OG photodegradation onto 2% Au-TiO ₂ surface under solar illumination; inset shows degradation percent.	114
3-50	Rate of OG photodegradation onto 4% Pt-TiO ₂ surface under solar illumination; inset shows degradation percent.	114
3-51	Effect of UVR and CR methods on the rate of OG degradation under visible illumination employing 2% Au-TiO ₂ : (a) 2-Oxoglutaric acid; (b) UV; (c) Sodium borohydride; (d) Citric acid .	116
3-52	Effect of UVR and CR methods on the rate of OG degradation under visible illumination employing 2% Pt-TiO ₂ : (a) UV; (b) Sodium borohydride; (c) 2-Oxoglutaric acid; (d) Citric acid.	116
3-53	Schematic diagram of degradation pathways of Orange G.	118

List of Tables

<i>No.</i>	<i>Table legend</i>	<i>page</i>
1-1	Relative oxidation power of some oxidizing species	2
1-2	Types and classification of advanced oxidation processes	5
1-3	reaction rate constants (k , in $\text{mol}^{-1}.\text{s}^{-1}.\text{L}$) of ozone vs. hydroxyl radical	14
2-1	The following chemicals were used throughout this research work	27
3-1	UV- reduction of Au and Pt onto TiO_2 surface analyzed by means of ICP-AES	65
3-2	Impact of initial pH on the percent of OG photodegradation using 2% Au- TiO_2	75
3-3	Impact of initial pH on the percent of OG photodegradation using 4% Pt- TiO_2	76
3-4	Quantum yields of photodegradation of OG obtained at different intensities	91
3-5	Variation of concentration and degradation percent of OG in the case of Au- TiO_2	94
3-6	Variation of concentration and degradation percent of OG in the case of Pt- TiO_2	95
3-7	Thermodynamic parameters for the photocatalytic degradation of Orange G using Au- TiO_2	110
3-8	Thermodynamic parameters for the photocatalytic degradation of Orange G using Pt- TiO_2	110

List of Abbreviations

AOP	Advanced Oxidation Process
·OH	Hydroxyl radical
UV	Ultraviolet
VB	Valance band
CB	Conduction band
E_g	Band gap energy
e⁻	Electron formed upon illumination of a semiconductor
h⁺	Hole formed upon illumination of a semiconductor
SPR	Surface plasmon resonance
LSPR	Localized surface plasmon resonance
NPs	Nano particles
Ads	Adsorbed species on a surface
SEM	Scanning Electron Microscopy
EDXS	Energy Dispersive X-Ray Spectroscopy
XRD	X-Ray Diffraction
TEM	Transmission Electron Microscopy
BET	Brunauer-Emmett-Teller
UV-VIS	Ultra Violet-Visible Spectrophotometer
k_{app}	Apparent rate constant
HOMO	Highest Occupied Molecular Orbital
LUMO	Lowest Unoccupied Molecular Orbital
PZC	Point of Zero Charge
NFDW	Nano Filtered Deionized Water
C_o	Initial concentration
C_t	Concentration at any time
E_a	Activation energy
FTIR	Fourier transforms infrared spectrometry
nm	Nanometer
ppm	Parts per million
T	Temperature (Kelvin)
λ	Wavelength
FWHM	Full width at half maximum



Chapter One
Introduction and
Literature Review

1.1 Advanced oxidation processes (AOP)

The typical environmental decontamination techniques involve classical methods such as coagulation, adsorption, ion flotation and sedimentation. All these techniques are many-sided and useful, but they all end up in producing additional products which need to be processed further [1]. Another set of techniques which are relatively newer, more powerful, and very promising is known Advanced Oxidation Processes (AOPs), which have been developed and employed to treat dye-contaminated wastewater effluents [1-2].

Dangerous organic wastes from industrial, military, and commercial operations represent one of the greatest challenges to environmental engineers. Advanced oxidation processes are replacements to the incineration of wastes, which has many disadvantages [3].

Advanced oxidation processes are techniques characterized by the generation of hydroxyl radicals ($\cdot\text{OH}$), which are highly reactive and non-selective substances used to degrade toxic organic compounds present in various media (such as wastewater and soil) [4]. AOPs include generation and subsequent reaction of hydroxyl radicals which can be used for the complete mineralization of many pollutants, like pesticides, pharmaceuticals dyes moieties that can not be oxidized entirely by traditional oxidants [5-6]. Hydroxyl radicals react normally with organic compounds via three types of reactions shown below: (1.1) hydrogen atom abstraction reaction; (1.2) electrophilic addition on double bond reaction; (1.3) electron transfer reaction [7].



where Ar an aromatic group and R represents an aliphatic chain. In the case of aromatic compounds, a hydroxylation of the ring might occur with a subsequent ring opening after successive $\cdot\text{OH}$ attacks, giving place to organic acids or conjugated structures. In every case, the process can lead to the total mineralization of the compound [8].

Hydroxyl radicals are secondary oxidants that can be generated from decayed ozone. They are stronger oxidizing agents than ozone itself, as a matter of fact, they are the most reactive oxidants utilized in water treatment having a standard reduction potential of 2.8 V see Table (1-1). Only fluorine gas has a higher electronegative oxidation potential, but it is not utilized in water treatment [9].

Table (1-1): Relative oxidation power of some oxidizing species [10].

Species	*E° (V, 25 °C)
Fluorine (F ₂)	3.06
Hydroxyl radical ($\cdot\text{OH}$)	2.80
Atomic oxygen (O ₂)	2.42
Ozone (O ₃)	2.07
Hydrogen peroxide (H ₂ O ₂)	1.78
Perhydroxyl radical (HO ₂)	1.70
Chlorine dioxide	1.57
Hypochlorous acid (HClO)	1.49
Chlorine (Cl ₂)	1.36
Bromine (Br ₂)	1.09
Iodine (I ₂)	0.54
*Potential refers to the standard hydrogen electrode (SHE)	

Taking the simple compound methanol as an example, the equations below show how the molecule CH_3OH is dissociated by $\cdot\text{OH}$ via intermediates to produce CO_2 gas and water H_2O Figure (1-1). The procedure with other more complex or larger molecules is similar but not always completely understood to date.

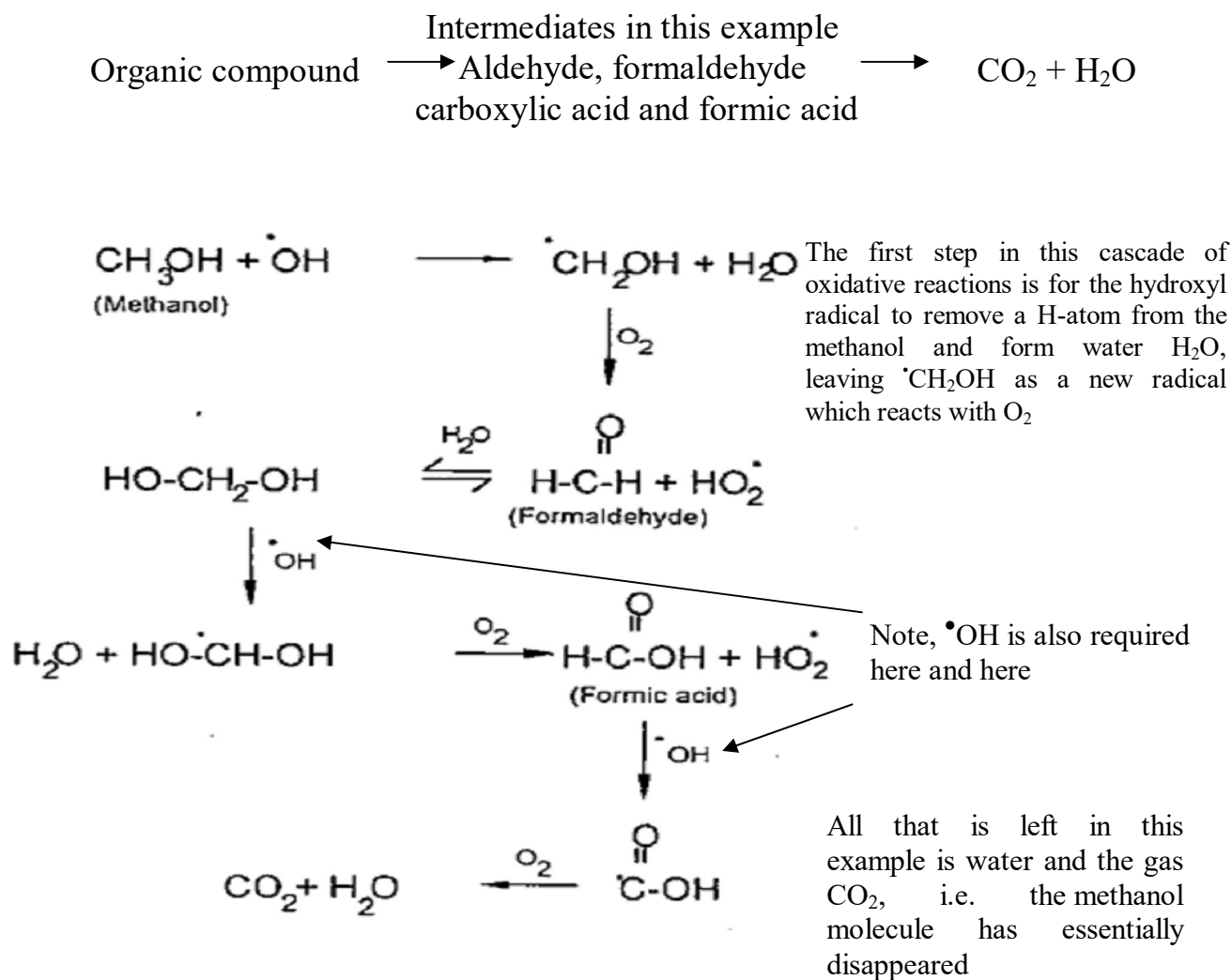


Figure (1-1): Mineralization of methanol by AOP [11].

Attack of the hydroxide radical on methanol in the presence of O₂ initiates a complex cascade of chemical reactions that requires a supply of •OH radicals and leads as in this example, to the vanishing of the contaminant. The issue of the possible production of intermediates in oxidation and AOP which may be more toxic than the original compound, if left un-oxidised, must always be considered. The generation of intermediates may be indicated by a color change or a change in pH. In theory, all organic compounds can be mineralized completely by some method or other but, costs might be expensive [11].

The use of AOPs as a pre-treatment step to enhance the biodegradability of wastewaters can significantly reduce operational costs and increase the efficiency of the overall process. Therefore, determining the biodegradability and toxicity of intermediate species is a critical point in evaluating the possibility of photocatalysis to be employed as a pre-treatment process [12].

Advantages of Advanced Oxidation Processes are as follows [13];

- a) Rapid reaction rates.
- b) Potential to reduce toxicity and possibly complete mineralization of the treated organics.
- c) Does not produce materials that require further treatment such as "spent carbon" from activated carbon adsorption.
- d) Does not make sludge as with physical-chemical process or biological processes.

While the disadvantages of Advanced Oxidation Processes are,

- a) Capital Intensive.
- b) Complex chemistry must be tailored to the specific application.

AOPs can be categorized by considering the phase where the process takes place. Hence, heterogeneous or homogenous processes can be differentiated. AOPs classification can also consider the different possible ways of hydroxyl radical production. In this way, non-photochemical and photochemical processes can be distinguished. Table (1-2) classifies some of the most important AOPs into photochemical and non-photochemical processes [14, 15].

Table (1-2): Types and classification of advanced oxidation processes.

Non-photochemical	Photochemical
Homogeneous processes	
<ul style="list-style-type: none"> •Ozonation in alkaline media (O₃/HO⁻), •(O₃/H₂O₂) •Fenton (Fe²⁺ or Fe³⁺/H₂O₂) •Electro-oxidation •Electrohydraulic discharge ultrasound •Wet air oxidation (WAO) •Supercritical water oxidation 	<ul style="list-style-type: none"> •Photolysis of water in vacuum ultraviolet (VUV) ($\lambda \leq 190$ nm) •UV/H₂O₂($\lambda \leq 300$ nm) •O₃/UV ($\lambda \leq 320$ nm) •O₃/H₂O₂/UV ($\lambda \leq 320$ nm) •Photo-Fenton (Fe²⁺ or Fe³⁺/H₂O₂/UV) ($\lambda \leq 550$ nm) •Photoelectro-Fenton($\lambda \leq 550$)
Heterogeneous processes	
<ul style="list-style-type: none"> • Catalytic wet air oxidation (CWAO) 	<ul style="list-style-type: none"> • Heterogeneous photocatalysis: ZnO/UV, SnO₂/UV, TiO₂/UV, TiO₂/H₂O₂/ UV

1.2 Photocatalysis

1.2.1 Heterogeneous Photocatalysis

The initial interest in heterogeneous photocatalysis started in 1972 when the photochemical dichotomy of the water into hydrogen and oxygen utilizing TiO_2 was shown to be possible [16]. From that date, broad work has been carried out to produce hydrogen from the water by this novel oxidation-reduction reaction using a variety of semiconductors. Furthermore, the heterogeneous photocatalysis has been examined and explored extensively by several researchers as a potentially viable alternative to classical "best" technologies for both environmental detoxification and for energy production [17], additionally it includes the increasing speed of photoreaction in presence of semiconductor photocatalyst [18]. Moreover, heterogeneous photocatalysis, which is a kind of AOPs, has been considered as a cost effective alternative for the purification of dye containing wastewater. Additionally, late studies have shown that photocatalysis can be utilized to mineralize organic compounds or degrade dyes under UV irradiation [19]. If the semiconductor remains intact and the charge transfer to the adsorbed species is continuous and exothermic, the process is termed "heterogeneous photocatalysis" [20].

A semiconductor consists of the highest occupied energy band, called the valence band (VB) and the lowest empty band, called the conduction band (CB). The difference energy between these two levels is called the band gap energy (E_g). Without light excitation, both the electrons and holes are in the valence band. When semiconductors are energized by photons with energy equal to or larger than their band gap, electrons get energy from the photons and are thus promoted from VB to CB with simultaneous generation of holes in the valence band.

The reaction is simply expressed as:



where D_{ads} are donors and A_{ads} are acceptors[21].

Titanium dioxide has a wide band gap, 3.2 eV, which can only absorb ultraviolet light with wavelengths of 387.5 nm or less [22]. When excitation of the semiconductor happens across the band gap, there is a sufficient lifetime, in the nanosecond regime, to create the electron-hole pair to undergo charge transfer to adsorbed species on the semiconductor surface from solution or gas phase contact [23]. Hence, the initial procedure for heterogeneous photocatalysis of organic and inorganic compounds is initiated with the photogeneration of $e^- - h^+$ pairs in the semiconductor particles. The quantity of photogenerated electron-hole pairs ($e^- - h^+$) depends on the semiconductor band structure and effective intensity and also on the energy of the incident light. Upon excitation, the fate of the separated electron and hole can follow few pathways [24]. The electrons and holes can migrate to the semiconductor surface where they are able to undergo charge transfer process with adsorbed species. Generally at the surface of the semiconductor, the photogenerated electrons can reduce an electron acceptor, usually oxygen in an aerated solution and the photogenerated holes can oxidize an electron donor [25] and further, the electron transfer process is more effective if the species are distributed on the surface. The probability and rate of the charge transfer reactions for electrons and holes depends on the respective positions of the band edges for the conduction and valence bands and the redox potential levels of the adsorbate species.

The photocatalytic events are illustrated in Figure (1-2) [26, 27]. Recombination of the separated electron and hole can happen at the surface (pathway A) in the volume of the semiconductor molecule (pathway B) or with the release of heat [27].

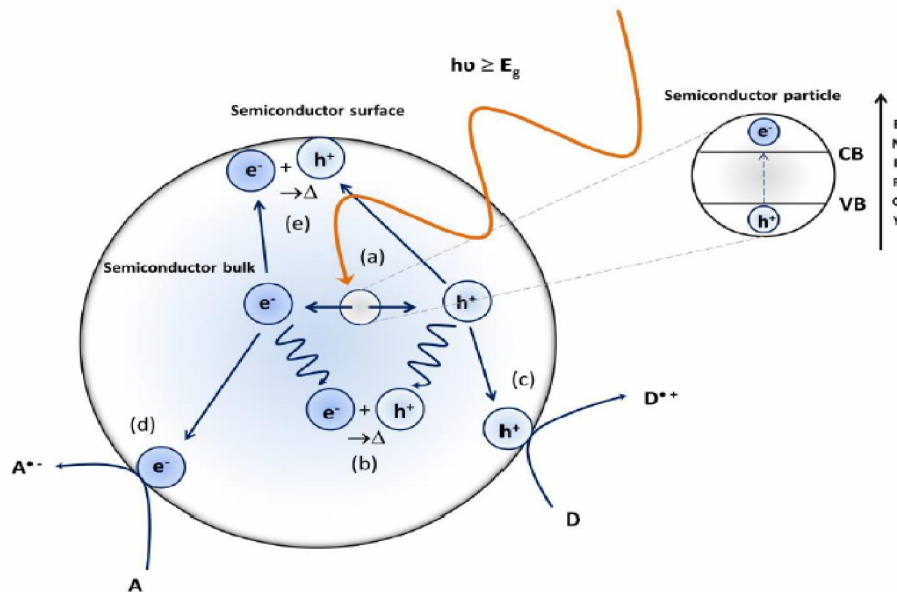


Figure (1-2): Photo-excitation of a semiconducting metal oxide particle (a) and the de-excitation events; (b) electron-hole recombination within the semiconductor bulk, (c) oxidation of surface adsorbed electron donors, (d) reduction of surface adsorbed electron acceptors and (e) electron-hole recombination at the semiconductor surface [27].

1.2.2 Homogeneous Photocatalysis

In homogeneous photocatalysis, the catalyst and the reactants are in the same phase. For instance, the ozonation of water to degrade organic materials, where ozone (O_3) acts as a direct photocatalyst that is separated upon UV illumination and generates $\cdot OH$ radicals after reacting with water [28]. The interest of homogeneous photocatalysis for researches is to study the degradation of toxic water pollutants. In this respect, can note that the most effective oxidation of organic contaminants can be obtained with the generation of a powerful oxidizing reagent, such as $\cdot OH$ or other radicals like atomic oxygen, anionic oxygen, superoxide anion and peroxy radical [29]. The most usually used homogeneous photocatalysts include ozone and photo-Fenton systems (Fe^{+2} and Fe^{+2}/H_2O_2). The reactive species is the $\cdot OH$ which is utilized for various purposes. Some of the examples of homogenous photocatalysis: Ultraviolet lamp (UV), $O_3/H_2O_2/UV$ and Photo-Fenton process [30].

The Combination of O_3 with UV accomplishes a net enhancement of dyes degradation due to a direct and indirect generation of hydroxyl radicals following O_3 decomposition and H_2O_2 formation, respectively as shown below [31]. $O(1D)$ is the excited oxygen atom (also known as a doublet multiplicity free radical).



The following processes are considered as homogeneous catalytic processes due to the catalytic role of iron in Fenton reagent, Eqs.(1.11-1.13).



Generated hydroxyl radicals play a major role in the degradation of organic pollutants. In photo-Fenton type processes, additional sources of hydroxyl radicals should be considered: through photolysis of H_2O_2 , Eq. (1.14), and through reduction of Fe^{3+} ions under UV light, Eq.(1.15) [32].



The efficiency of Fenton type processes is impacted by several operating parameters like concentration of hydrogen peroxide, pH and intensity of UV light. The main advantage of this process is the ability of using sunlight with light sensitivity up to 450 nm, thus avoiding the high expenses of UV lights and electrical energy. These reactions have been proven more effective than the alternate photocatalysis but the disadvantages of the process are the low pH values which are required, since iron precipitates at higher pH values and the fact that iron must be removed after treatment [33].

1.3 Dyes as environmental pollutants

Textile and other industrial dyes constitute one of the biggest groups of organic compounds that represent an expanding ecological danger. About 1–20% of the total world production of dyes is lost during dyeing process and is accordingly released in the textile wastewaters [34].

Different types of dyes are utilized in many industries such as textile, paint, ink, plastics and cosmetics. There are various classes of dyes such as acidic, basic, neutral, azo, disperse, direct.... etc. Out of these dyes, azo dyes are most frequently utilized [35].

Azo dyes represent more than half of all dyes in common use because of their chemical stability and versatility, and most of them are non-biodegradable, toxic and potentially carcinogenic in nature [36]. However, even if dyes are not toxic, the toxicity of their by-products has to be considered. Certainly, dyes degradation ends with aromatic amines, which are known to be toxic [37]. Dyes can be classified into anionic, cationic, and nonionic dyes. Anionic dyes include direct, acid and reactive while the cationic dyes are basic dyes [38].

Dyes embrace a wide variety of structural types depending on the precise nature of electron acceptor (A) and electron donor (D) groups and can be subdivided into three main categories [39]: anionic ($z = -1$), cationic ($z = +1$) and neutral ($z = 0$). Cationic dyes are positively charged and the most important group of this type of dye contains nitrogen atoms in both the D and A groups. On the other hand, a characteristic feature of anionic dyes is the presence of at least one sulfonate ($-\text{SO}_3^-$) groups, usually as sodium (Na^+) salts. These groups ensure that the dyes carry a negative charge [40].

Azo dyes absorb light in the visible spectrum due to their chemical structure, which is described by one or more azo groups ($-\text{N}=\text{N}-$). Mono azo dyes ($\text{N}=\text{N}$) imply only one double bond while diazo and triazo dyes contain two and three ($\text{N}=\text{N}$) double bonds, respectively [41]. Figure (1-3) illustrates the molecular structures of three examples for mono, di and tri azo dyes.

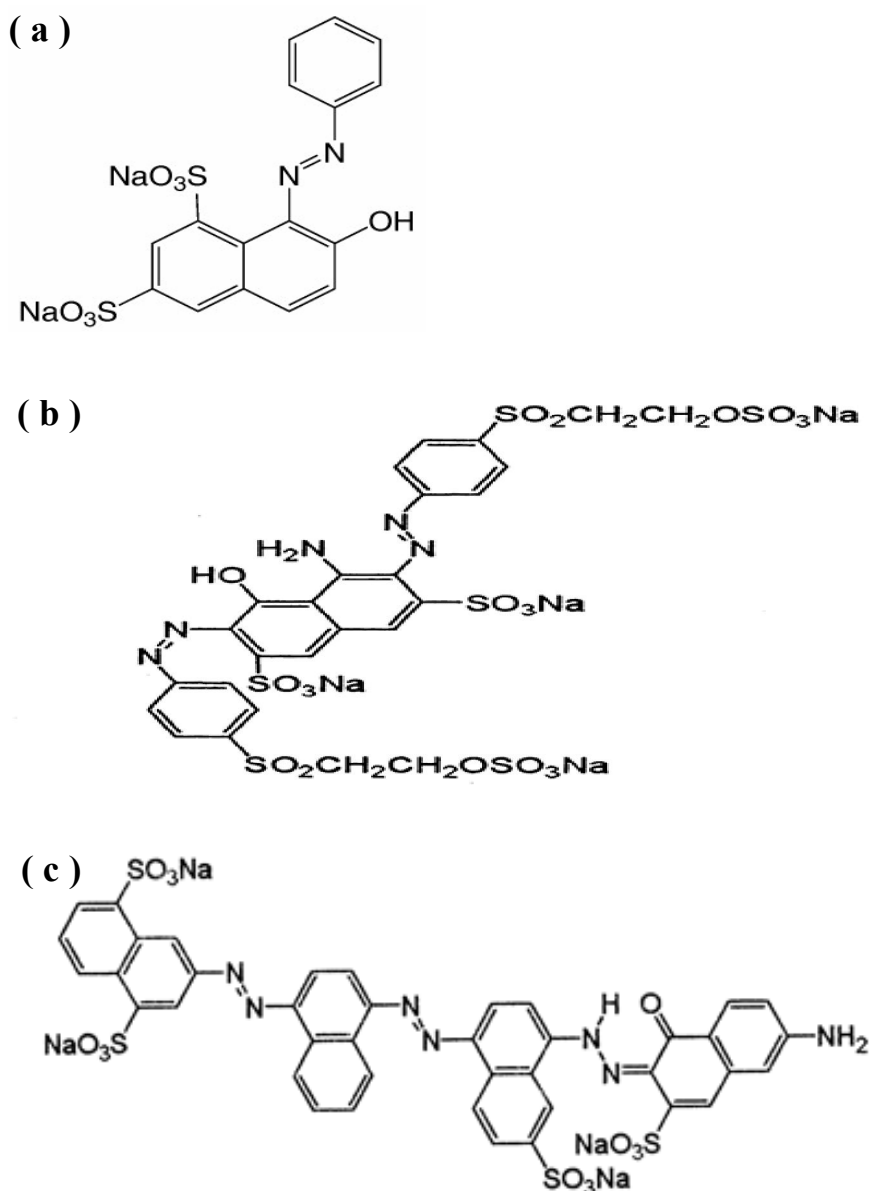


Figure (1-3): The molecular structures of (a) mono azo dye Orange G (b) di azo dye Reactive black 5 (c) tri azo dye direct blue 71

A dye molecule composes of nucleophiles which are referred to as auxochromes and aromatic groups (benzene and naphthalene rings) which are called chromophores. Together, the dye molecule is often described as a chromogen. Synthesis of most azo dyes includes diazotization of a primary aromatic amine, followed by coupling with one or more nucleophiles. Amino and hydroxy groups are usually used coupling components [42].

All aromatic compounds absorb electromagnetic energy but only those that absorb light with wavelengths in the visible range (400-700 nm) are colored. Dyes include chromophores, electron systems delocalized with conjugated double bonds, and auxochromes, electron withdrawing or electron donating substituents that cause or intensify the color of the chromophore by altering the general energy of the electron system [43].

The most important chromophores are azo ($-\text{N}=\text{N}-$), carbonyl ($-\text{C}=\text{O}$), nitro ($-\text{NO}_2$), and methine ($-\text{CH}=\text{}$) and quinoid groups. To summarize the groups which are necessary for generation of color are called chromophores and the groups which improve the color are known auxochromes; examples contain: $-\text{OH}$, $-\text{NHR}$, $-\text{NR}_2$, $-\text{COOH}$, $-\text{NH}_2$, and $-\text{SO}_3\text{H}$ groups [44].

1.4 Hydroxyl radical chemistry

In chemistry, radical is an atom, molecule or ion that has unpaired valence electrons. Radicals and radical pairs often assume a very important role as intermediates in thermal, radiation, and photochemical reactions [45]. The hydroxyl radical ($\cdot\text{OH}$) is one of the most powerful oxidizing agents, able to react unselectively and instantaneously with the surrounding chemicals, including organic pollutants [46]. The mechanism detailed of the OH radical generation has not been experimentally cleared up yet, because it is difficult to detect $\cdot\text{OH}$ due to its short lifetime and high reactivity [47]. Figure (1-4) shows some extraordinary characteristics of $\cdot\text{OH}$ that make AOPs a powerful method for the removal of refractory compounds [48].



Figure (1-4): Features of hydroxyl radical [48].

Table (1-3) compares the reaction rates of different organic contaminants with ozone and the hydroxyl radical. The hydroxyl radical reacts normally a million to a billion times faster than hydrogen peroxide and ozone, resulting in greatly reduced treatment costs and system size [49].

Table (1-3): reaction rate constants (k , in $\text{mol}^{-1} \cdot \text{s}^{-1} \cdot \text{L}$) of ozone vs. hydroxyl radical [50].

Compound	O_3	$\cdot\text{OH}$
Chlorinated Alkenes	10^{-1} to 10^3	10^9 to 10^{11}
Phenols	10^3	10^9 to 10^{10}
N-containing Organics	10 to 10^2	10^8 to 10^{10}
Aromatics	1 to 10^2	10^8 to 10^{10}
Ketones	1	10^9 to 10^{10}
Alcohols	10^{-2} to 1	10^8 to 10^9
Alkanes	10^{-2}	10^6 to 10^9

From Table (1-3) it can be seen that chlorinated alkenes treat most effectively because the double bond is very susceptible to hydroxyl attack. Saturated molecules as mentioned before have smaller rate constants and therefore are harder to oxidize [51].

The oxidation potentials of molecular hydroxyl radicals and ozone are 2.80 and 2.07 V, respectively. Molecular ozone reactions are selective to the organic molecules having nucleophilic moieties such as aromatic rings, carbon-carbon double bonds and the functional groups bearing sulfur, nitrogen, phosphorus and oxygen atoms, whereas, hydroxyl radicals reactions are non-selective toward different inorganic and organic compounds through electrophilic addition, radical-radical reactions, hydrogen abstraction and electron transfer reactions [52].

Upon UV light irradiation (Figure 1-6), electron-hole pairs are formed in the nanocrystal titanium dioxide photocatalyst semiconductor. Holes are positive charges, which when in contact with water molecules, generate $\cdot\text{OH}$ and H^+ ions. Electrons react with disintegrated oxygen to form superoxide ions ($\text{O}_2^{\cdot-}$), which react with water molecules to generate peroxide radicals ($\cdot\text{OOH}$) and hydroxide ions (^-OH). Peroxide radicals consolidate with H^+ ions to form ^-OH and $\cdot\text{OH}$, and holes oxidize ^-OH to $\cdot\text{OH}$. Thus, all species at last facilitate the formation of $\cdot\text{OH}$, and these radicals attack the contaminations present in the aqueous solution as indicated in the following Eqs. 1.16–1.19 [53, 24]:

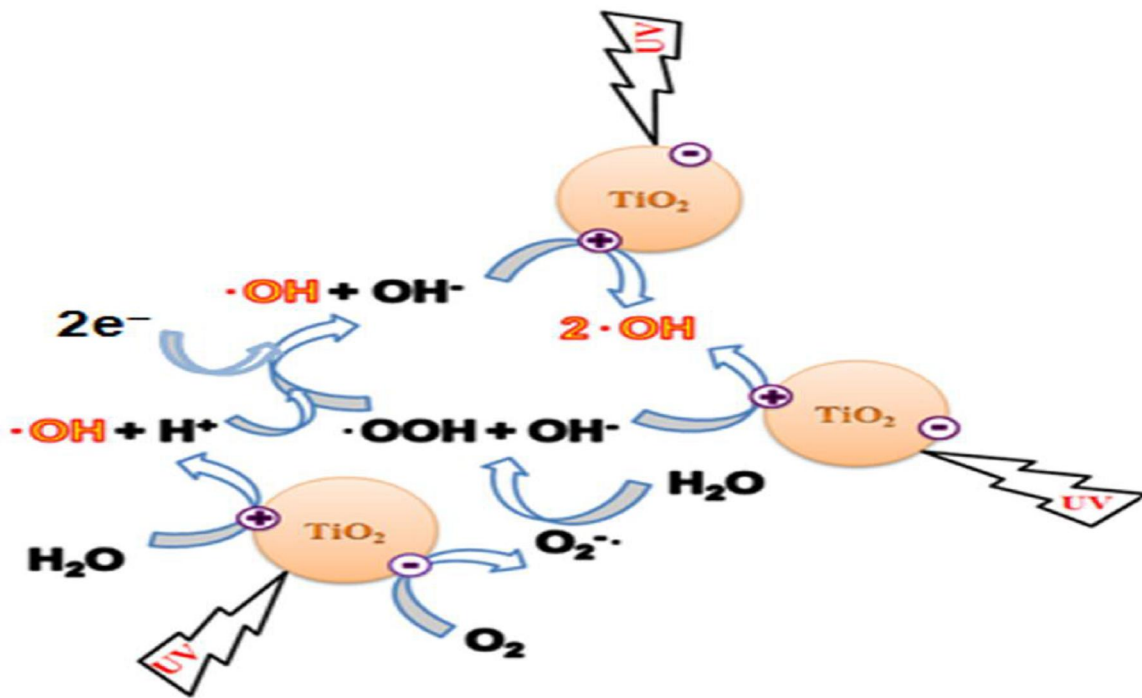
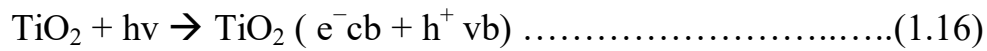


Figure (1-6): Photocatalytic production of hydroxyl radicals [53].

1.5 Surface plasmon resonance (SPR)

The basis of the localized surface plasmon resonance (LSPR) effect has been described in a recent review by Hafner and Mayer [54], and the detailed illustrations of the mechanisms of the plasmonic enhancement to photocatalysis have been shown by Zhang et al. [55]. These two surveys provide an understanding of the physical principles of the SPR [56]. Localized surface plasmon resonance (LSPR) is an optical phenomena produced by a light wave trapped within conductive nano particles (NPs) smaller than the wavelength of light.

The phenomenon is a result of the interactions between surface electrons in a conduction band and the incident light [57]. At the point when a small spherical metallic nanoparticle is irradiated by light, the oscillating electric field causes the conduction electrons to oscillate coherently. This is schematically shown in Figure (1-7) [58].

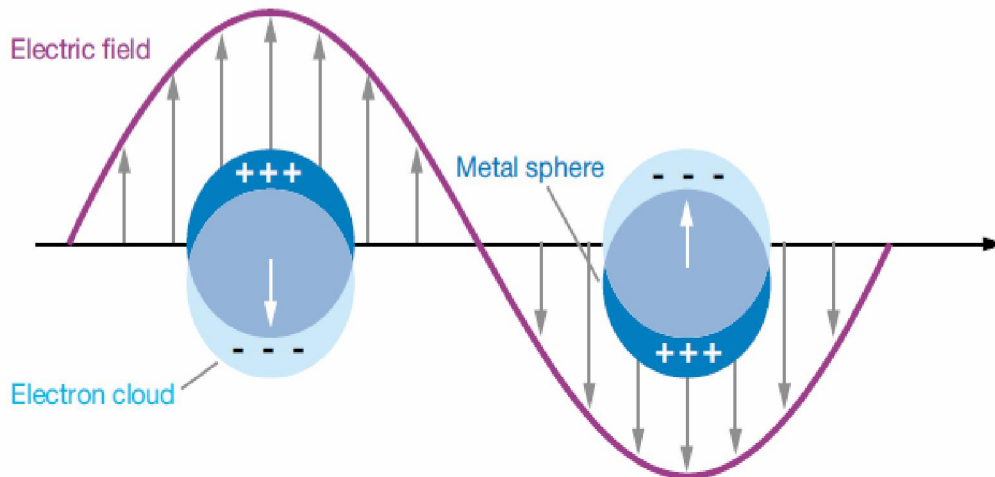


Figure (1-7): Schematic diagram illustrating a surface plasmon resonance [58]

Light in resonance with the surface plasmon oscillation causes the free electrons in the metal to oscillate. As the wave front of the light passes, the electron density in the particle is polarized to one surface and oscillates in resonance with the light's frequency making a standing oscillation. The resonance condition is determined from absorption and scattering spectroscopy and is found to depend on the dielectric constants, shape, particles size, and of both the surrounding material and the metal [59]. The SPR band is stronger for plasmonic nanoparticles (noble metal, especially Au and Ag) than other metals because of d-d band transitions, the plasma frequency is pushed into the visible part of the spectrum [57]. Figure (1-8) shows the extinction cross-section for various metal NPs with 10 nm in size.

It is noted that for noble metal NPs (such as Au, Ag) the extinction cross section can be up to 10 times their geometrical section; that is, the NPs are capable of absorbing and scattering photons with a relative high excitation cross-section in the visible regime.

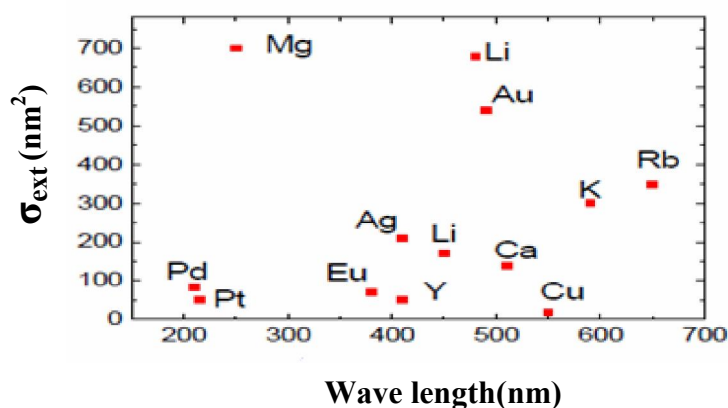


Figure (1-8): The extinction cross-section and corresponding resonant wavelength for isolated metallic nanoparticle with 10 nm in size [60].

In addition, these two metals are chemically inert in addition to processing a high charge carrier density. Thus, both Au and Ag NPs are frequently utilized as an essential part of plasmonic composites [60].

The noble metal-TiO₂ composite photocatalyst forming a Schottky barrier delay the electron-hole recombination and generates oxygen radicals by means of photogenerated electron capturing reduction reaction, increases the photocatalysts efficiency. [61].

The synergetic promotion effects of Au particles on the photocatalytic activity of titanium dioxide are represented in Figure (1-9). Electrons in large AuNPs are excited by LSPR and transferred to the conduction band of adjacent TiO₂, during which the local electric field of adjacent TiO₂ and separation of e⁻-h⁺ pairs are enhanced. Meanwhile, little Au nanoparticles on TiO₂ can act as efficient co-catalysts and trap the photo-excited electrons from the conduction band of TiO₂ [56].

Under UV-visible light illumination, triple synergetic promotion effect on the separation of photogenerated electron–hole pairs over TiO_2 by gold deposition with both large and small particles can be achieved [62].

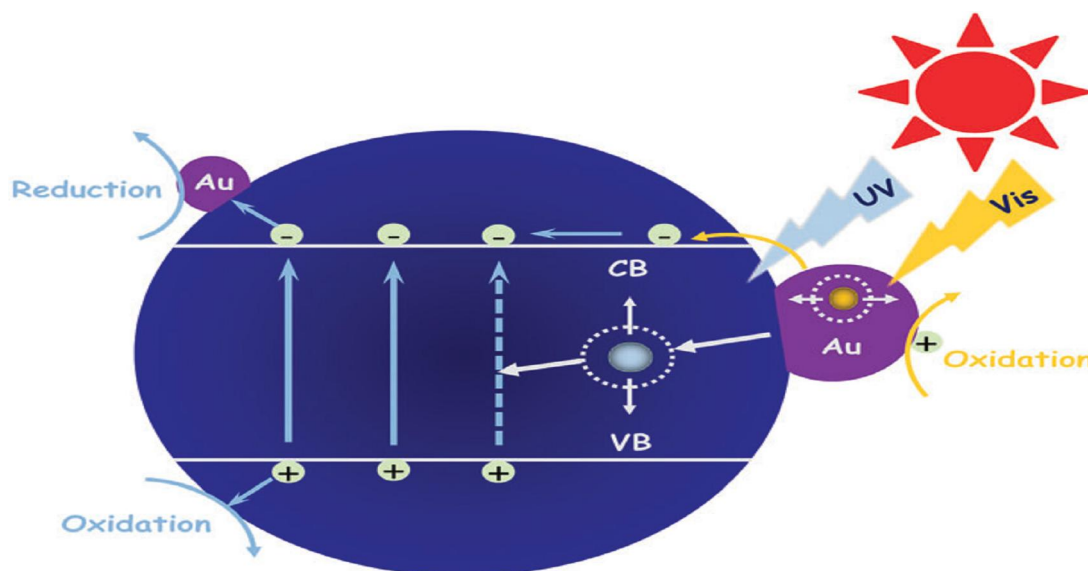


Figure (1-9): The whole mechanism for LSPR affects the photocatalytic [62].

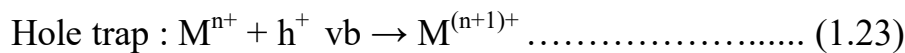
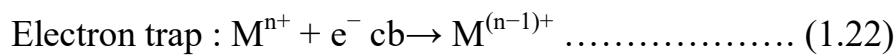
1.6 Precious metal doping

Among different semiconductors, titanium dioxide photocatalyst was considered as one of the most demanding catalyst due to its chemical stability, optical and electronic properties, low cost, non-toxicity, easily available, and efficient photocatalytic activity [34]. There are two types of problems which limit the photocatalytic activity of TiO_2 : firstly, the fast recombination rate of photogenerated electron-hole pairs results in a low photocatalytic reaction rate. Secondly, due to its large band gap ($E_g = 3.2$ eV), it can be photoactivated only in the ultraviolet region (~ 380 nm). Therefore, only about 5% of the solar energy can be used for photoexcitation of this material [63]. Titanium dioxide nanoparticles modified with precious metals have been extensively employed in photocatalytic water decontamination process [64].

Noble metal particles can be deposited onto the catalyst's surface by either photoreduction, sonochemical method or chemical reduction (in liquid phase with e.g., hydrazine or sodium borohydride). The size and amount of noble metal particles on the titanium dioxide surface are very important factors that can influence the general activity of the catalyst. Larger quantities of metal particles on the titania can block the active sites and a large amount of metal deposits can decrease charge carrier space distance which leads to expand electron-hole recombination rates [65]. Transition metal ion doping and rare earth metal ion doping have been widely experimented to enhance the photocatalytic efficiency. Choi et al.[66] exhibited a systematic investigation on the influence of 21 types of metal ion doping to titanium dioxide. The incorporation of metal ion into the lattice of TiO₂ enables the visible-light absorption by generating of impurity energy levels in the E_g as indicated in reactions (1.20) and (1.21).



where M and Mⁿ⁺ represent metal and metal ion dopant, respectively. Besides, the e⁻ transfer between metal ion and TiO₂ can retard the recombination of photogenerated e⁻/h⁺ (reactions 1.22 and 1.23)



The energy level of Mⁿ⁺/M⁽ⁿ⁻¹⁾⁺ must be less negative than the CB edge of TiO₂ while the energy level of Mⁿ⁺/M⁽ⁿ⁺¹⁾⁺ must be less positive than that of VB edge of TiO₂ [67].

The doping of TiO₂ with transition metal ions, for example Cu, Fe, V, Mn, Ni, Co, and Cr, are mostly unsuccessful to start efficiently the photocatalytic reaction under visible light illumination, because the doping sites may become reactive centers for rapid charge recombination. However, the surface or bulk modification of TiO₂ by noble metal ions (Chloridized Rh³⁺, Pt⁴⁺ and Au³⁺) can generate a visible active center for the degradation of organic pollutants [23].

Since the photocatalytic activity of the doped TiO₂ photocatalyst depends on different experimental conditions, preparation methods, nature and concentration of the dopants ion, it is very difficult to compare the results reported for doped samples [68]. The noble metal nanoparticles coupled with the semiconductor photocatalysts could behave as electron sinks to efficiently separate the photogenerated electron-hole pairs [69]. As the Fermi levels of these noble metals are lower than that of titanium dioxide, photo-excited electrons can be transferred from a conduction band to metal particles deposited on the surface of TiO₂. While photo-generated valance band holes stay on the TiO₂. These activities greatly reduce the possibility of electron-hole recombination, resulting in efficient separation and stronger photocatalytic reactions [70].

Gold is a noble metal that does not suffer corrosion under photocatalytic conditions, it can be prepared strongly anchored on the titania surface and it exhibits a characteristic surface plasmon band in the visible region because the collective excitation of electrons in the gold nanoparticles [71].

One of the most active metals for photocatalytic enhancement is platinum (Pt), which can generate the highest Schottky barrier among the metals that facilitate electron capture.. The capture of electrons by Pt is postulated to generate a longer electron–hole pair separation lifetime [72], Schottky barrier is a potential energy barrier for electrons formed at a metal–semiconductor junction. Therefore, prevent the recombination of electron– hole pairs and enhance the transfer of holes and possibly electrons to O_2 adsorbed on the TiO_2 surface. Afterwards, excited electrons migrate to the metal, where they get trapped and the electron–hole pair recombination is suppressed [73] as it is illustrated in Figure (1-10).

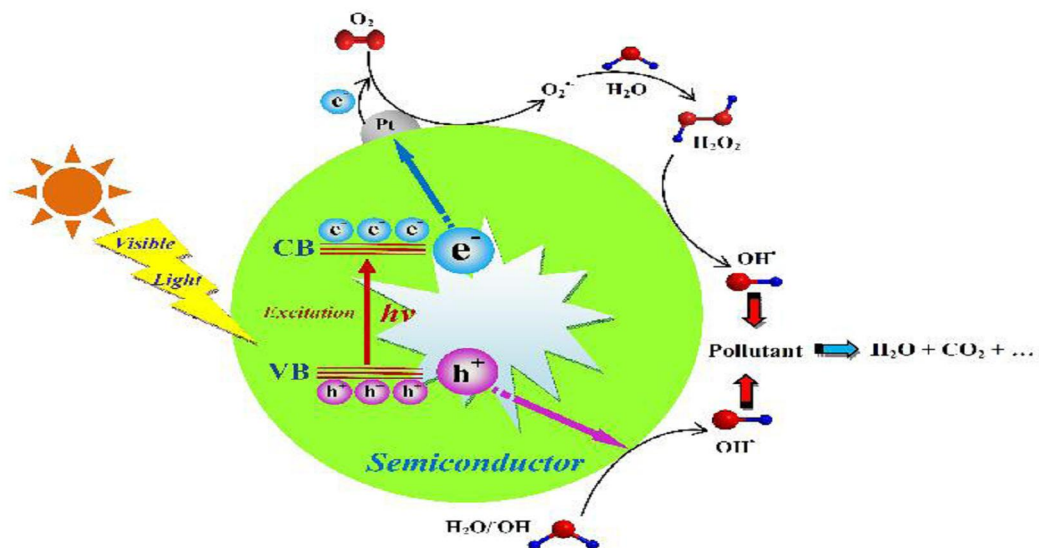


Figure (1-10): Mechanism of photocatalytic action of Pt-TiO₂ nanoparticles under visible light irradiation [73].

1.7 Photodeposition of metal ions

Photodeposition has been utilized to recover noble metals, to remove metal cations from aqueous effluents, and to prepare metal-supported catalysts and photocatalysts ever since Bard et al. [74], reported it in 1978. The illumination of a semiconductor powder (e.g., TiO_2) with UV light results in the reduction of metal cations having appropriate redox potential by the photoexcited electrons, creating metal particles on TiO_2 [75]. We can distinguish between two types of photodeposition: oxidative photodeposition and reductive photodeposition. A schematic overview of both reductive and oxidative photodeposition is depicted in Figure (1-11) [76].

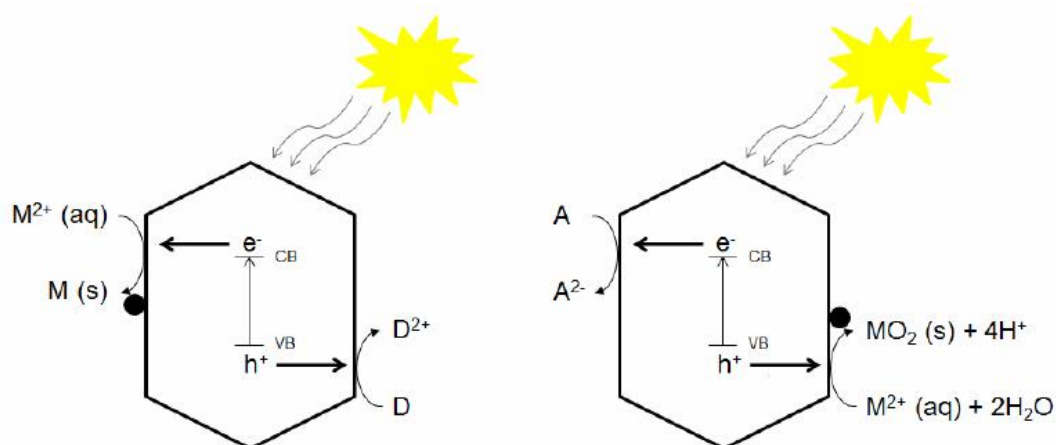


Figure (1-11): schematic overview of both reductive and oxidative photodeposition [76].

Heterogeneous photocatalysis utilizing TiO_2 has been proven to effectively degrade a great number of organic pollutants in air and wastewaters, being a promising environmental cleaning technology, especially for low levels of contaminants. In photocatalysis, deposition of noble metals, such as Au, Pt or Ag, over TiO_2 has been utilized for many years as a means for improving the photocatalytic activity of this photocatalyst [77].

In most studies on Au/TiO₂ plasmonic photocatalysts, the photodeposition technique was used for loading Au nanoparticles on the TiO₂ support. This method uses photogenerated electrons for reduction of the Au source. Since Au nanoparticles are believed to be formed on “reduction sites” of the TiO₂ surface, effective photocatalytic reduction is expected for prepared Au/TiO₂ [78].

Another possibility for the producing of noble metal nanoparticles is the addition of a reducing agent to the solution containing the noble metal precursor, e.g. hydrazine, ascorbic acid, citrate, or sodium borohydride. The effectiveness of the catalyst depends strongly on the amount of noble metal loaded onto the TiO₂ surface. The active sites of the catalyst can be blocked if there are too numerous metal nanoparticles on the surface, while if the metal content is too low, the desired activity enhancement might not be achieved [79].

1.8 Literature survey

Dopants, such as transitional metals have been added to the TiO₂ catalyst to improve its response, to reduce the recombination of photogenerated electrons and photogenerated holes and to induce a bathochromic shift, i.e., a decrease of the band gap which results in more visible light absorption. [1]. Tanabe et al. [80] stated that the addition of dopants may influence the suspension properties such as agglomeration behavior of particles due to alteration of the net surface charge on the particle.

According to the model proposed by Zhou et al. [81] the formation rates of hydroxyl radicals, and photocatalytic decolorization of Rhodamine-B aqueous solution were significantly enhanced by those embedded Au nanoparticles in the Au-TiO₂ nanocomposites due to surface plasmon resonance of Au nanoparticles.

Masakazu and Takeuchi [82] employed Electron Spin Resonance signals to investigate electron transfer from TiO₂ to Pt particles in Pt doped TiO₂ powder. It was found that Ti⁺³ signals increased with irradiation time and the loading of Pt reduced the amount of Ti⁺³. This observation indicates the occurrence of electron transfer from TiO₂ to Pt particles.

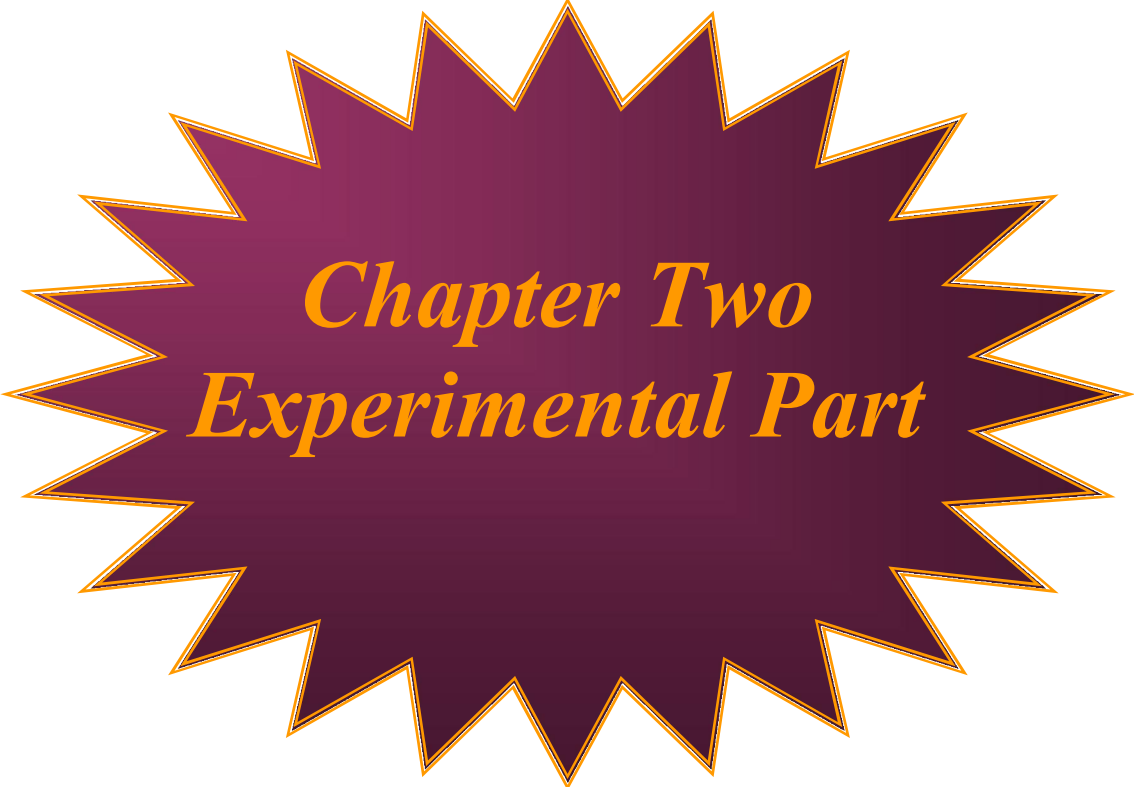
As accumulate electrons on the noble metal particles, their Fermi levels shift closer to the conduction band of TiO₂ resulting in more negative energy levels [70]. The removal of OG increased from 36.3 to 78.3% by decreasing initial concentration OG from 125 to 50 mg/L. This trend is due to the availability of fixed adsorbent sites for a fixed amount of adsorbent reported by Roy et al. and Z. Barzgari et al. [83-84]. For higher concentrations, the ratio of adsorbent sites to dye species decreases, which leads to the decrease in removal percent.

Thennarasu et al. [85] reported that the degradation efficiency of OG slowed down on increase of the initial pH from 7.0 to 10. The reason for lower percentage degradation of dye molecules in the range of acidic pH may be that more H⁺ ions are available for the adsorption to mask the surface of the catalyst thus preventing the photoexcitation of semiconductor particles, thereby reducing the generation of free radicals.

1.9 Scope of the work

In the present work the first purpose has been impregnation of nano anatase TiO₂ with different levels of Au or Pt abundance employing photodeposition technique by means of UV irradiation and chemical reduction methodologies exploiting various reducing agents. The second objective was planned to investigating the impacts of several operational parameters namely, initial pH of photocatalysis media, visible light illumination time, initial concentration of the Orange G model dye (OG), doped TiO₂ loading, Au or Pt content, visible light source intensity and temperature on the photocatalytic degradation of OG.

In addition, the characterization of the prepared doped anatase Au-TiO₂ and Pt-TiO₂ nano photocatalysts has been another objective implying the morphology, composition, particle size and specific surface area using several instrumental techniques namely, Scanning Electron Microscopy (SEM), Energy Dispersive X-Ray Spectroscopy (EDXS), X-Ray Diffraction (XRD), Transmission Electron Microscopy (TEM) and N₂-adsorption Brunauer–Emmett–Teller (BET) methodology. The kinetic and thermodynamic studies for the photocatalysis of OG dye have also been one of the aims of this research work as well.



Chapter Two
Experimental Part

2.1 Chemicals

Table (2-1): The following chemicals were used throughout this research work.

<i>Material</i>	<i>Purity</i>	<i>Source</i>
$(\text{NH}_4)_2 \text{SO}_4 \cdot \text{FeSO}_4 \cdot 6\text{H}_2\text{O}$	99.5 %	BDH
$\text{H}_2\text{C}_2\text{O}_4 \cdot 2\text{H}_2\text{O}$	99.6 %	HW
$\text{FeSO}_4 \cdot 7\text{H}_2\text{O}$	99 %	Riedel-Dehaen
CH_3COONa	98 %	Riedel-Dehaen
1-10 phenanthroline	97 %	BDH
Isopropanol alcohol	99.5 %	Fluka
Ti-isopropoxide	99.7 %	Aldrich
Orange G	99 %	Fluka
H_2PtCl_6	99.95%	Aldrich
$\text{HAuCl}_4 \cdot 3\text{H}_2\text{O}$	99.99 %	ABCR GmbH
TiO_2	99.7 %	Aldrich
NaBH_4	96 %	Fluka
Sodium citrate tribasic dihydrate	99 %	Sigma-Aldrich
α - Ketoglutaric acid (2-Oxoglutaric acid)	99 %	Fluka
Acetone	99 %	Analyt
Ethanol	97 %	Fluka
H_2O_2	50 % wt/wt	Scharlau
H_2SO_4	98%	Himedih

2.2 Procedures

2.2.1 Preparation of Potassium Trisoxalatoferrate(III) Trihydrate.

1- Weigh about 5 g of $(\text{NH}_4)_2 \text{SO}_4 \cdot \text{FeSO}_4 \cdot 6\text{H}_2\text{O}$ was weighed in a 125 ml Erlenmeyer flask and dissolved in 20 ml hot nanofiltered deionized water (NFDW) and finally 1 ml of 3M H_2SO_4 was added.

2- About 2.5 g of oxalic acid ($\text{H}_2\text{C}_2\text{O}_4$) was dissolved in 25 ml of NFDW, this solution was mixed with the above solution, mentioned in step one, and warmed to boiling while stirring constantly to prevent bumping.

3- The Erlenmeyer flask was removed from the heat source and allowed the yellow precipitate of FeC_2O_4 to settle for 10 ml.

4- The supernatant liquid was decanted (poured the liquid away from the solid) and the precipitate was washed utilizing 15 ml of hot NFDW. The mixture was filtered and swirled.

5- About 10 ml of hot NFDW that contains 3.5g of $\text{K}_2\text{C}_2\text{O}_4$ was added to the precipitate, then was stirred and heated to 40°C . While the temperature was at 40°C , immediately, 8 ml of H_2O_2 was added dropwise and stirred continuously. Periodically the temperature of the solution was checked and made sure that it was at least 40°C (but not more than 50°C) during the addition of H_2O_2 . A precipitate of brown $\text{Fe}(\text{OH})_3$ was observed at this time.

6- The resulting solution was heated to boiling. 20 ml of $\text{H}_2\text{C}_2\text{O}_4$ was added (prepared by dissolving 1 g in 30 ml of NFDW). It was stirred continuously and the last 10 ml of $\text{H}_2\text{C}_2\text{O}_4$ was added dropwise, while maintaining the temperature near boiling. The solution was turned clear green.

7- Roughly 20 ml of ethanol was added to solution of rejected precipitate (when crystals were formed, it was dissolved by heating in water bath).

8- The solution was left in dark about 24 hours.

9- The solution was filtered under vacuum and washed with 10 ml of 1:1 NFDW / ethanol solution.

10- Finally, the precipitate (potassium ferrioxalate) was washed utilizing ten milliliters of acetone [40].

2.2.2 Measurement of light intensity using actinometric method

The intensity measurement of the incident light was carried with a potassium ferrioxalate actinometer as described by Parker and Hatchard [86] and examined extensively through a previous work in our research laboratory [87]. This method is commonly utilized to determine the number of quanta entering the reaction vessel and consequently, the apparent quantum yields for the photocatalytic reaction will be estimated. The actinometer solution $6 \times 10^{-3} \text{ mol.L}^{-1}$ was set up by dissolving 2.947g of $\text{K}_3\text{Fe}(\text{C}_2\text{O}_4)_3 \cdot 3\text{H}_2\text{O}$ in 800 ml of NFDW.

About 100 ml of 1N H_2SO_4 was added and the whole solution was diluted to 1 L with NFDW.

The method which was utilized for the determination of light intensity involves irradiation of actinometer solution for known period time (1 hour).

Calibration curve

A calibration curve for Fe^{+2} was drawn using the following solutions:

- 1- 0.1% w/v phenanthroline monohydrate in water.
- 2- 4×10^{-4} mol.L⁻¹ of FeSO_4 in 0.1 N H_2SO_4 .
- 3- Buffer solution, was prepared by mixing 600 ml of 1N sodium acetate and 360 ml of 1N H_2SO_4 then diluted to 1L .

Different concentrations of Fe^{+2} solutions were prepared by further dilution of solution (1) above in 25 ml volumetric flask. Then after, the followings are added to each flask;

- a- 5 ml of buffer solution.
- b- 2 ml phenanthroline solution.
- c- Different volumes of 0.1N H_2SO_4 solution were utilized to make equivalent to 10 ml 0.1 N H_2SO_4 and finally dilute the whole solution to 25 ml with NFDW.

The volumetric flask was covered with aluminum foil and kept in the dark for 30 min. Then the optical densities at wavelength of 510 nm were measured. A blank solution was utilized as reference which contained all the liquids except the ferrous ion solution. Draw the Plot for optical density versus ferrous ion concentration, Figure (2-1). The slope of the straight line gives the absorptivity (extinction coefficient) of FeSO_4 solution.

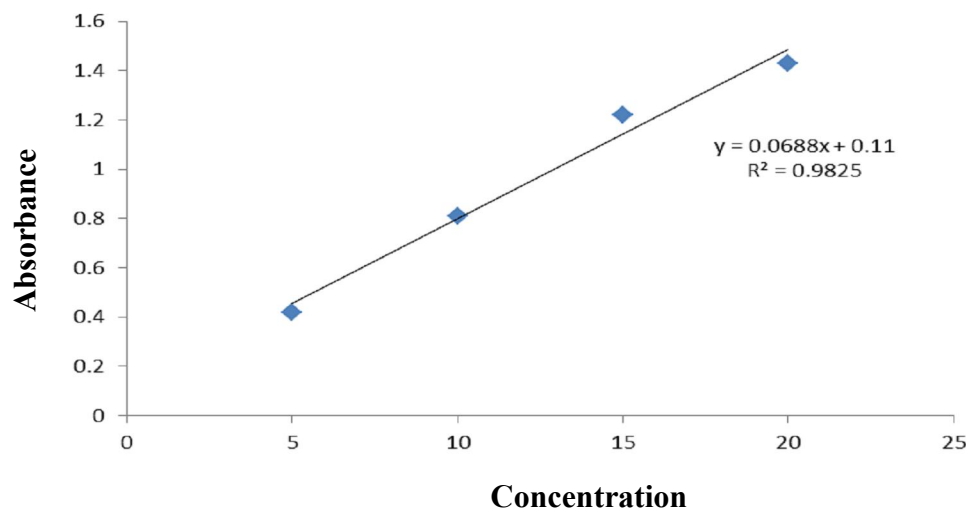


Figure (2-1): Calibration curve for Fe^{+2}

In order to **determine the intensity light**, 100 ml of actinometer solution was irradiated in the irradiation cell. Post illumination, 1ml of the irradiated solution was transferred into 25 ml volumetric flask, 0.5 ml of buffer solution and 2 ml of phenanthroline solution were added to the flask, and then it was diluted to 25 ml using NFDW.

A Blank solution was prepared by mixing 1 ml of unirradiated potassium ferrioxalate solution with other components. The optical density was measured.

The incident light intensity was calculated as follows:

$$I_0 = A \times V_1 \times 10^{-3} \times V_3 / Q_y \times \epsilon \times V_2 \times t$$

Where:

I_0 = photo flow (incident light intensity)

A = optical density (absorbance) at 510 nm

V_1 = initial volume (100 ml)

V_3 = final volume (25 ml)

Q_y = quantum yield at 365 nm which equals to 1.21 [88].

ϵ =extinction coefficient = slope of calibration curve of Fe^{+2} (1.235×10^4 L. mol⁻¹.cm⁻¹).

V_2 = volume taken from irradiated solution (1 ml).

t = Irradiation time in seconds .

The apparent quantum yield is calculated using the following expression :

Φ_{app} = rate of reaction / rate of absorbed photons (I_0).

the computed intensities using above expression have been as follows;

high intensity equals = 3.39×10^{-7} (Ein./L.sec)

medium intensity equals = 1.47×10^{-7} (Ein./L.sec)

low intensity equals = 0.38×10^{-7} (Ein./L.sec)

2.2.3 Synthesis of TiO₂ nanoparticles catalyst.

Titanium dioxide nanosized catalyst was synthesized by the sol-gel procedure by means of a gradual addition of a solution of titanium isopropoxide (5 ml isopropanol + 5ml titanium isopropoxide) onto 200 ml of DNFW at pH=5 with a rate of addition of 2 ml /min. The mixture was kept, after completion of addition, under continuous vigorous mixing at room temperature until the completion of hydrolysis for two hours. The resulting transparent colloidal solution was left aging for 24 hours then filtered, dried at 90 °C for two hours, and finally was calcined at 400 °C for 4 hours. Grinding into fine powder, if needed, overcomes the agglomeration [89].

2.2.4 Preparation of doped TiO₂ with Au and Pt by UV-irradiation.

- 1- About 110 ml of NFDW were contained 0.05g of hydrogen tetrachloro aurate (III) trihydrate and 0.5g of TiO₂, and the procedure was repeated with 0.1 g of dihydrogen hexachloro palatinate (IV) for Pt doping.
- 2- The solutions were stirred and irradiated for 24 hours with 15 watt UV-lamp (Figure 2-2 a).
- 3- The solutions were filtered using cellulose membrane (0.45μm) and then dried at 80-90 °C for 2 hours.

2.2.5 Preparation of doped TiO₂ with Au-TiO₂ and Pt-TiO₂ via chemical reduction.

- 1- About 0.1 M of each reductant was prepared (sodium borohydrate, sodium citrate and ∞-ketogultaric acid) in 10 ml volumetric flask.
- 2- Roughly 0.1g of HAuCl₄.3H₂O salt and 0.5g of TiO₂ were taken and mixed by means of a magnetic stirrer in 100 ml NFDW. Similar procedure was followed in the case of H₂PtCl₆ salt.
- 3- Take 5 ml of 0.1M reductants' solution was added dropwise during 15 min with vigorous stirring for 1 hour (Figure 2-2 b).
- 4- The solutions were kept stirring gently overnight. Then, filtered using cellulose membrane (0.45μm) and dried at 80 °C for 2 hours.

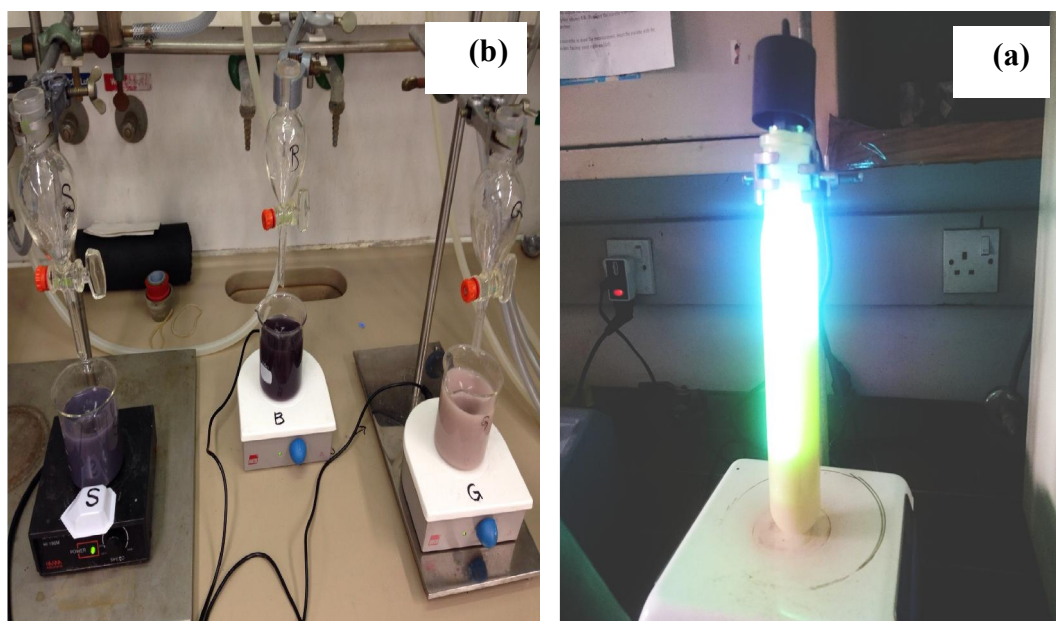


Figure (2-2): (a) Irradiative doping of TiO_2 ; (b) Chemical reductive doping of TiO_2 .

2.2.6 Effect of gold and platinum content of Au-TiO_2 and Pt-TiO_2 on the degradation of Orange G.

- 1- Take 100 ml of OG (10 mg/L) was taken and its pH was adjusted to 3.
- 2- About 40mg of the following powders (Au-TiO_2), and similar procedure was repeated to (Pt-TiO_2) was added to above solution.
 - a- 1% Au-TiO_2 , and repeated for 1% Pt-TiO_2
 - b- 2% Au-TiO_2 , and repeated for 2% Pt-TiO_2
 - c- 4% Au-TiO_2 , and repeated for 4% Pt-TiO_2

Note: Every single Au-TiO_2 and Pt-TiO_2 powder refer to separate experiment.

- 3- The solutions were stirred with O₂ bubbling in the dark for 25 min to ensure the adsorption equilibrium which was established prior to irradiation.
- 4- The samples were irradiated using halogen lamp at high intensity with stirring for 270 min for Au-TiO₂ and 200 min for Pt-TiO₂.
- 5- About 5 ml was withdrawn after every 45 min for Au-TiO₂ and every 30 min for Pt-TiO₂ of irradiation time.
- 6- The catalysts were separated from the suspension by centrifuge for 10 minutes using 3000 RPM, and filtered using cellulose membrane of 0.45 μm pore size.
- 7- The absorbance of OG was measured to estimate the degradation percent.

2.2.7 Effect of reductants (sodium borohydrate, sodium citrate and α-ketogutaric acid) and UV-irradiation on the degradation of Orange G.

- 1- About 100 ml of OG (10 mg/L) was taken and its pH was adjusted to 3 for Au-TiO₂, and the process was repeated but the pH was adjusted to 5 for Pt-TiO₂. (i.e., both was carried out in acidic media).
- 2- About 40mg of the following powders (Au-TiO₂), and similar procedure was repeated for (Pt-TiO₂), was added to above solution.
 - a- 2% Au-TiO₂ of sodium borohydrate, and repeated for 2% Pt-TiO₂
 - b- 2% Au-TiO₂ of sodium citrate, and repeated for 2% Pt-TiO₂
 - c- 2% Au-TiO₂ of α-ketogutaric acid, and repeated for 2% Pt-TiO₂
 - d- 2% Au-TiO₂ UV-Irradiation, repeated for 2% Pt-TiO₂

Note: Every single Au-TiO₂ and Pt-TiO₂ powder refer to separate experiment.

3- The solutions were stirred with O₂ bubbling in the dark for 25 min to ensure the adsorption equilibrium which was established prior to irradiation.

4- The samples were irradiated using halogen lamp at high intensity with stirring 270 min for Au-TiO₂, and 200 min for Pt-TiO₂.

5- About 5 ml was withdrawn after every 45 min for Au-TiO₂, and every 30 min for Pt-TiO₂ of irradiation time.

6- The catalysts were separated from the suspension by centrifuge for 10 min using 3000 RPM, and filtered using cellulose membrane of 0.45 μm pore size.

7- The absorbance of OG was measured to estimate the degradation percent.

2.2.8 Preparation of Orange G solution.

1- A stock solution of OG of 50 ppm was set up by dissolving 0.05 g of OG dye into 1 L of NFDW.

2- Different concentrations (5, 10, 15, 20, 30 and 40 ppm) of Orange G were prepared from stock solution by a series of dilution in order to prepare the calibration curve.

3- The calibration curve was drawn by measuring absorbance at 478 nm for all prepared OG solutions mentioned previously in steps 1 and 2, as shown in Figure (2-3).

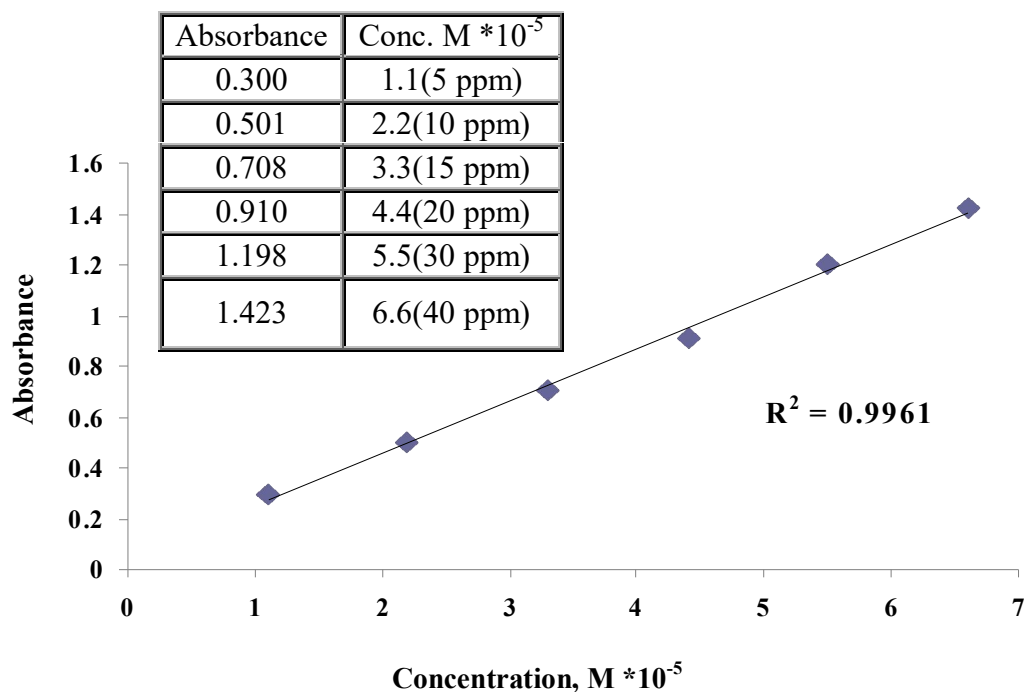


Figure (2-3): Calibration curve for orange G together with the inset which presents the absorbance at relevant concentrations

The UV-VIS spectrophotometric scan in the range of 275-600 nm was used to record the absorbance as shown in Figure (3-3). The molar extinction coefficient (absorptivity, ϵ) from 5 to 30 ppm of OG in NFDW was measured at the maximum absorption wavelength, 478 nm, using Beer-Lambert equation ($A = \epsilon_{\max}bc$), where A = absorbance, b = absorption light path, 1 cm and c = molar concentration of OG.

The absorptivity (ϵ_{\max}) has been 22480 L.mol⁻¹.cm⁻¹ for molar concentration from $1.105 \cdot 10^{-5}$ to $6.632 \cdot 10^{-5}$ mol/L.

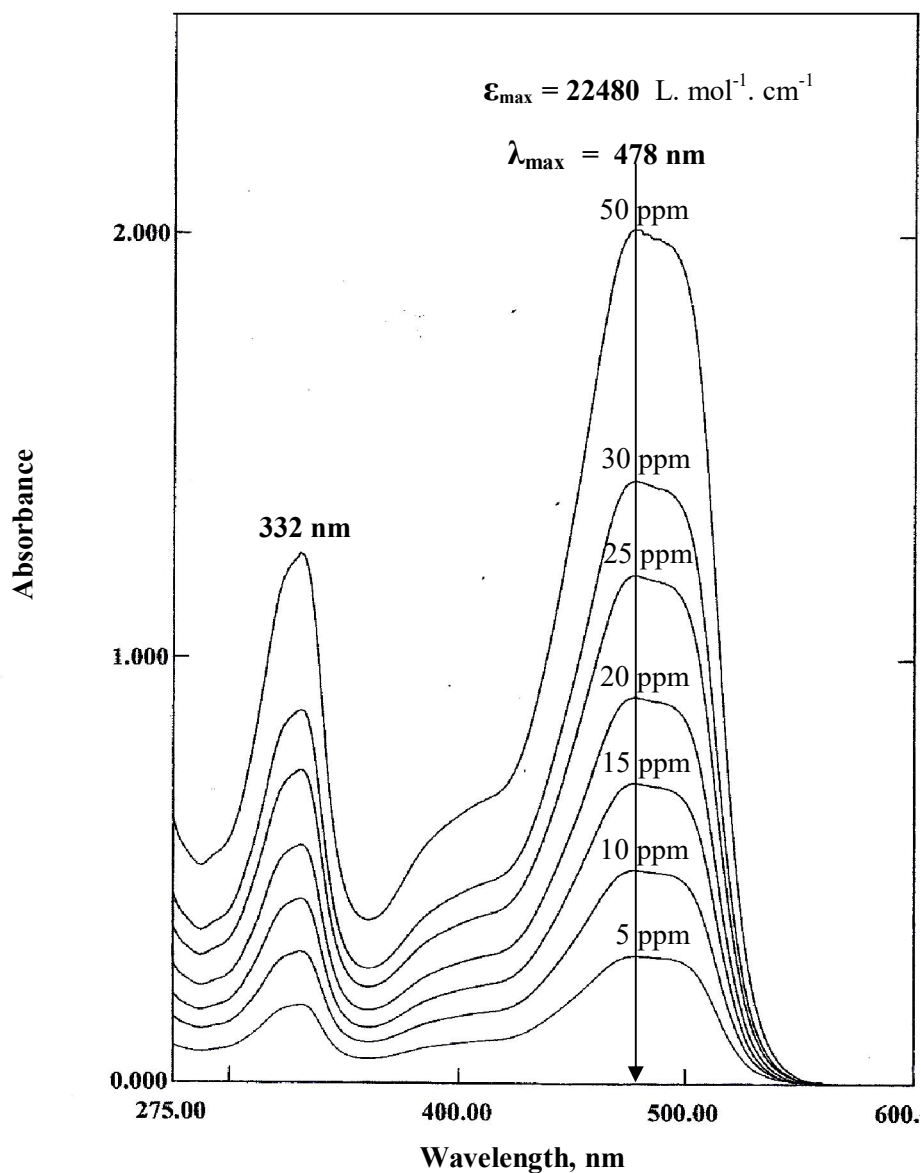


Figure (2-4): UV-VIS spectrum of OG at various concentrations.

2.2.9 Testing of degradation of Orange G under visible light.

The effect of visible light on degradation of Orange G was studied as follows;

- 1- Take 100 ml of OG (10 mg/L) aqueous solution was illuminated using halogen lamp at high intensity with stirring for 180 min.
- 2- At every 60 min of irradiation time, samples of 5 ml was withdrawn for analysis.

3-The disappearance of OG was monitored using the visible absorbance feature at $\lambda = 478$ nm as function of irradiation time.

2.2.10 Testing of degradation of Orange G in the dark.

- 1- Take 100 ml of OG (10 mg/L) was added into a beaker.
- 2- A mass of 40 mg of (2% Au-TiO₂) was added into 100 ml of Orange G aqueous solution, and similar procedure was repeated to (4% Pt-TiO₂).
- 3- The solutions were kept in the dark for 180 min for Au-TiO₂ and 210 min for Pt-TiO₂ with continuous stirring.
- 4- Roughly 5 ml was withdrawn after every 60 min for Au-TiO₂ and every 30 min for Pt-TiO₂ of stirring time.
- 5- The catalysts (Au-TiO₂, Pt-TiO₂) were separated from the suspension by centrifuge for 10 min using 3000 RPM, and filtered using cellulose membrane of 0.45 μ m pore size.
- 6- The absorbance was measured for OG at 478 nm to estimate the changes in concentration.

2.2.11 Testing of degradation of dye by visible Light in presence of TiO₂ without O₂.

- 1- Take 100 ml of OG (10 mg/L) aqueous solution was irradiated using halogen lamp at high intensity with stirring .
- 2- A mass of 40 mg of powder (TiO₂) was contacted with 100 ml of OG aqueous solution.
- 3- The water suspension of dye and nanosized TiO₂ powder were stirred in the dark for 25 min to ensure the adsorption equilibrium was established prior to irradiation.

4- The sample was irradiated using halogen lamp at high intensity with stirring for 180 min.

5- About 5 ml was withdrawn after every 60 min of irradiation time.

6- The catalyst (TiO_2) was separated from the suspension by centrifuge for 10 minutes using 3000 RPM and filtered using 0.45 μm cellulose membrane.

7- Absorbance of OG was measured to estimate the degradation percent.

2.2.12 Testing of degradation of dye by visible Light in presence of TiO_2 and O_2 .

1- Take 100 ml of OG (10 mg/L) aqueous solution

2- A mass of 40 mg of powder (TiO_2) was contacted with 100 ml of azo dyes aqueous solution.

3- The water suspension of dye and nanosized TiO_2 powder were stirred with O_2 bubbling in the dark for 25 min to ensure the adsorption equilibrium was established prior to irradiation.

4- The sample was irradiated using halogen lamp at high intensity with stirring for 180 min.

5- About 5 ml was withdrawn after every 60 min of irradiation time.

6- The catalyst (TiO_2) was separated from the suspension by centrifuge for 10 min using 3000 RPM and filtered using 0.45 μm cellulose membrane.

7- Absorbance of dye was measured to estimate the degradation percent.

2.2.13 Testing of degradation of Orange G by visible light in presence of Au-TiO₂, O₂ and Pt-TiO₂, O₂.

- 1- A mass of 40 mg of (2% Au-TiO₂), and similar procedure was repeated to (4% Pt-TiO₂), were contacted with 100 ml of OG (10 mg/L) aqueous solution.
- 2- The solution were stirred with O₂ bubbling in the dark for 25 min to ensure the adsorption equilibrium which was established prior to irradiation.
- 3- The samples were irradiated using halogen lamp at high intensity with stirring 180 min for Au-TiO₂ and 210 min for Pt-TiO₂.
- 4- Roughly 5 ml was withdrawn after every 60 min for Au-TiO₂ and every 30 min for Pt-TiO₂ of stirring time.
- 5- The catalysts (Au-TiO₂, Pt-TiO₂) were separated from the suspension by centrifuge for 10 min using 3000 RPM, and filtered using cellulose membrane of 0.45 μm pore size.
- 6- The absorbance of OG was measured at 478 nm to estimate the degradation percent.

2.2.14 Testing of degradation of azo dye by visible light in presence of Au-TiO₂ without O₂ and Pt-TiO₂ without O₂.

- 1- A mass of 40 mg of (2% Au-TiO₂), and similar procedure was repeated to (4% Pt-TiO₂), were contacted with 100 ml of Orange G (10 ppm) aqueous solution.
- 2- The solutions in the dark were stirred for 25 min to ensure the adsorption equilibrium which was established prior to irradiation.

- 3- The samples were irradiated using halogen lamp at high intensity with stirring 180 min for Au-TiO₂ and 210 min for Pt-TiO₂.
- 4- Roughly 5 ml was withdrawn after every 60 min for Au-TiO₂ and every 30 min for Pt-TiO₂ of stirring time.
- 5- The catalysts (Au-TiO₂, Pt-TiO₂) were separated from the suspension by centrifuge for 10 min using 3000 RPM, and filtered using cellulose membrane of 0.45 μm pore size.
- 6- The absorbance of OG was measured at 478 nm to estimate the degradation percent.

2.2.15 Effect of initial pH on the degradation of Orange G.

- 1- Roughly 100 ml of OG (10 mg/L) was taken and whose pH was changed as follows (2, 3, 4, 5, 6, 8, and 9) in the case of Au-TiO₂, and (1.9, 3, 4, 5, and 6) in the case of Pt-TiO₂ using diluted (0.1M) H₂SO₄ and diluted (0.1M) NaOH. then 40 mg of powder (2% Au-TiO₂), similar procedure was repeated to (4% Pt-TiO₂), was added.
- 2- The solutions were stirred with O₂ bubbling in the dark for 25 min to ensure the adsorption equilibrium which was established prior to irradiation.
- 3- The samples were irradiated using halogen lamp at high intensity with stirring for 240 min for Au-TiO₂ , and 120 min for Pt-TiO₂ .
- 4- About 5 ml was withdrawn after every 60 min for Au-TiO₂, and every 20 min for Pt-TiO₂ of irradiation time.
- 5- The catalysts were separated from the suspension by centrifugation for 10 min using 3000 RPM, and filtered using cellulose membrane of 0.45 μm pore size.

6- The absorbance of OG was measured at 478 nm to estimate the degradation percent.

2.2.16 Effect of Au-TiO₂ and Pt-TiO₂ loading on the degradation of Orange G .

1-Take 100 ml of OG (10ppm) and adjust to pH = 3 using dilute (0.1M) H₂SO₄.

2-Add different amounts of (2% Au-TiO₂) to the cell (20, 30, 40, 50, and 60 mg), similar procedure was repeated to (4% Pt-TiO₂).

3- The solutions were stirred with O₂ bubbling in the dark for 25 min to ensure the adsorption equilibrium which was established prior to irradiation.

4-The samples were irradiated using halogen lamp at high intensity with stirring for 270 min for Au-TiO₂ and 90 min for Pt-TiO₂.

5- About 5 ml was withdrawn after every 45 min for Au-TiO₂, and every 15 min for Pt-TiO₂ of irradiation time.

6- The catalysts were separated from the suspension by centrifuge for 10 min using 3000 RPM and filtered using cellulose membrane of 0.45 μm pore size.

7- The absorbance of OG was measured to estimate the degradation percent.

2.2.17 Effect of light intensity on the degradation of Orange G

1- Take 100 ml of OG (10 mg/L) was stirred and adjusted to pH = 3.0

2- About 40 mg of 2 % Au-TiO₂ powder was added to above solution.

3- The solution was stirred with O₂ bubbling in the dark for 25 min to ensure the adsorption equilibrium which was established prior to irradiation.

4- The sample was irradiated at low, medium, and high intensities with stirring for 270 min.

5- About 5 ml was withdrawn after every 45 min of irradiation time.

6- The catalyst was separated from the suspension by centrifugation for 10 min using 3000 RPM and filtered using cellulose membrane of 0.45 μm pore size.

7- The absorbance of OG was measured to estimate the degradation percent.

2.2.18 Effect of initial OG concentration on the rate of reaction

1- Roughly 100 ml of various initial concentrations of azo dye (5, 10, 15, 20, 25, 30, and 40) ppm, then pH was adjusted to 3.

2- About 40 mg of (2% Au-TiO₂), similar procedure was repeated to (4% Pt-TiO₂) powder, was added to above solution.

3- The solution was stirred with O₂ bubbling in the dark for 25 min to ensure the adsorption equilibrium which was established prior to irradiation.

4- The samples were irradiated using halogen lamp at high intensity with stirring for 270 min for Au-TiO₂ and 60 min for Pt-TiO₂.

5- About 5 ml was withdrawn after every 45 min for Au-TiO₂ , and every 15 min for Pt-TiO₂ of irradiation time.

6- The catalysts were separated from the suspension by centrifuge for 10 min using 3000 RPM, and filtered using cellulose membrane of 0.45 μm pore size.

7- The absorbance of OG was measured to estimate the degradation percent.

2.2.19 Effect of temperature on the degradation of dye.

1- Roughly 100 ml of OG (10 ppm) were taken and adjusted to $\text{pH} = 3$, using diluted H_2SO_4 (0.1M).

2- Take 40 and 50 mg of 2%Au-TiO₂, similar procedure was repeated to 4% Pt-TiO₂, were added onto the cell containing the above solutions for OG.

3- The solutions were equilibrated with O₂ for 25 min in the dark where water bath circulator was used to keep the temperature of solution at (20, 25, 30, 35, and 45 °C).

4- The samples were irradiated using halogen lamp at high intensity with stirring for 270 min for Au-TiO₂ and 60 min for Pt-TiO₂.

Note : the flow rate of O₂ is 50-55 ml/min.

5- About 5 ml was withdrawn after every 45 min for Au-TiO₂ , and every 15 min for Pt-TiO₂ of irradiation time.

6- The catalysts were separated from the suspension by centrifuge for 10 min using 3000 RPM and filtered using cellulose membrane of 0.45 μm pore size.

7- The absorbance of OG was measured to estimate the degradation percent.

2.2.20 Determination of pH of point zero charge (pH_{pzc})

- 1- 0.01M NaCl aqueous solution was prepared at pH (2, 4, 6, 8, 10).
- 2- The pH value of the solutions were adjusted with H₂SO₄ (0.1M) or NaOH (0.1M) solutions.
- 3- take 20 ml from each solution kept in contact with 0.02g 2% Au-TiO₂, and the procedure was repeated for 4% Pt-TiO₂ for 48hours under vigorous stirring.
- 4- The supernatant was decanted and its pH was measured.
- 5- The pH_{pzc} value was determined using the plot of pH_i vs. pH_f.

2.2.21 Influence of solar irradiation.

- 1- Roughly 100 ml of OG (10 ppm) were taken and adjusted to pH = 3 using diluted H₂SO₄ (0.1M).
 - 2- Take 40 mg of 2% Au-TiO₂ nanoparticles was added to the solution, and the procedure was repeated for 4% Pt-TiO₂.
 - 3- The above solution was irradiated through direct sun light, with O₂ bubbling and stirring for 120 min for Au-TiO₂ , 25 min for Pt-TiO₂.
- Note: the flow rate of O₂ is 50-55 ml\min.
- 4- About 5 ml was withdrawn after every 15 min for Au-TiO₂ , and every 5 min for Pt-TiO₂ of irradiation time.
 - 5- At given irradiation time intervals, samples of 5 ml of the suspension were withdrawn and filtered post centrifugation for 10 min using 3000 RPM to remove the catalyst.
 - 6- The dye concentration was determined by measuring its absorbance using a UV-VIS spectrophotometer.

Note: The solar light experiments were carried out at 10: 15 am during June (summer season) in Baghdad city.

2.3 Instruments

2.3.1 Refrigerated circulating bath. Model (WCR-P12), wisecircu.

2.3.2 Nanofiltered-deionized water supply unit. model (Sm-11), Waterpia.

2.3.3 Centrifuge (K centrifuge PLC series.).

2.3.4 Muffle furnace (SX-5-12).

2.3.5 Drying cabinet (K Hot Air Sterilizer).

2.3.6 Apel PD-303 single beam spectrophotometer has been used for visible light absorption measurements.

2.3.7 Double beam Shimadzu UV-VIS spectrophotometer. Model (1650 PC) has also been used throughout this work.

2.3.8 Thermostat shaker water bath JEIOTECH (BS-11).

2.3.9 Fourier Transform Infrared (FTIR) spectrometer.

2.3.10 X-ray Spectrometer .

Pananalytical Philips diffractometer using a Cu target Ka radiation ($\lambda = 1.541 \text{ \AA}$) to determine the crystalline size. The accelerating voltage and the applied current were 40 kV and 30 mA, respectively. The XRD patterns were at the scanning range 2θ from 5° to 120° . (Figure 2-5), (Karlsruhe Institute of Technology (KIT), Germany).



Figure (2-5): Pananalytical Philips diffractometer (Karlsruhe Institute of Technology, Germany).

2.3.11 Scanning Electron Microscopy (SEM) coupled with Energy dispersive X-ray spectroscopy (EDXS) .

The LEO 982 SEM coupled with EDX was used to characterize the morphological and structural properties of the samples. Nearly 1 mg of a sample was mounted on a SEM sample holder and was sputtered with gold prior to analysis for better conductivity and resolution of the sample. This SEM permits ultra high resolution imaging of semiconductor materials, (Figure 2-6).

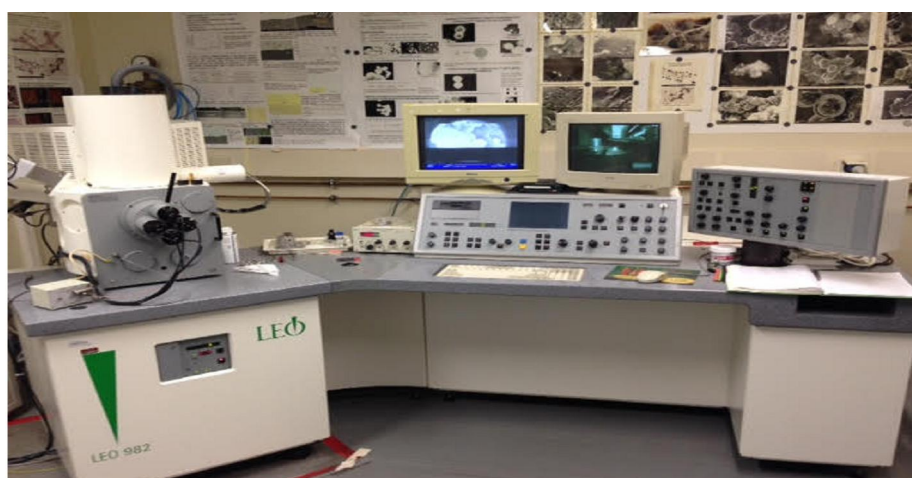


Figure (2-6): LEO 982 SEM coupled with EDX (Karlsruhe Institute of Technology, Germany).

2.3.12 Chemisorption Analyzer Brunauer, Emmett and Teller (BET).

Surface area and pore distribution of the samples were determined using nitrogen adsorption/desorption isotherm by means of micromeritics Autochem Chemisorption analyzer, (Figure 2-7).



Figure (2-7): Micromeritics AutoChem HP Chemisorption Analyzer (BET) (Karlsruhe Institute of Technology, Germany).

2.3.13 Transmission Electron Microscopy (TEM)

High resolution TEM for nanoscale analysis was used for the image observation for specimen and particle size analysis well. Images are supported by means of DF-STEM where Z-contrast imaging facilitates further structural analysis, (Figure 2-8).

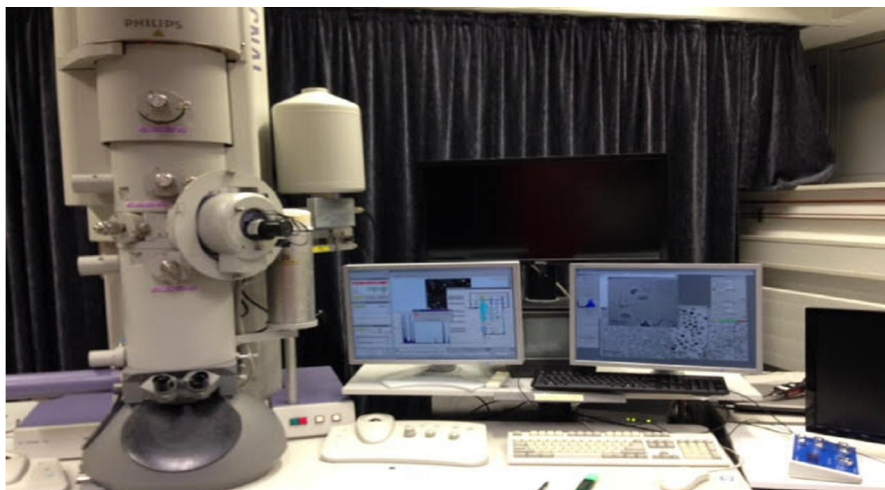


Figure (2-8): Philips Technai TEM (Karlsruhe Institute of Technology, Germany).

2.2.14 Inductively Coupled Plasma - Atomic Emission Spectrometry (ICP- AES).

Agilent Technologies 700 series ICP-AES was used for the determination of metal ions concentration. Also referred to as inductively coupled plasma optical emission spectrometry, ICP-OES, which is an analytical technique used for the detection of trace metals. It is a type of emission spectroscopy that uses the inductively coupled plasma to produce excited atoms and ions that emit electromagnetic radiation at wavelengths characteristic of a particular element, (Figure 2-9).



Figure (2-9): Inductively Coupled Plasma - Atomic Emission Spectrometry (Karlsruhe Institute of Technology, Germany).

2.3.15 Photoreactor system.

The Photoreactor configuration shown in Figure (2-10), is local market made and consists of 500W halogen lamp (Philips) which is vertically fixed into stainless steel hollow cylinder of ten centimeter in diameter and twenty seven centimeter in height.

The heating effect stemmed from the lamp was minimized by circulating the water in the hollow cylinder through outlet and inlet slots in cylinder using circulating thermostate chilled water bath. The internal walls of the cylinder were covered with aluminum foil to avoid radiation losses and temperature rising. Convex Lens is used for light collection and focusing. The solutions/suspensions of dye and photocatalyst were magnetically stirred. The flow rate of O₂ was kept at 50-55 mL /min with continuous stirring using a hot plate-stirrer. The concentration of dye was determined from its visible absorbance characteristic and calibration

curve method at the wavelength of maximum absorption (478nm) for OG.

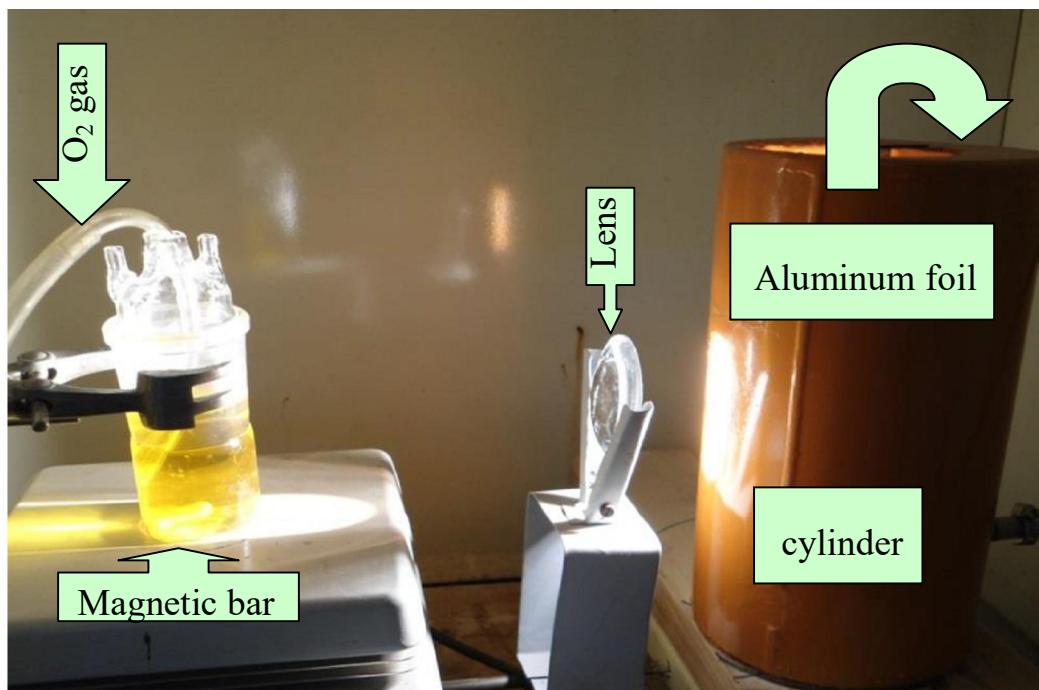
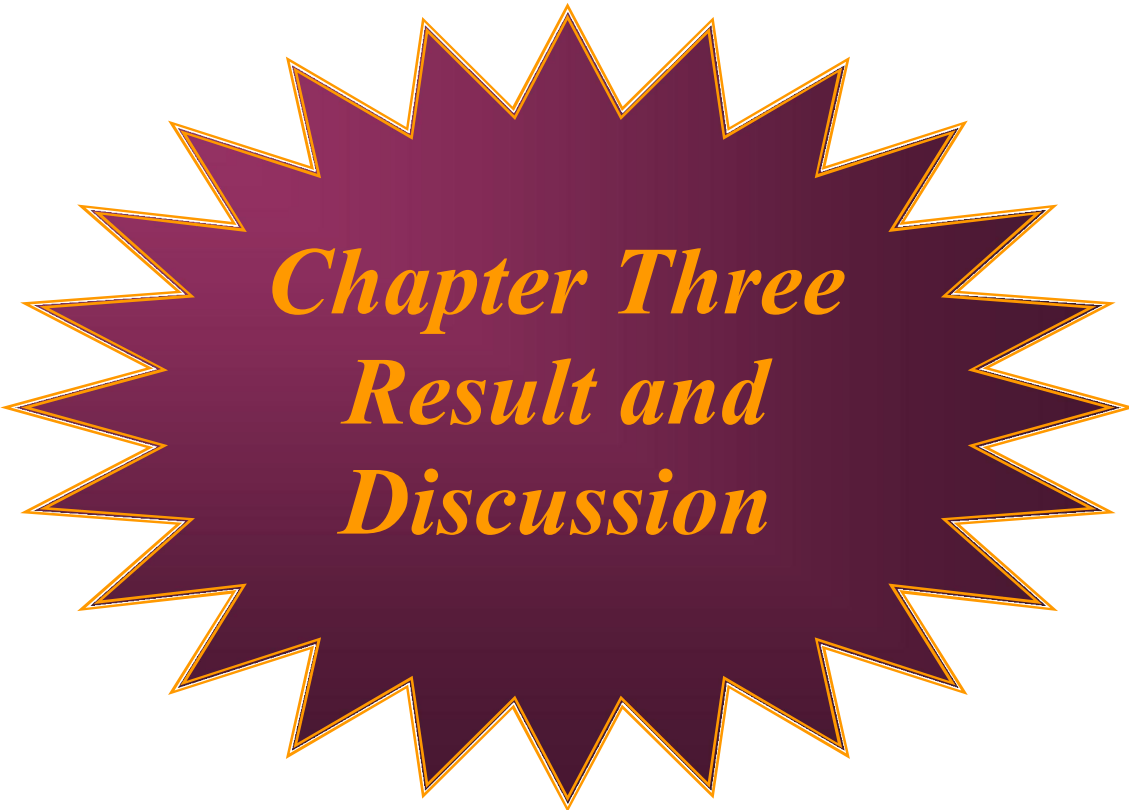


Figure (2-10): Photolysis unit of visible light source.



Chapter Three
Result and
Discussion

3.1 UV-Visible spectroscopic aspects of Orange G dye

Orange G (OG), is a mono water-soluble anionic azo dye which was selected as target compound for this photocatalytic decolorization study, whose molecular formula is ($C_{16}H_{10}N_2Na_2O_7S_2$). The molecular structure of OG is shown in Figure (3-1).

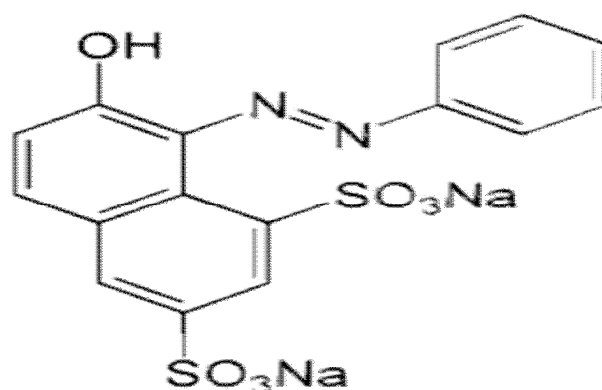


Figure (3-1): Molecular structure of Orange G dye.

OG azo dye solution at various concentrations was prepared with NFDW water. The UV-Vis spectrum of OG consists of two absorption bands at 478 and 332 nm as it is illustrated in Figure (3-2). The weak band at 332 nm arises from the $\pi-\pi^*$ transition related to the aromatic ring attached to the N=N group in the dye molecule, whereas the 478 nm band could be assigned to the $n-\pi^*$ transition of the -N=N- group [90].

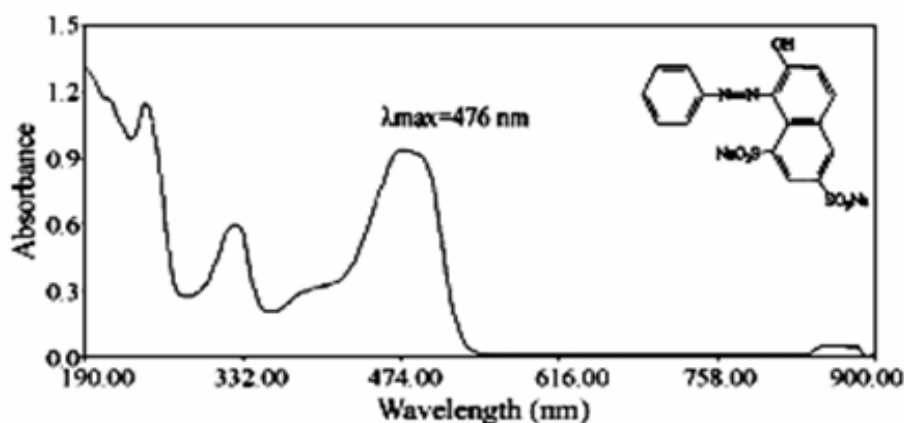


Figure (3-2): UV-VIS absorption spectrum of OG.

Upon variation of solution pH towards lower values (protonation), with increasing the pH of a solution, no tautomeric equilibrium is revealed as it is noticed in Figure (3-3) which reflects the standard UV-VIS scan for Orange G at different initial pH values.

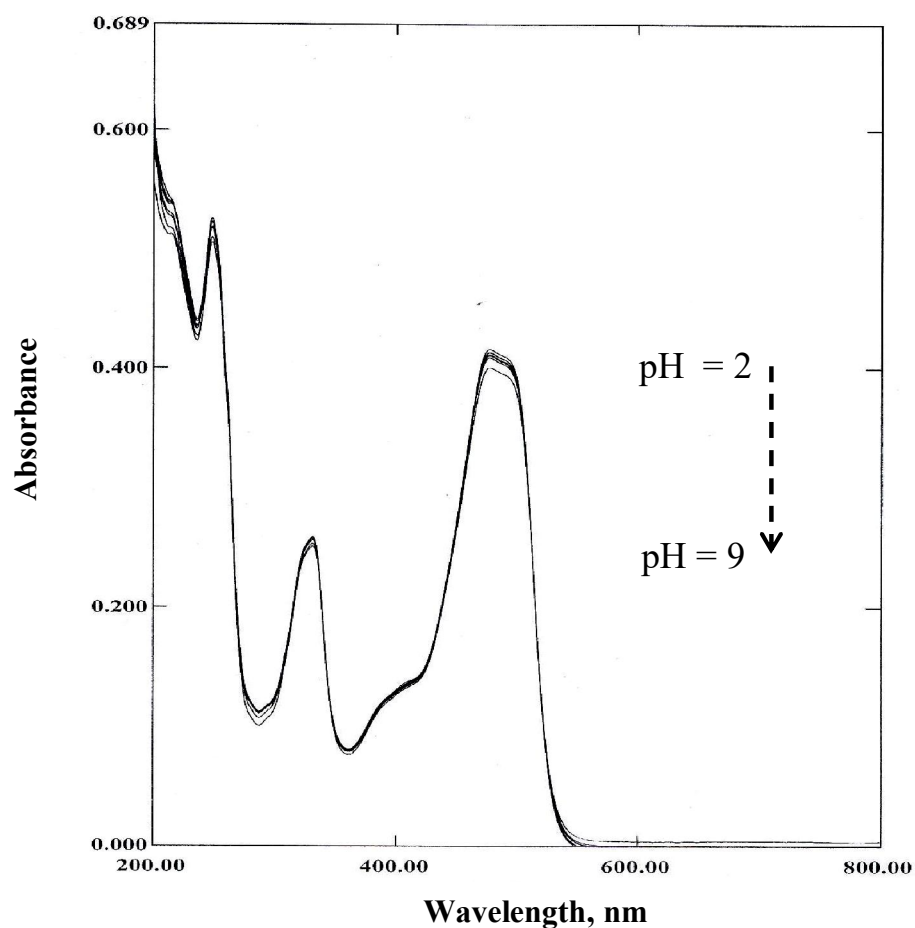


Figure (3-3): Standard scan of Orange G at different pH values.

3.2 Characterization of Au / Pt doped anatase TiO₂ nanoparticles.

3.2.1 Surface morphology and composition aspects.

Scanning Electron Microscope (SEM) was used for the surface morphology study of the mesoporous Au-TiO₂ and Pt-TiO₂ powders. Figures (3-4) and (3-5) exhibit smooth and homogeneous surfaces for gold and platinum doped TiO₂, respectively. The insets show the precious metals distribution onto the photocatalyst surface at two different magnifications.

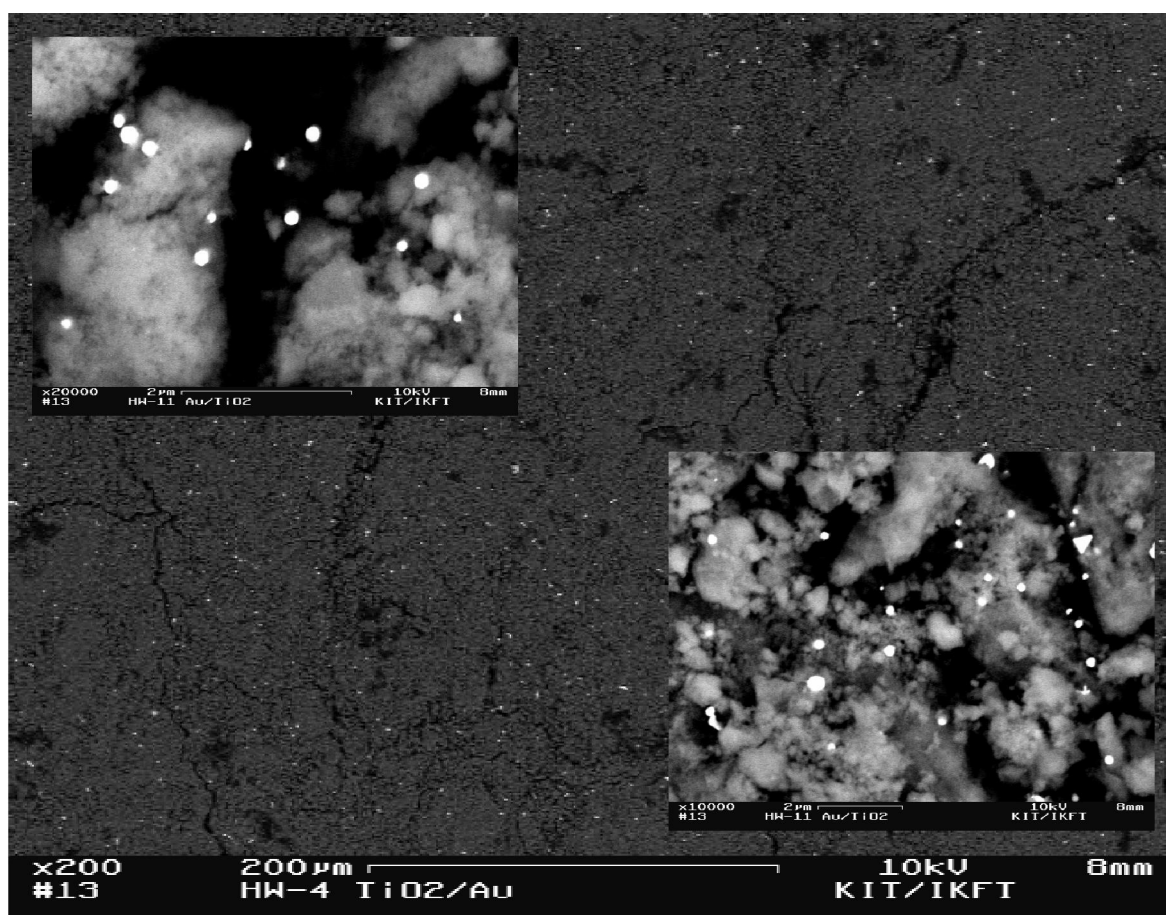


Figure (3-4): Scanning Electron Microscope (SEM) micrographs for Au-doped anatase TiO₂ with different magnifications.

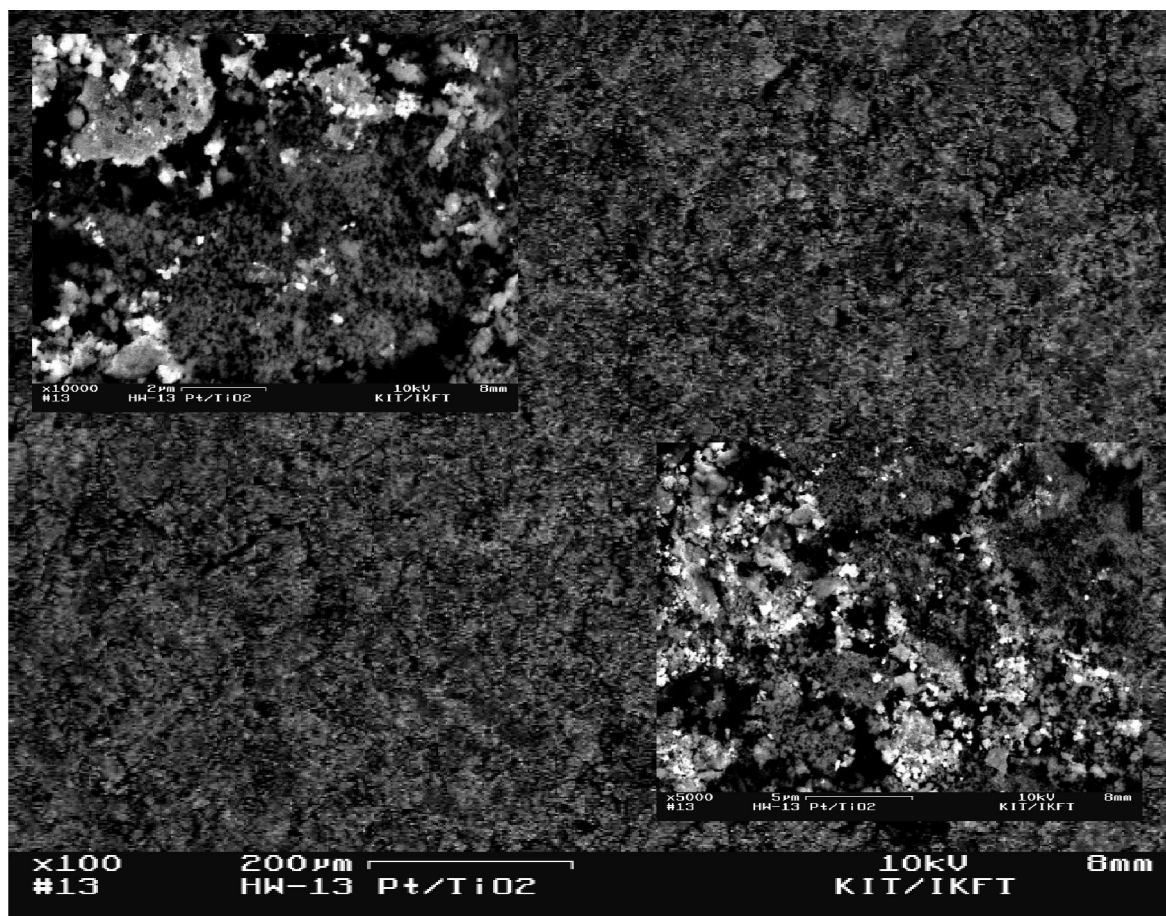


Figure (3-5): Scanning Electron Microscope (SEM) micrographs for Pt-doped anatase TiO₂ with different magnifications.

The surfaces have also been explored by Transmission Electron Microscope (TEM) coupled with TECNAI device for nanoscale analysis. Figures (3-6) and (3-7) reveal the excellent dispersion of irregular spherically shaped Au and Pt metals over TiO₂ particles which are more explicitly presented, in terms of metal atoms content, in the accompanied EDXS templates.

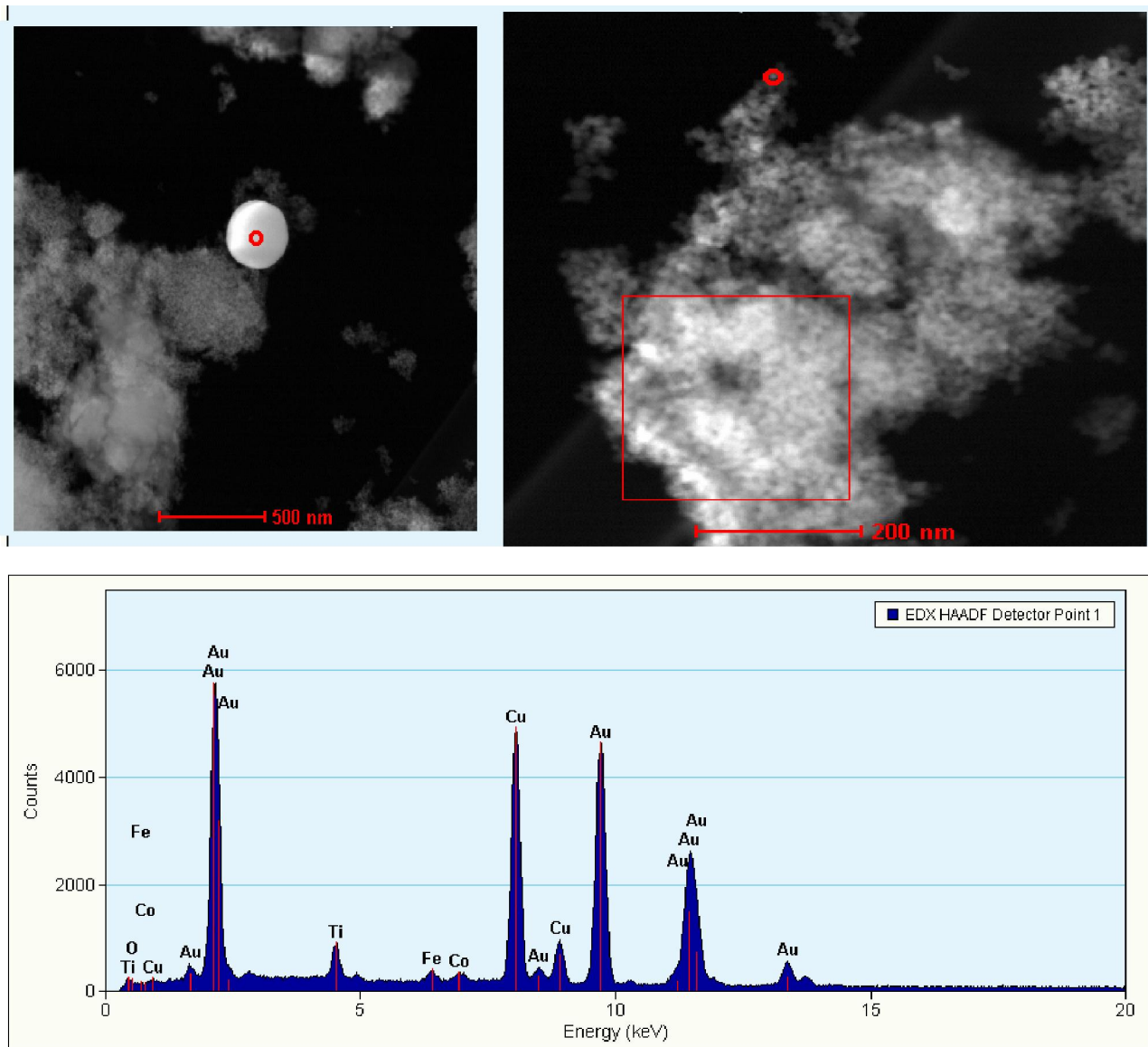


Figure (3-6): Transmission Electron Microscope (TEM) micrograph for Au-doped nano TiO_2 powder and EDXS composition.

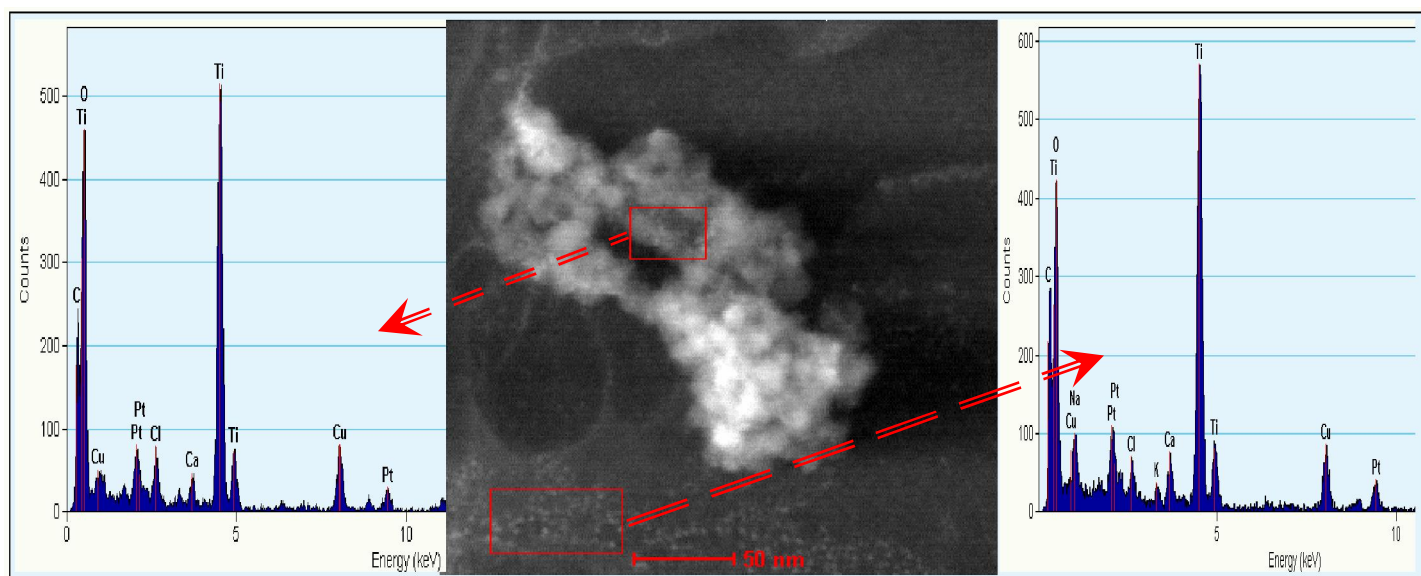


Figure (3-7): Transmission Electron Microscope (TEM) micrograph for Pt-doped nano TiO_2 powder and EDXS composition.

Moreover, the overall surfaces for both Au- TiO_2 Figure (3-8) and Pt- TiO_2 Figure (3-9) have been scanned and explored employing Energy Dispersive X-ray Spectrometer (EDXS). These Figures (3-8) and (3-9) show obviously the abundance of the precious (Au and Pt) metals encompassed into the prepared nano TiO_2 powders.

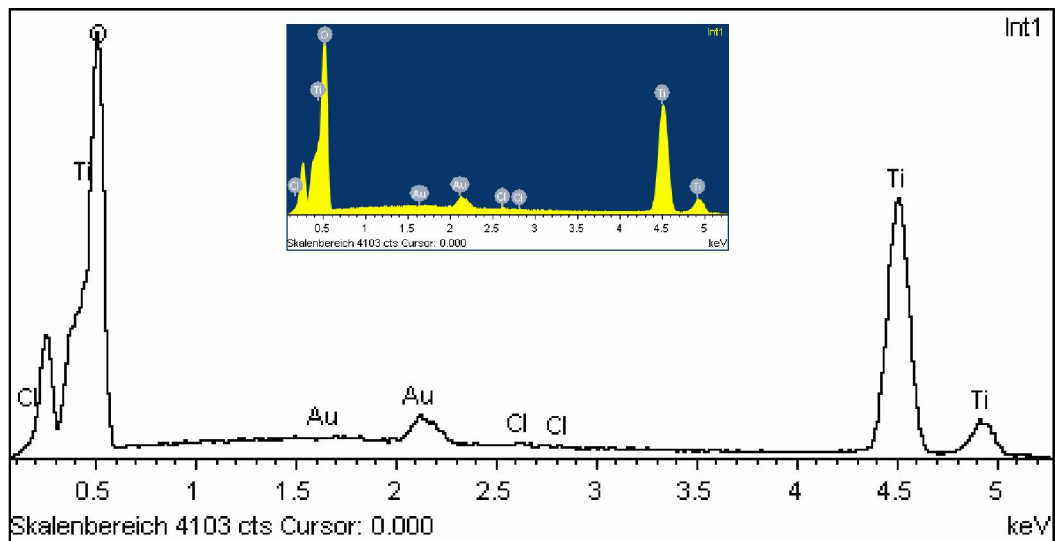


Figure (3-8): Energy Dispersive X-ray spectroscopy (EDXS) image of Au-doped nano TiO₂ powder.

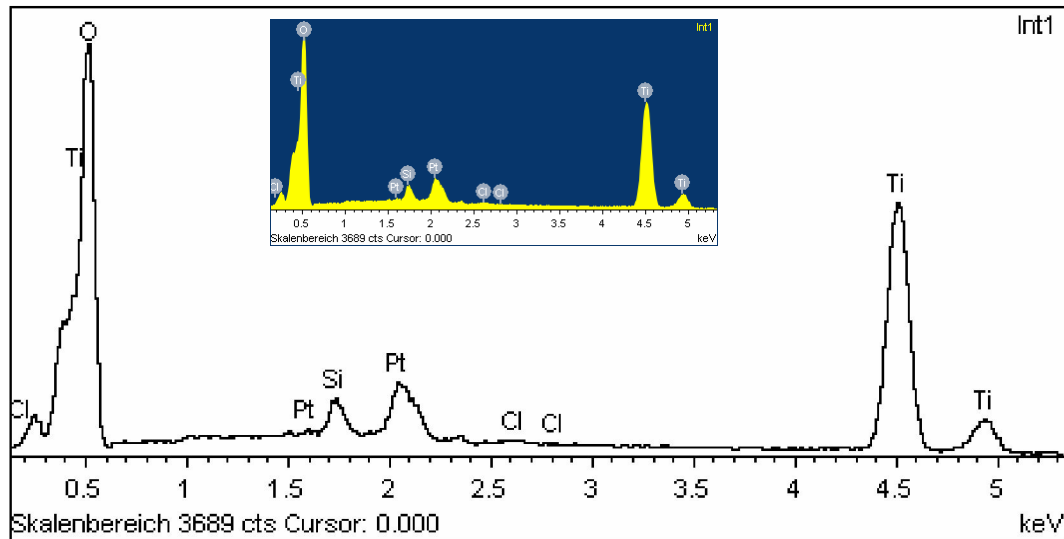


Figure (3-9): Energy Dispersive X-ray spectroscopy (EDXS) image of Pt-doped nano TiO₂ powder.

3.2.2 Porosity and surface area analysis.

Brunauer–Emmett-Teller (BET) theory aims to explain the physical adsorption of gas molecules on a solid surface and serves as the basis for an important analysis technique for the measurement of the specific surface area of materials. Brunauer-Emmett-Teller (BET) nitrogen adsorption methodology was employed for the measurement of both pore size and surface area of the Au and Pt doped anatase TiO₂ nanoparticles after the samples were vacuum degassed at 110 °C (2 °C/min) for 720 min. Figure (3-10) presents the measured pore sizes for the synthesized nano TiO₂ particles, Au-doped and Pt-doped powders. The maxima at pore sizes of 6.8, 7.8 and 7.8 nm are illustrated for TiO₂ nanoparticles, Au-TiO₂ and Pt-TiO₂ composites, respectively. These values of pore size indicate the mesoporosity of the neat and doped powders. Furthermore, the insets in Figure (3-10) show adsorption-desorption isotherm plots which result in surface area of 130, 121 and 109 m²/g for TiO₂, Au-TiO₂ and Pt-TiO₂ specimen, respectively. Also from Figure (3-10), one could observe the impacts of precious metals doping on the pore size and surface area of the prepared nano powder. The pore sizes were increased, whereas surface areas have been decreased, particularly in presence of Pt. The porous structure could provide abundant active sites and suitable mass transfer resistant for the degradation reaction [91].

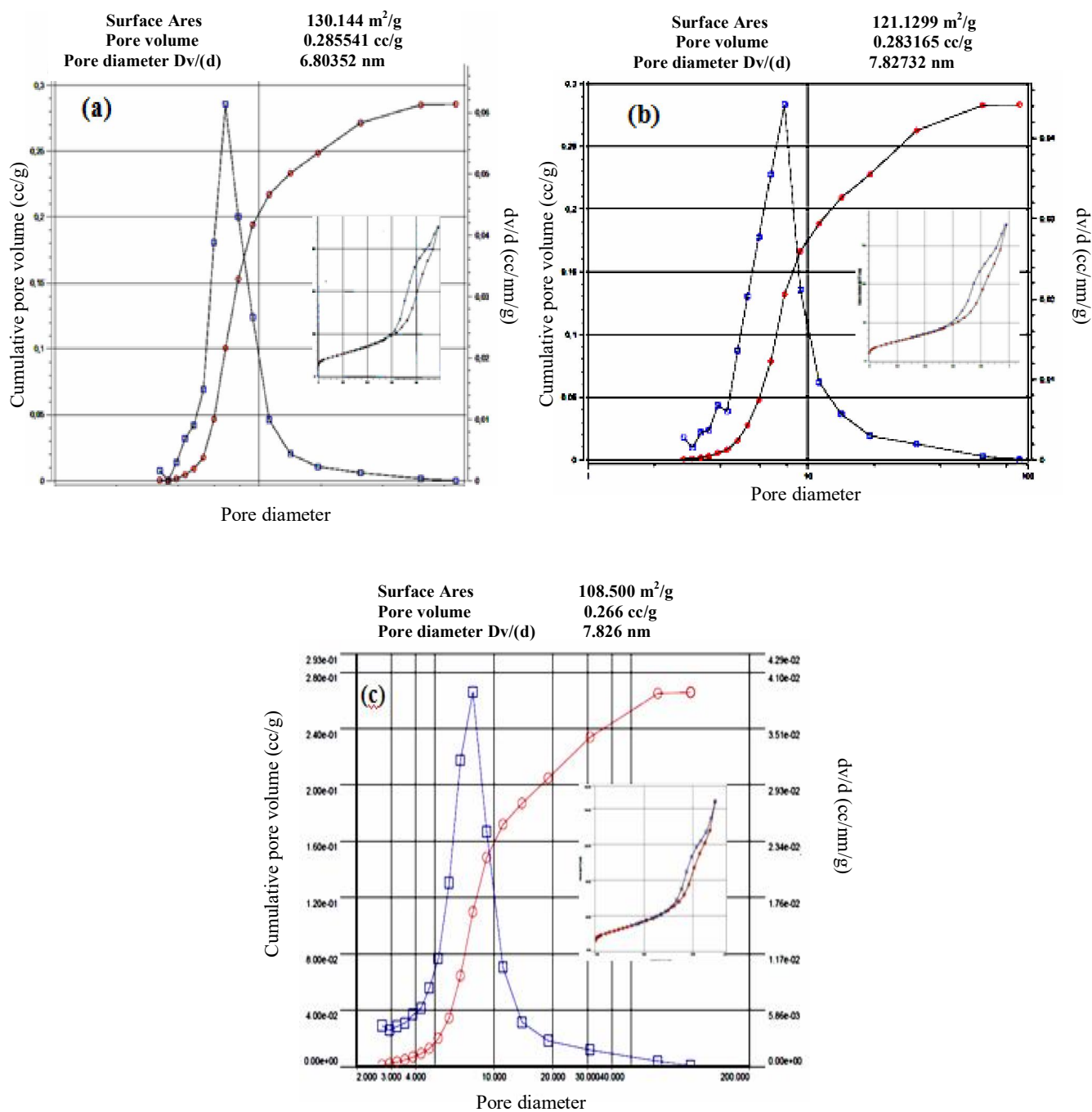


Figure (3-10): Pore size measurements for (a) Synthesized nano anatase TiO_2 ; (b) Au-doped nano anatase TiO_2 ; (c) Pt-doped nano anatase TiO_2 ; insets represent adsorption-desorption isotherms.

3.2.3 Phase and crystalline size features

X-ray diffractometer with Cu K α radiation (0.15425 nm) in the range of 2θ from 0° to 120° was employed for the X-ray Diffraction (XRD) spectroscopy patterns of Au and Pt doped anatase TiO₂ powders. Diffraction signal assigned to the anatase (101) structure at 25.3° (25.4° - 25.6° in this work) is explicitly observed in TiO₂ [92]. From Figure (3-11), the diffraction signals which are located at 38.2, 44.4, 64.6, 77.5, 81.7, 110.8 and 115.3 degrees are assigned for Au (111), Au (200), Au (220), Au (311), Au (222), Au (331) and Au (420) allotropes, respectively. Whereas, Figure (3-12) presents diffraction signals located at 39.8, 46.3, 82.3 and 117.7 degrees which belong to Pt (111), Pt (200), Pt (311) and Pt (331) allotropes, respectively. Both Figures (3-11) and (3-12) don't show any rutile phase (110) diffraction signals, which consequently concludes that appropriate conditions were employed for the sol gel impregnation methodology.

The average crystalline sizes for Au-TiO₂ and Pt-TiO₂ powders were computed by Sherrer's equation using the XRD line broadening method [93]. The crystal size C.S. = $0.9 \lambda / (B \cos \theta)$ where λ represents the wavelength of X-ray, B the FWHM and the θ diffraction angle. By using the experimental data, an average crystalline size of 15.3, 14.2 and 12.4 nm were derived for TiO₂, Au-TiO₂ and Pt-TiO₂.

The crystalline size relates reciprocally with the peak width in which by increasing the peak width the size of nano TiO₂ decreases [94]. Consequently, Figures (3-11) and (3-12) confirm this phenomenon in which the synthesized nano TiO₂ band shows less broadening than that of the doped TiO₂ bands.

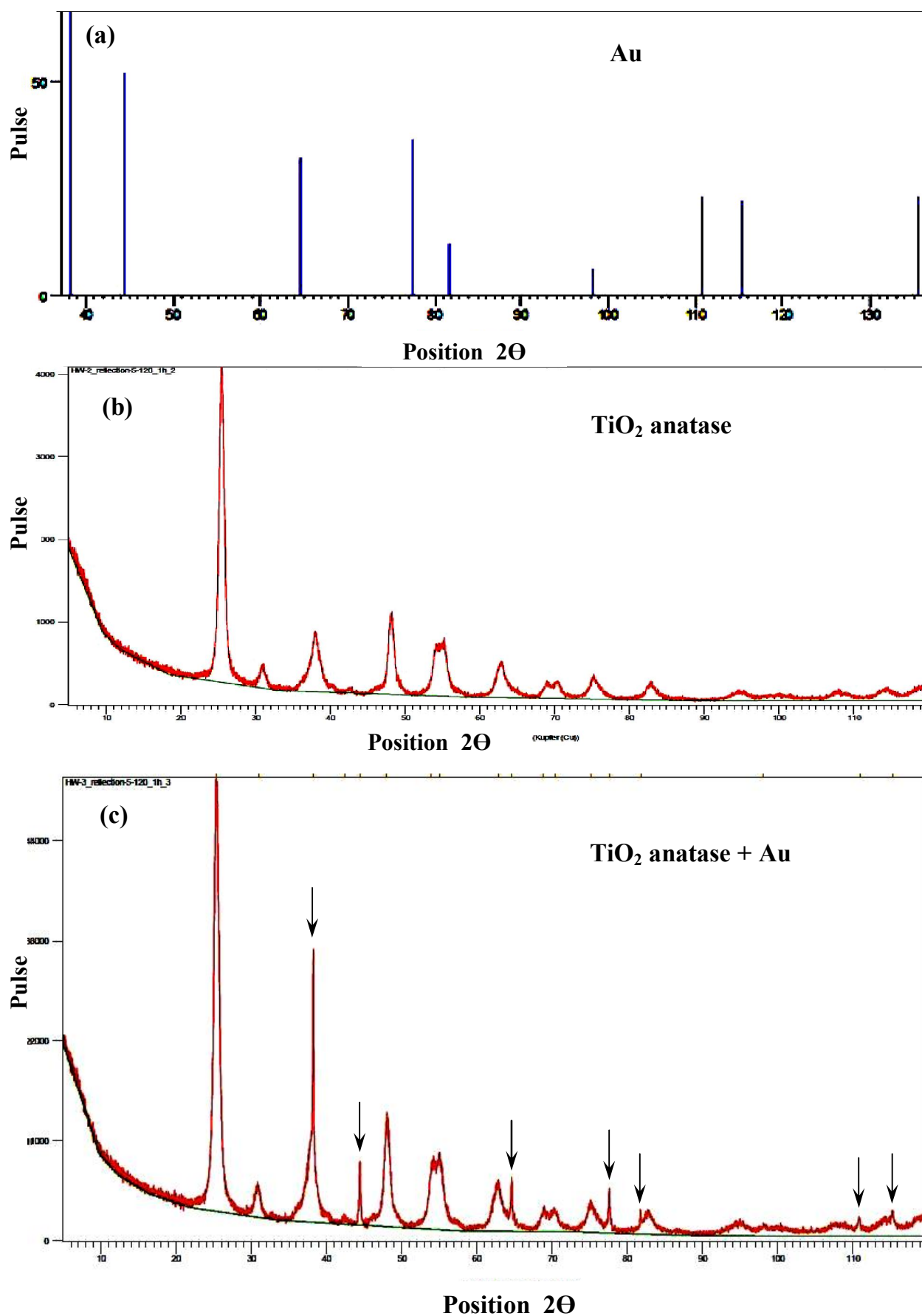


Figure (3-11): X-ray Diffraction Spectroscopy (XRD) patterns of (a) Au; (b) anatase TiO₂; (c) Au-doped anatase TiO₂; arrows present gold positions

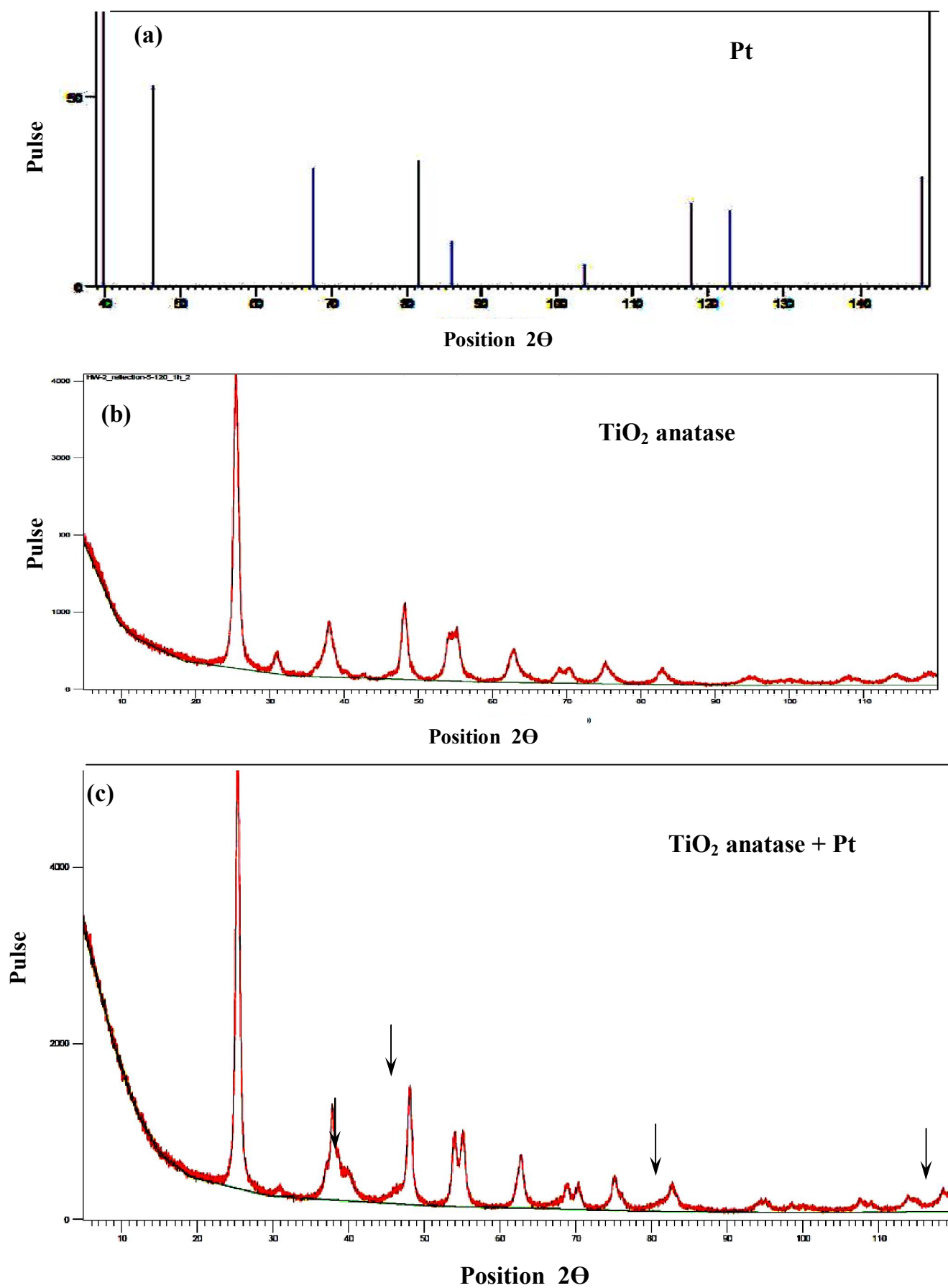


Figure (3-12): X-ray Diffraction Spectroscopy (XRD) patterns of (a) Pt; (b) anatase TiO_2 ; (c) doped anatase TiO_2 ; arrows present platinum positions

3.2.4 Quantification of doped precious metals

Inductively Coupled Plasma Atomic Emission Spectrometry (ICP-AES) was used for the quantification of the precious metals (Au and Pt) contained into the doped TiO₂ powders. UV irradiation (15 W) and chemical (sodium citrate, sodium tetrahydroborate and α -ketoglutaric acid) reduction techniques have been used for the reduction of Au from H₂AuCl₄.3H₂O solution and Pt from H₂PtCl₆ solution.

Table (3-1) illustrates the results of TiO₂ doping by means of Au and Pt exploiting the UV illumination at a power of 15 watts and for 24 hours irradiation. We observe from Table (3-1) that the accuracy of Pt ion reduction for doping of the photocatalyst with UV irradiation has been much better than that of Au ion reduction, and further, for all the levels of abundance. Interestingly, the 2% abundance of both dopants has reflected better doping than the other investigated abundances for Au and Pt.

Table (3-1): UV- reduction of Au and Pt ion onto TiO₂ surface analyzed by means of ICP-AES.

Prepared, wt%	Analyzed, wt%	Accuracy%*
Au 1%	0.86%	86
Au 2%	1.92%	96
Au 4%	3.23%	81
Pt 1%	0.95%	95
Pt 2%	1.96%	98
Pt 4%	3.89%	97

* Accuracy% = (Analyzed / Prepared) x 100

Accordingly, the 2% Au or Pt abundance doping has been selected for the chemical reduction route. Figure (3-13) depicts excellent dispersion of irregular reduced Au over TiO_2 particles using 2-Oxoglutaric acid as reducing agent, and further, the composition was quantified by the accompanied EDXS spectrum. In comparison of Figure (3-13) with Figure (3-14 a and b) we may conclude that 2-Oxoglutaric acid exhibits better reduction for Au ions onto TiO_2 than sodium tetrahydroborate (Figure 3-14 a) and sodium citrate (Figure 3-14 b). Whereas, sodium tetrahydroborate shows better reducing capability for platinum doping (Figure 3-15) than the other two reductants, 2-Oxoglutaric acid and sodium citrate. These two reducing agents have presented approximately similar distribution of Pt onto TiO_2 (SEM) and further, resemble quantification (EDXS) as obviously illustrated in Figure (3-16 a and b).

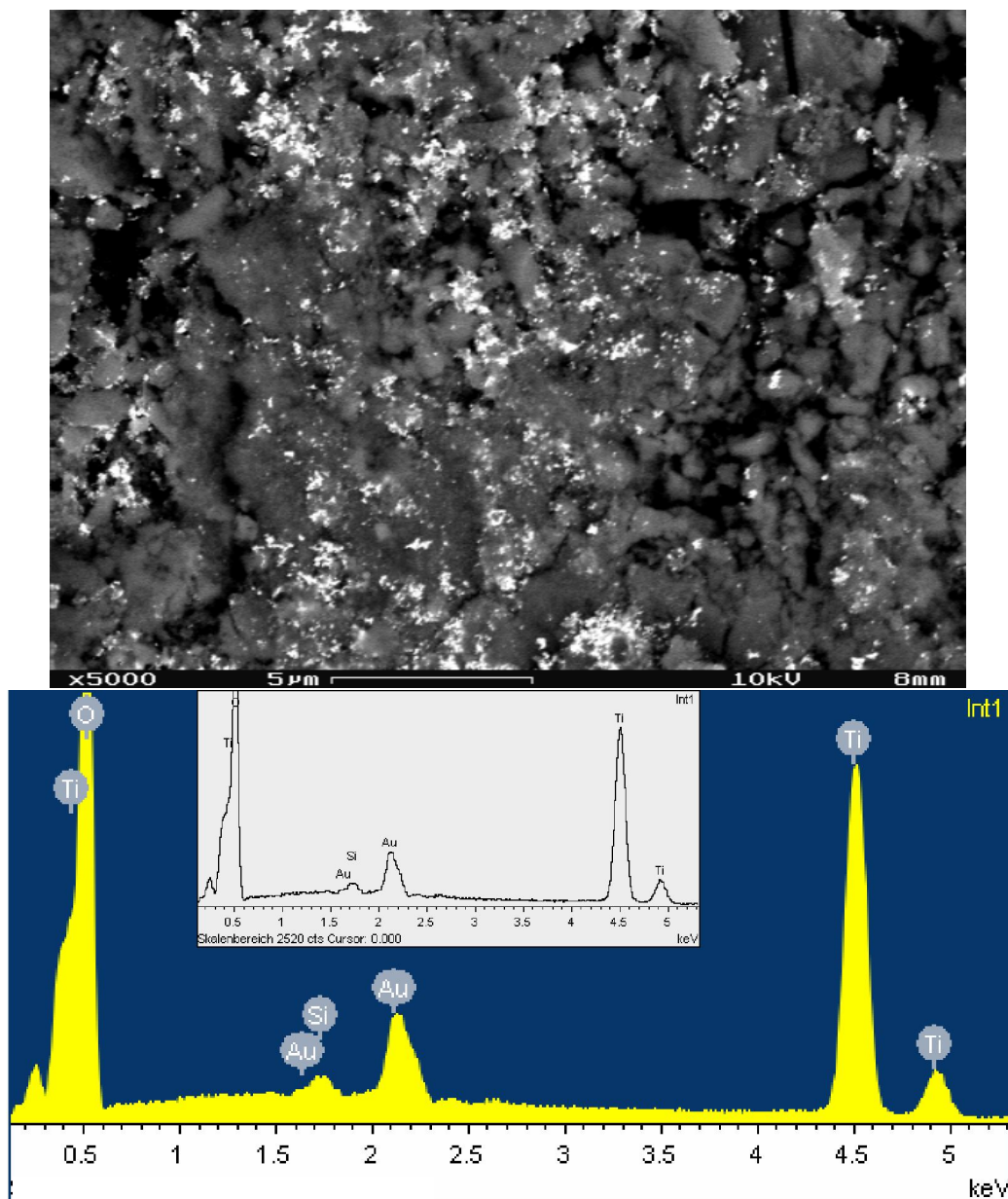


Figure (3-13): SEM micrograph and EDXS composition for Au-doped anatase TiO₂ using 2-Oxoglutaric acid as a reductant.

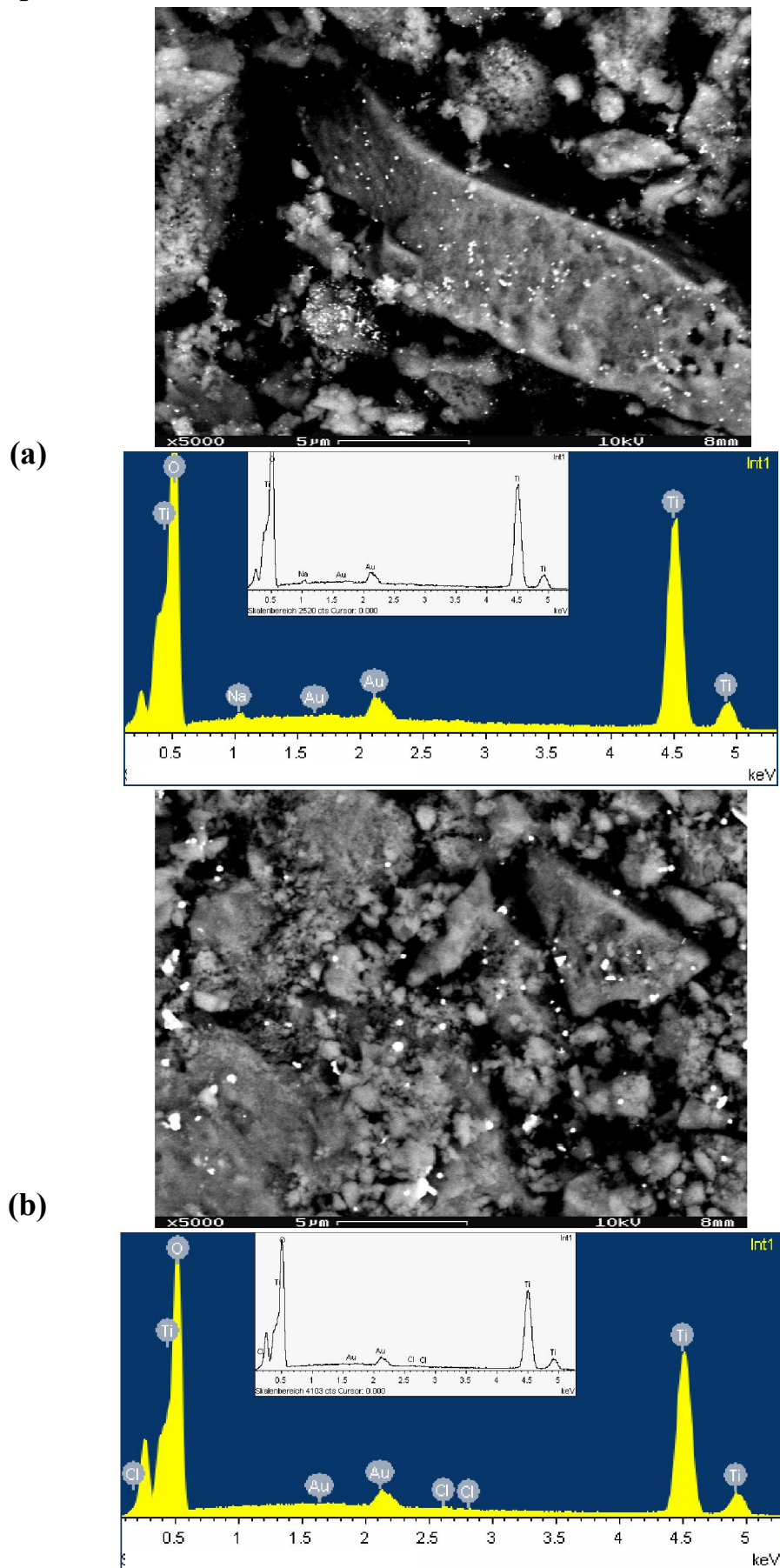


Figure (3-14): SEM micrograph and EDXS composition for Au-doped anatase TiO₂ using; (a) NaBH₄ as a reductant and (b) sodium citrate as a reductant .

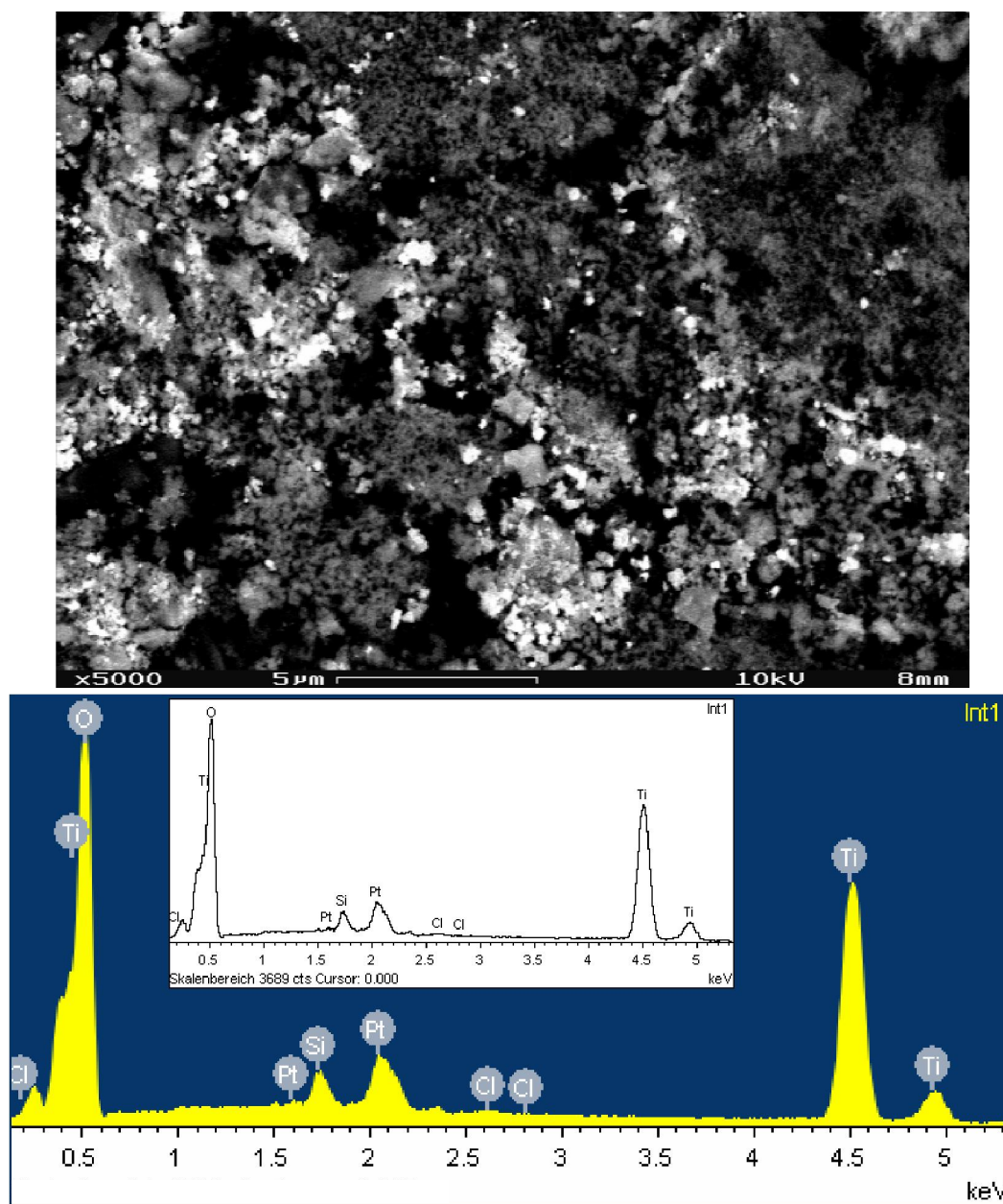


Figure (3-15): SEM micrograph and EDXS composition for Pt-doped anatase TiO_2 using sodium tetrahydroborate as a reductant .

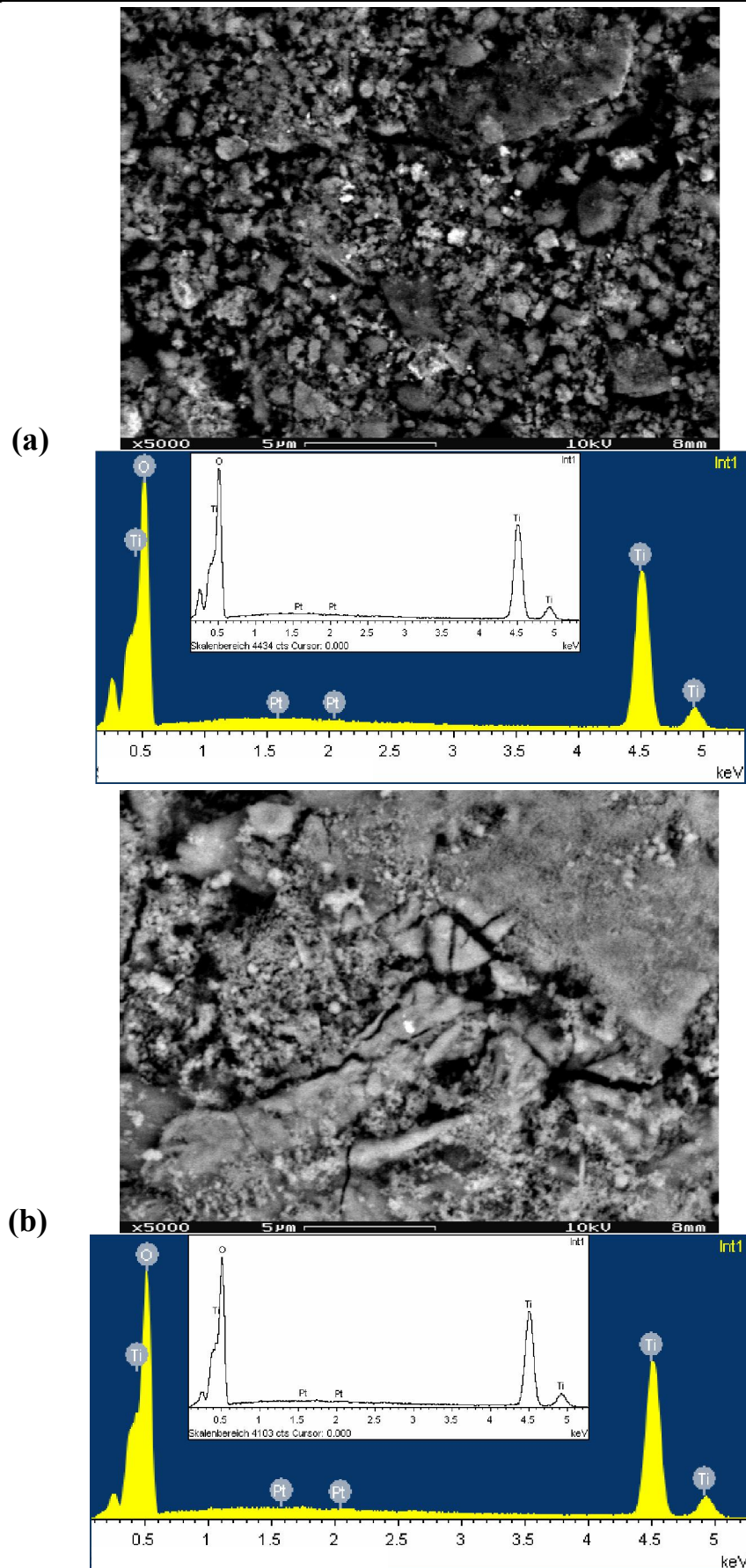


Figure (3-16): SEM micrograph and EDXS composition for Pt-doped anatase TiO_2 using; (a) 2-Oxoglutaric acid as a reductant and (b) sodium citrate as a reductant.

3.3 Control experiments

Several control experiments were carried out to explore the optimum conditions that essentially impact the efficient bleaching and degradation of OG. One set that was performed with OG solution exposed to visible light irradiation with an absence of catalysts (TiO_2 , Au-TiO_2 , Pt-TiO_2), for a duration of 180 min and at pH of Orange G solution about 5, showed that the degradation of OG was almost negligible under visible illumination. The second set was implemented by exposing OG solution with catalysts but without visible light irradiation (in dark). Under the dark conditions, similar experiments were also conducted in the presence of catalysts for comparison purpose. Minimal dye degradation was observed under the dark conditions or in other words the obtained degradation results may probably be due to adsorption of dye molecules onto the surface of the semiconductor photocatalyst [85]. The third set was accomplished in the presence of visible light and TiO_2 semiconductor but in the absence of O_2 gas. While, the fourth set was conducted in the presence of visible light, TiO_2 semiconductor and O_2 gas. The fifth set was carried out by exposing OG to visible light in the presence of doped catalysts (Pt-TiO_2 , Au-TiO_2) and without O_2 gas. The last set was implemented under visible light illumination with the doped catalysts (Pt-TiO_2 , Au-TiO_2) and in the presence of O_2 gas. The absorption changed clearly when the dye was mixed with a catalyst under visible illumination, which represents the photocatalysis circumstances, as obviously shown in Figures (3-17) and (3-18) and relevant tables for Au-TiO_2 and Pt-TiO_2 , respectively.

The color removal of OG pollutant is almost complete in 180 min using Au-TiO_2 while with Pt-TiO_2 , the quantitative degradation takes about 210 min.

Under similar conditions of halogen lamp illumination, initial pH = 5 and 40 mg photocatalyst loading. The examination of the outcomes of these sets of experiments may conclude that the employment of doped photocatalyst (Pt-TiO₂ or Au-TiO₂) presents better photodegradation of OG in comparison to those without a doped semiconductor. This phenomenon is ascribed to the plasmonic behavior in case of Au under visible illumination and the propensity of Pt for containment of electrons which subsequently are transferred to the adsorbed O₂ onto Au-TiO₂ or Pt-TiO₂ slurries yielding O₂⁻, OH and HO₂ radicals. Finally, these radicals enhance the mineralization of intermediates formed during catalytic degradation into the final mineralized end-products [95].

Time	(a)	(b)	(c)	(d)	(e)	(f)
0	0.400	0.400	0.400	0.400	0.400	0.400
60	0.400	0.386	0.383	0.341	0.342	0.313
120	0.400	0.387	0.334	0.271	0.235	0.187
180	0.400	0.388	0.220	0.191	0.127	0.069

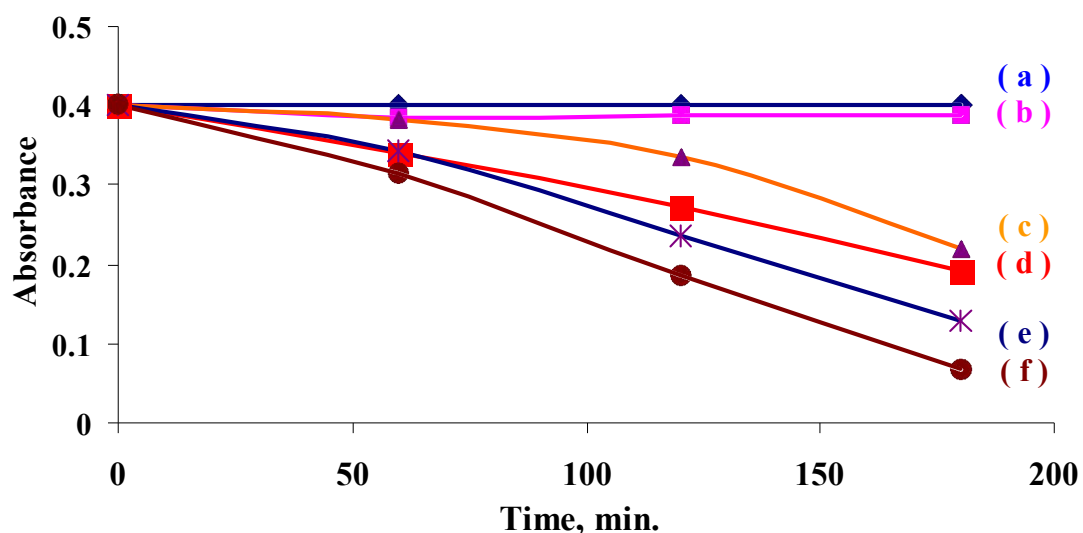


Figure (3-17): The relative decrease in absorption intensity of Orange G as a function of irradiation time (a) VIS+OG; (b) Au-TiO₂ + OG in dark; (c) VIS+TiO₂+OG in absence of O₂ gas;(d) VIS+TiO₂+OG+ O₂; (e) VIS+Au-TiO₂+OG in absence of O₂ gas;(f)) VIS+Au-TiO₂+OG+ O₂ .

Time	(a)	(b)	(c)	(d)	(e)	(f)
0	0.413	0.413	0.400	0.400	0.412	0.413
30	0.413	0.411	0.370	0.390	0.324	0.171
60	0.413	0.408	0.341	0.383	0.279	0.070
90	0.413	0.406	0.31	0.36	0.233	0.034
120	0.413	0.404	0.271	0.334	0.185	0.018
150	0.413	0.402	0.230	0.280	0.145	0.013
180	0.413	0.399	0.191	0.220	0.115	0.007

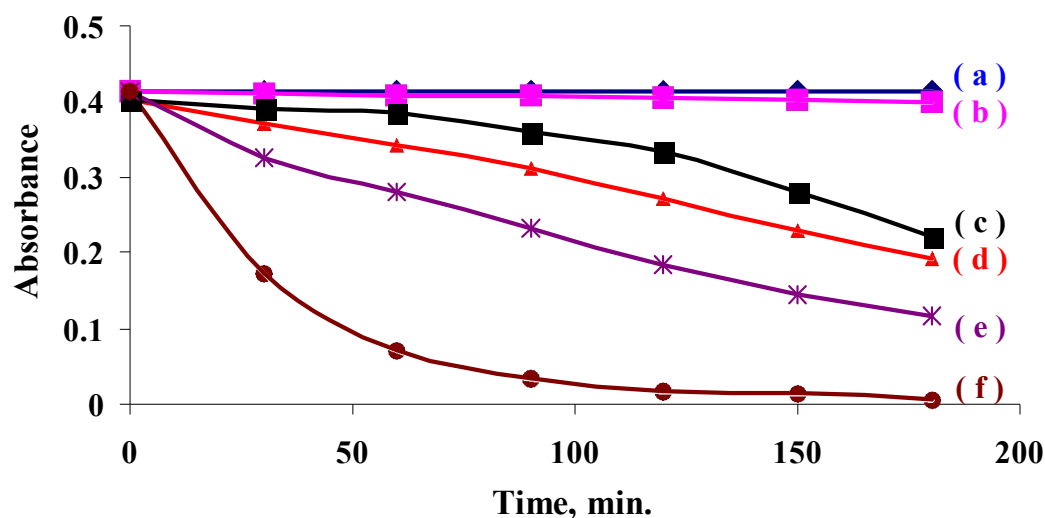


Figure (3- 18): The relative decrease in absorption intensity of Orange G as a function of irradiation time: (a) VIS +OG; (b) Pt-TiO₂ + OG in dark; (c)VIS+TiO₂+OG in absence of O₂ gas; (d) VIS+TiO₂+OG+ O₂; (e) VIS+Pt-TiO₂+OG in absence of O₂ gas; (f)) VIS+Pt-TiO₂+OG+ O₂ .

3.4 Experimental optimization of photocatalysis parameters.

In photocatalytic degradation of dye, the following operating parameters affect the process: initial pH of the OG solution to be degraded, dopants type and content, catalysts loading and temperature. These parameters will be considered one after the other as they influenced the photocatalytic degradation of OG dye which is considered in this study.

3.4.1 Effect of initial pH.

The impact of pH on the photocatalytic reaction is generally attributed to the surface charge of the photocatalyst and its relation to the ionic form of the organic compound (cationic or anionic) [16].

The pH of a solution is the key factor in photocatalysis. This parameter affects the surface charge of the catalysts (Au-TiO₂, Pt-TiO₂) and the ionization state of the compound. Points of zero charges is a concept relating to the phenomenon of adsorption, and it describes the condition when the electrical charge density on a surface is zero. The ionization state of the photocatalyst surface can be protonated and deprotonated under acidic (pH < pH_{Pzc}) and alkaline (pH > pH_{Pzc}) conditions, respectively [96]. The points of zero charges of Au-doped TiO₂ particle and Pt-doped TiO₂ particle are 6.0 and 6.2, respectively.

Thus, the following equations, 3.1 and 3.2, may apply on the surfaces of Au-doped TiO₂ and Pt-doped TiO₂ at different pH values:



Figures (3-19) and (3-20) present point of zero charges for Au-doped TiO₂ and Pt-doped TiO₂ surfaces.

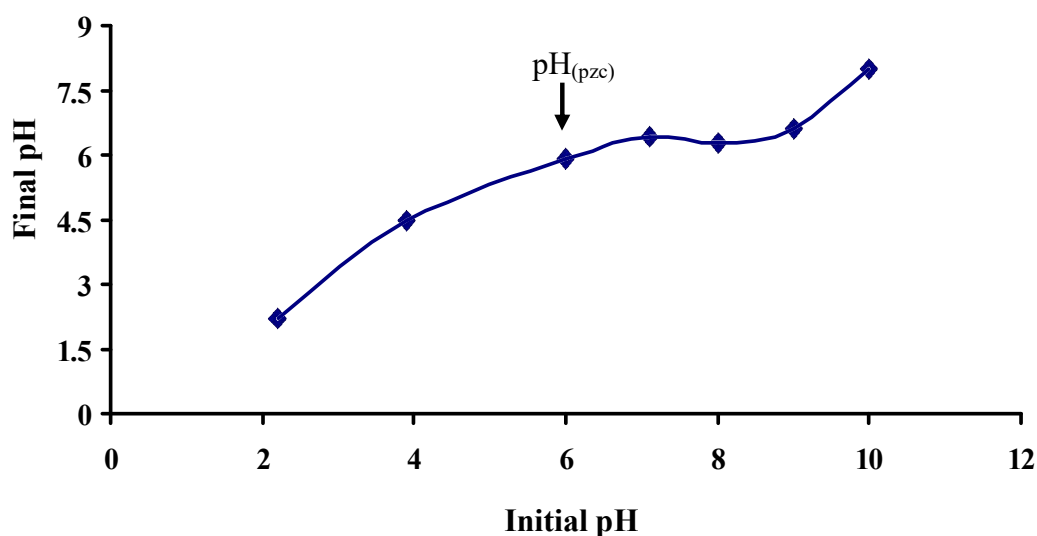


Figure (3-19): Zero point charge pH of 2% Au-TiO₂.

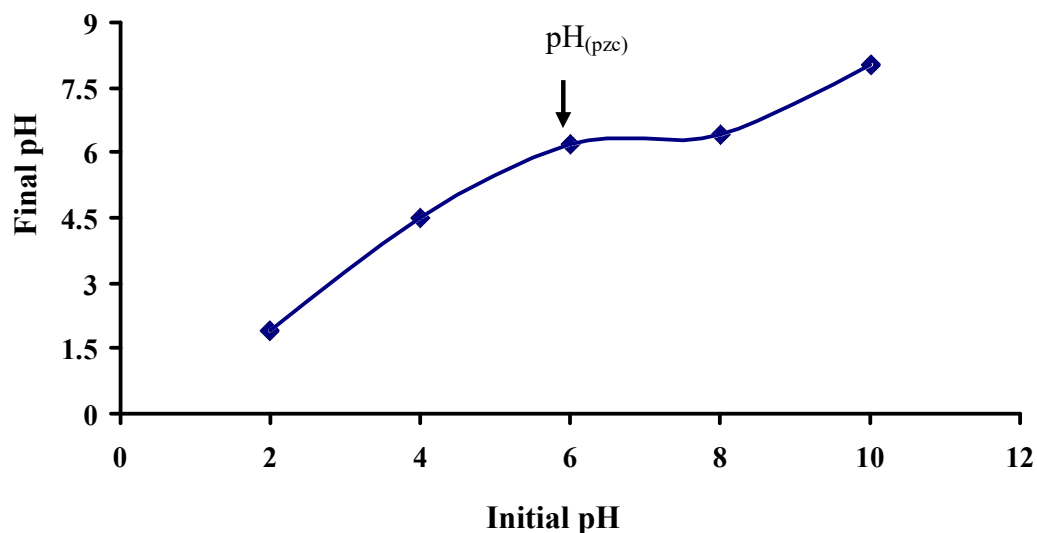


Figure (3-20): Zero point charge pH of 4% Pt-TiO₂.

The degradation of OG onto the catalyst was investigated at different pH values. For altering pH in the acidic and in alkaline regions, H₂SO₄ and NaOH solutions were used, with initial OG dye concentration of 10 mg L⁻¹ and catalyst dosages of 40 mg for Au-TiO₂ and Pt-TiO₂, respectively. The results are presented in Figures (3-21) and (3-22) with accompanied tables (3-2) and (3-3). It can be seen that the degradation efficiency percents increase with decreasing pH value, and a maximum efficiency was observed at pH = 3 (99% degradation in 80 min. for Pt-TiO₂, and 89% degradation in 240 min. for Au-TiO₂).

Table (3-2): Impact of initial pH on the percent of OG photodegradation using 2% Au-TiO₂.

Time, min.	% Deg. pH=2	% Deg. pH=3	% Deg. pH=4	% Deg. pH=5	% Deg. pH=6	% Deg. pH=8	% Deg. pH=9
0	0	0	0	0	0	0	0
60	21	40	21	13	9	5	3
120	46	61	39	36	16	14	11
180	62	78	62	53	37	20	24
240	75	89	81	72	51	31	35

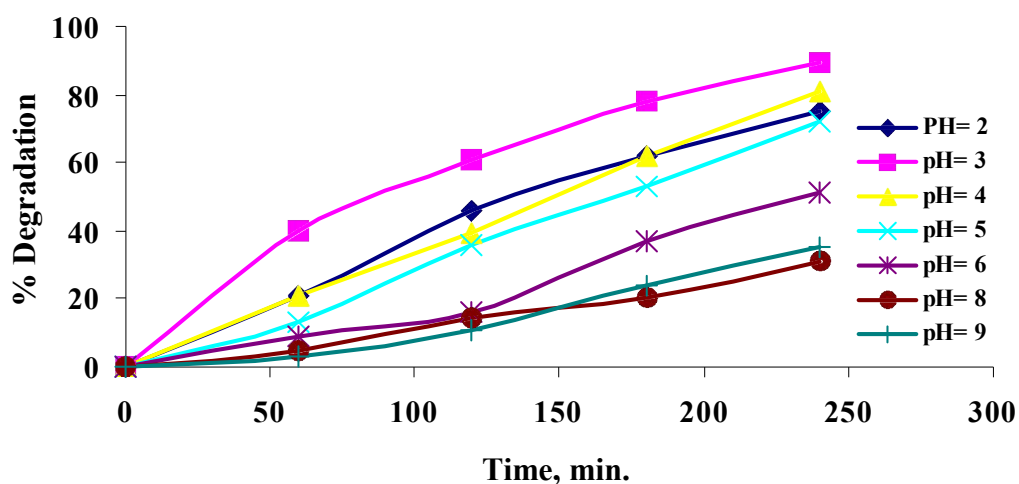


Figure (3-21): Impact of initial pH on the percent of OG photo-degradation using 2% Au-TiO₂.

Table (3-3): Impact of initial pH on the percent of OG photodegradation using 4% Pt-TiO₂.

Time min.	%Deg. pH=1.9	%Deg. pH=3	%Deg. pH=4	%Deg. pH=5	%Deg. pH=6
0	0	0	0	0	0
20	43	68	51	60	47
40	65	85	79	79	67
60	75	94	93	88	78
80	83	99	99	94	87
100	89			97	93
120	92			99	97

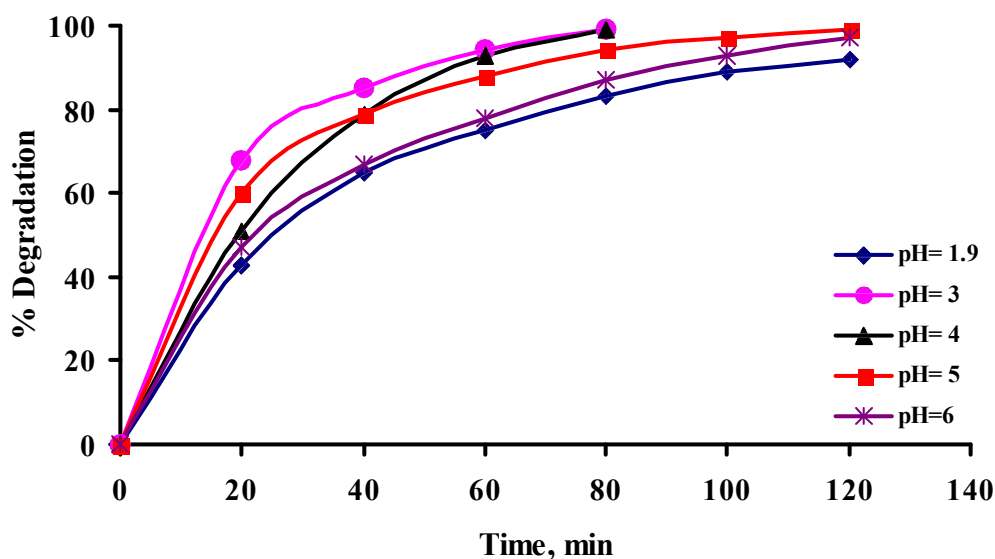


Figure (3-22): Impact of initial pH on the percent of OG photodegradation using 4% Pt-TiO₂

Hence, the effect of pH on the decolorization rate constant (k) of OG on the catalysts (Au-TiO₂ and Pt-TiO₂) are remarkable in our experiments in which (k) increased with decreasing initial pH, exhibiting maximum efficiency ($k = 0.0089 \text{ min}^{-1}$) at pH 3 for OG photodecomposition in case of Au-TiO₂, while it is ($k = 0.0543 \text{ min}^{-1}$) at pH 3 for OG photodecomposition in case of Pt-TiO₂ as shown in Figures (3-23) and (3-24), respectively.

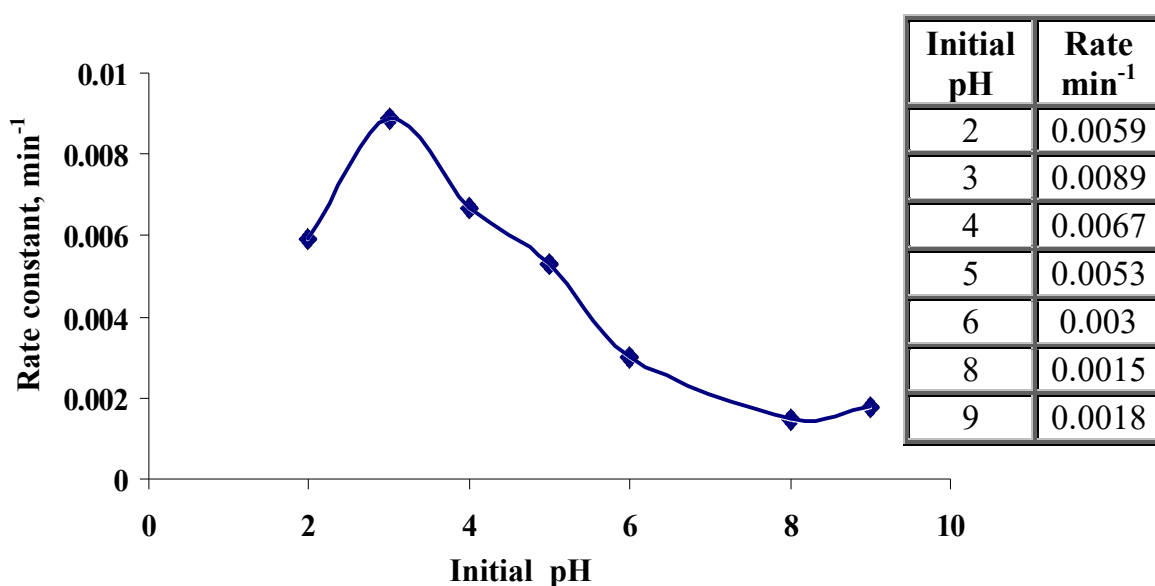


Figure (3-23): Influence of initial pH on photobleaching rate of OG using Au-TiO₂.

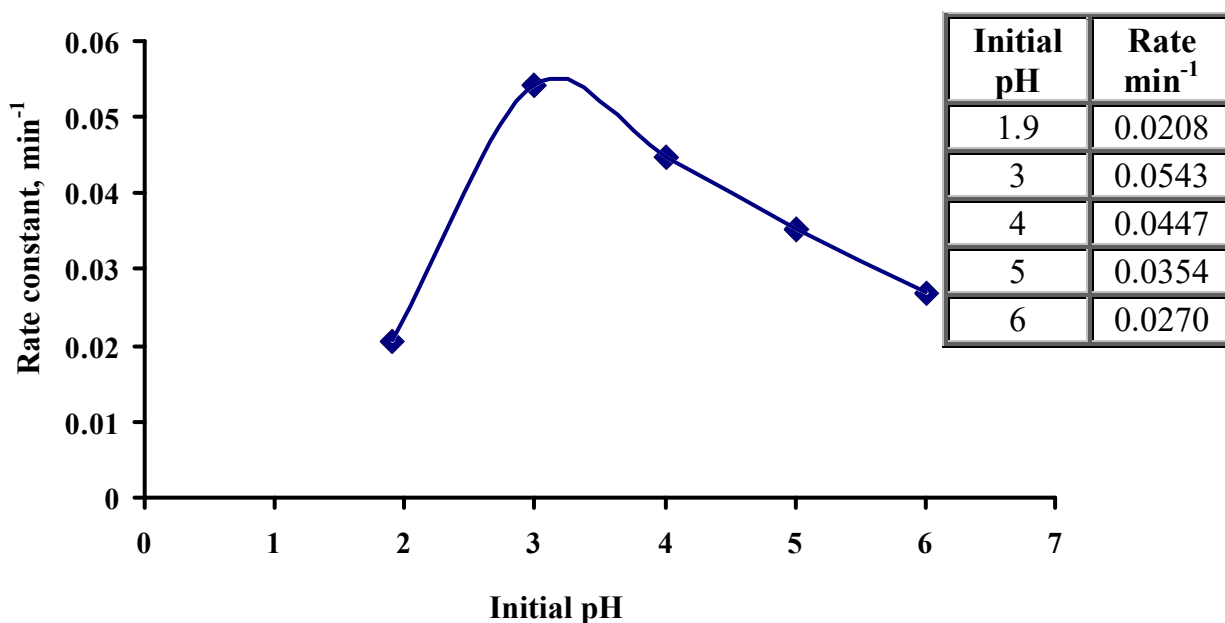


Figure (3-24): Influence of initial pH on photobleaching rate of OG using Pt-TiO₂.

At low pH ($\text{pH} \leq 2$) the concentration of H^+ is in excess, and the H^+ ions interact with the azo group ($\text{N}=\text{N}$), which is particularly susceptible to be electrophilic attacked by hydroxyl radical, decreasing the electron densities at azo group. Consequently, the reactivity of hydroxyl radical by electrophilic mechanism decreases. [97, 83]. Whereas, at high pH value, Sun et al. [98] reported that the OH^- on the surface of catalysts replaced by ONa^- , and the catalytic activity of catalysts decreased accordingly due to some sort of repulsion occurs between the catalyst surface and OG dye. Furthermore, Naik and coworkers [99] stated that the photocatalytic activity of Au/TiO₂ when used to degrade Methyl Orange at $\text{pH} \geq 9$, the catalytic activity became negligible because gold nanoparticles do not show surface plasmon resonance peak at high pH due to the agglomeration of gold nanoparticles.

On the other hand, Dunn et al. [100] reported that Pt/TiO₂ accumulated less negative species on catalyst surfaces, which deteriorates reaction rates, than pure TiO₂ in an acidic condition.

This might be one of the reasons resulting in the better photocatalytic ability of Pt/TiO₂ than pure TiO₂ [101]. This is actually in a good agreement with our findings (Figure (3-18 d and f)).

Generally and for the sake of clarification, the adsorption of OG moiety onto the electrophilic (Ti⁺⁴) sites at the TiO₂ surface is favored in acidic media [83] and hence impacts its photodegradation at different initial pH values. Some authors [83, 87] reported that the adsorption linkages of sulphonated dyes onto TiO₂ surface at low pH values take place through sulphonato anchoring groups as it is virtually depicted in Figure (3-25).

More interestingly, Wang et al. [102] reported that the state of the chemical species which exist in water is not affected only by pH, but also closely related to the dissociation constant (pK_a) of the species. When pH > pK_a the species exists as the ionic state, but when pH < pK_a of the species, it primarily presents in the molecular state. Accordingly, since the pK_a value of OG is 11.5 [103], which is less than the optimum adsorption and further degradation pH, we also expect that the OG exists in a molecular state and adsorbs onto the doped catalyst surfaces via the donation of the azo nitrogen and hydroxyl oxygen lone pairs into the partially empty 3d orbital of titanium [104], which represents the adsorption center, because the Ti lowest unoccupied molecular orbital, LUMO (the empty d orbital), can accept electrons from the ligand [105]. Thus, Figure (3-26) might be suggested as virtual adsorption geometry of OG onto doped TiO₂ particle as well.

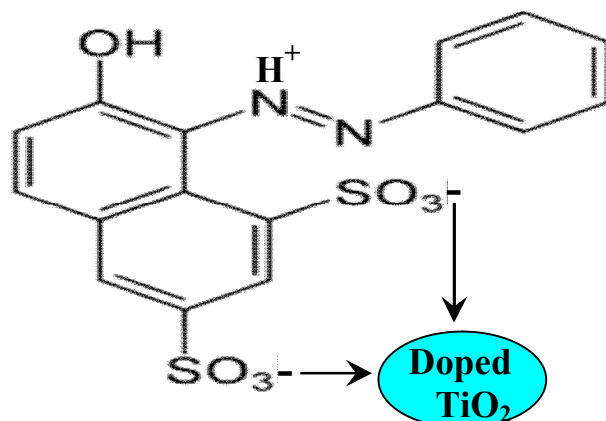


Figure (3-25): Virtual adsorption geometry of OG onto doped TiO₂ particle via sulphonate anchoring groups .

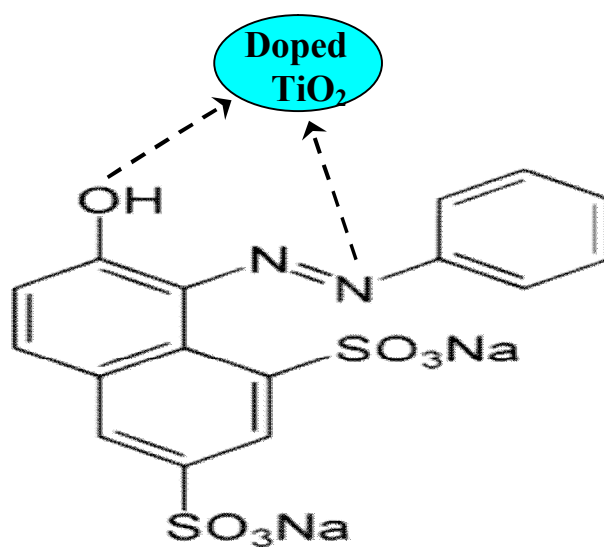


Figure (3-26): Virtual adsorption geometry of OG onto doped TiO₂ particle via azo nitrogen and hydroxyl oxygen groups.

3.4.2 Effect of catalyst loading.

The effect of Au-TiO₂ and Pt-TiO₂ catalysts loading on the degradation rate of OG in aqueous solution has been carried out at initial pH = 3 and OG concentration = 10 ppm by varying catalyst dosage from 20 mg to 60 mg. The results which are illustrated in Figures (3-27) and (3-28) reveal the variation in degradation rate constant of OG against the dosage of Au-TiO₂ and Pt-TiO₂, respectively. It was found that the decolorization degradation of OG increased significantly with increased amount of catalysts and then decreased with further increase of the catalyst dosage due to screening effect and light scattering [106]. The screening impact of the suspended particles is the primary cause of this phenomenon, because the overloaded photocatalyst particles may reduce the incident light intensity by reflection, despite a large number of the active sites present [87].

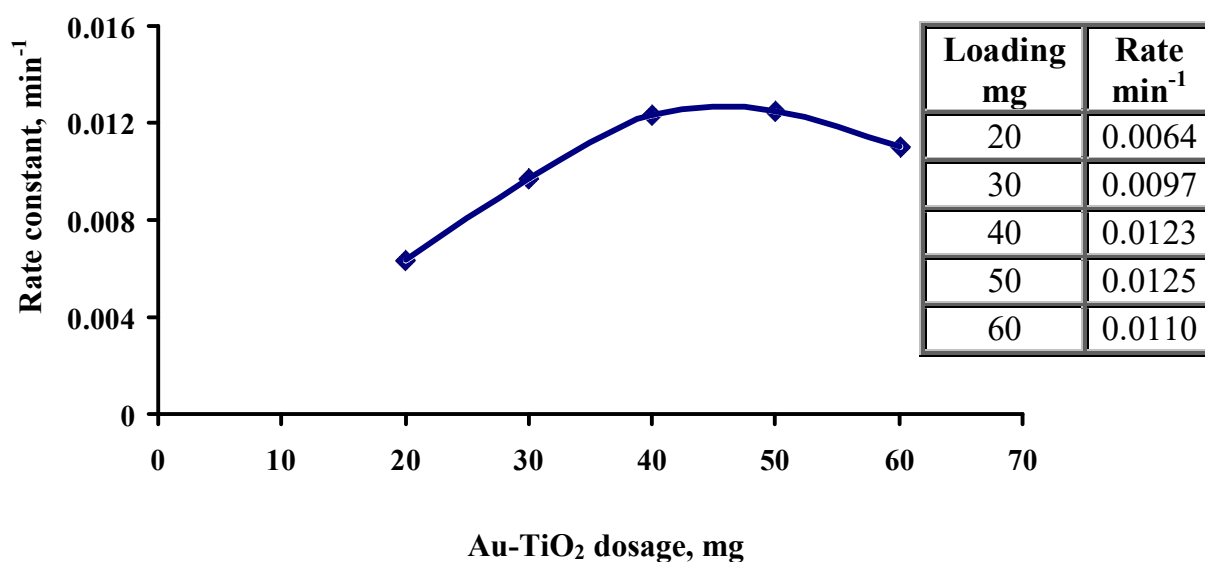


Figure (3-27): Effect of Au-TiO₂ loading on the removal of OG.

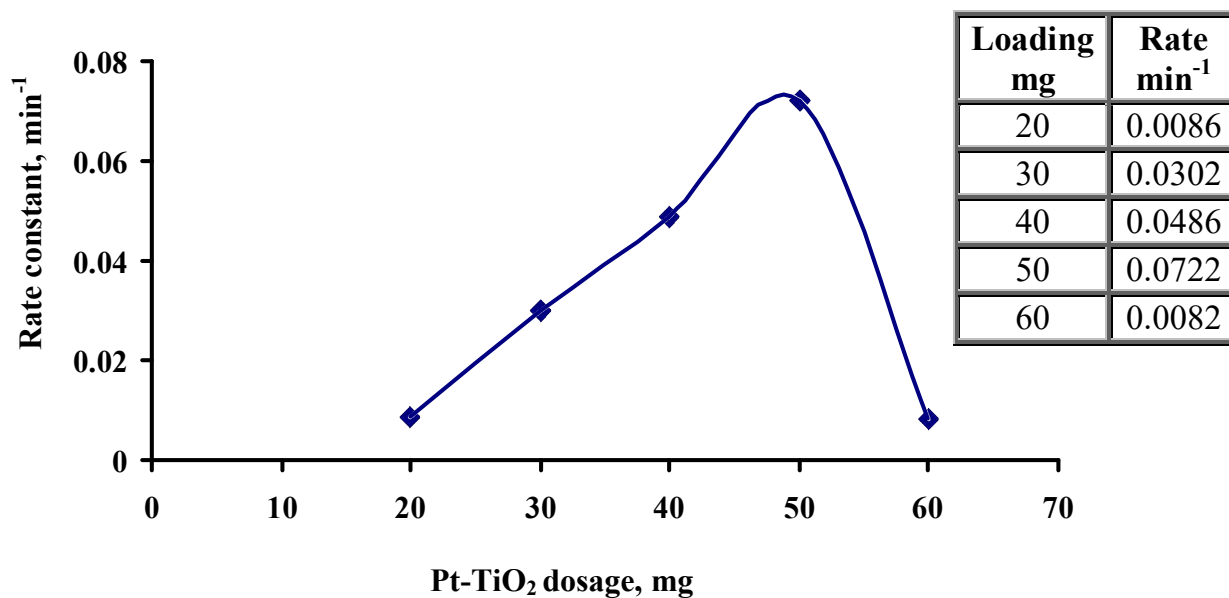


Figure (3-28): Effect of Pt-TiO₂ dosage on the degradation of OG .

The trend in Figures (3-29) and (3-30) show clearly that the loading of Au-TiO₂ and Pt-TiO₂ photocatalysts has a similar influence on OG degradation percent.

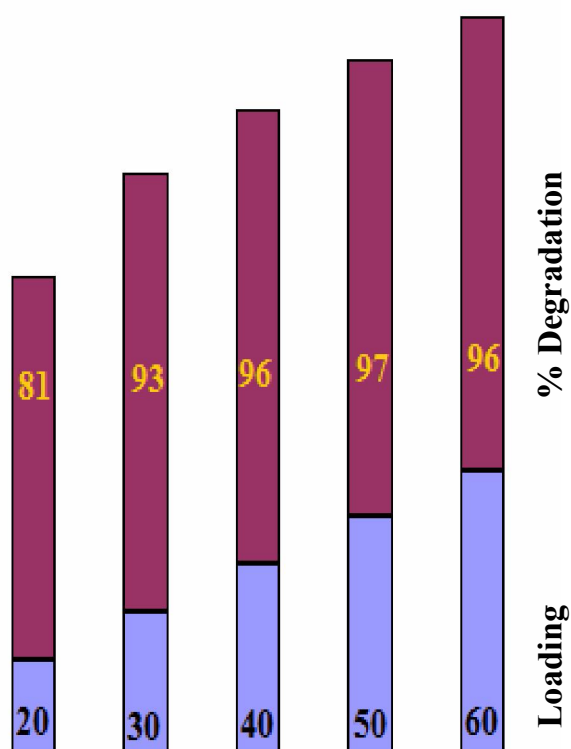


Figure (3-29): Effect of Au-TiO₂ catalyst loading on the degradation yield of Orange G after 270 min of visible light illumination; red columns represent % degradation and blue columns represent Au-TiO₂ dosage.

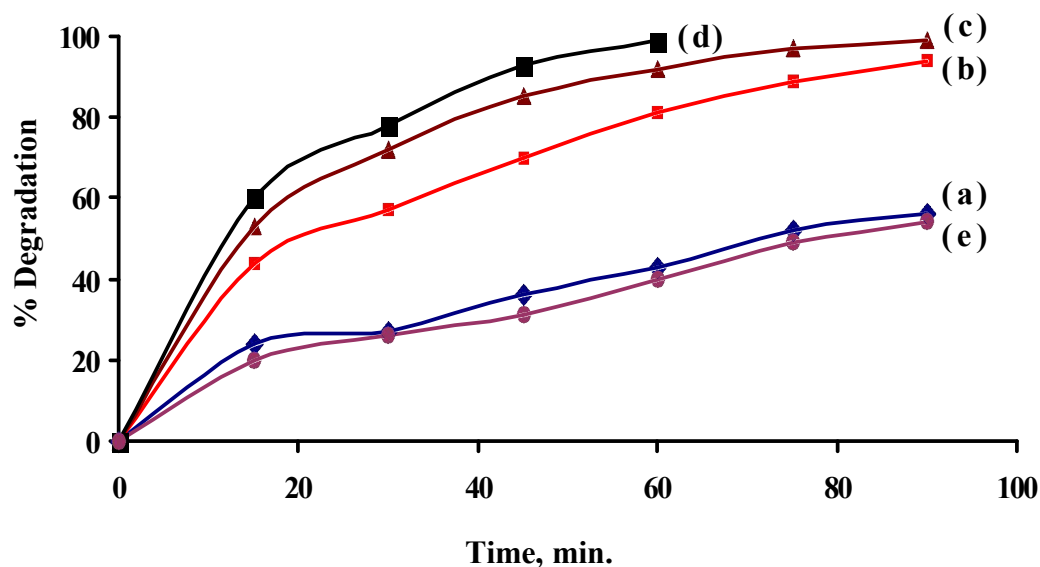


Figure (3-30): Effect of Pt-TiO₂ dosage on the degradation% of OG at pH = 3 and initial OG conc. 10 ppm: (a) 20; (b) 30; (c) 40; (d) 50 and (e) 60 mg .

Figures (3-29) and (3-30) ascertain that the optimum amount of Au-TiO₂ and Pt-TiO₂ catalysts are about 50 mg. This optimum amount has to be added to photocatalysis cell in order to avoid unnecessary excess catalyst and also to ensure total absorption of light photons for efficient photo mineralization of OG dye.

To analyze the effect of the catalysts dosage on the photocatalytic degradation process, two different situations will be described, low and high catalysts dosages; at low loading levels (below optimum dosage), the catalyst surface and absorption of light by this surface are the limiting factors. Thus, an increase in catalysts loading greatly enhances the process efficiency, probably because of the increase of active sites and the production of hydroxyl radicals [107]. Then with increasing dosage above a certain value (optimum), the reactive sites increase and the solution turns cloudy and opaque, which consequently reduce the light penetration and lead to the reduction of the active sites.

Furthermore, Jodat and collaborators [108] have concluded that the increase of catalyst dosage above certain optimum value results in the agglomeration of the catalysts particles. Hence, the catalyst's surface became unavailable for photon absorption and dye adsorption, thus, the decolorization rate decreases.

3.4.3 Effect of initial concentration of OG.

The effect of OG initial concentration in water on the photocatalytic process has also been examined. The photocatalytic degradation of OG at initial concentrations (5, 10, 15, 20, 30, 40 ppm) for a catalyst loading of 40 mg Au-TiO₂ and initial concentrations (7, 10, 15, 20, 30, 40 ppm) for a catalyst loading of 50 mg Pt-TiO₂ were investigated under visible light irradiation and at pH=3 for both catalysts. The effect of initial OG concentration on decolorization rate constant is depicted in Figures (3-31) and (3-32) for Au-TiO₂ and Pt-TiO₂, respectively. It is generally noted that the degradation rate increases with the increase in dye concentration to a certain level and a further increase in dye concentration lead to decrease in the degradation rate of the dye. Based on the above results, the optimum OG concentration for quantitative degradation is 10 ppm for illumination periods of 270 min in the case of Au-TiO₂ and 60 min in the case of Pt-TiO₂. At higher concentrations the photocatalytic process runs with some lower efficiency, however, better results can be appeared by extension of reaction time. Also noted that at low concentration of OG the degradation rate constant is higher in comparison to that at a higher concentration.

O'shea and collaborators [109] stated that the number of catalytic sites at low concentrations is not the limiting factor of the degradation rate which is proportional to the substrate concentration in accordance with apparent first-order kinetics.

On the other hand, the high concentrations of the dye promote the adsorption of OG molecules causing a full surface coverage which consequently reduce the generation of hydroxyl radicals on the catalyst surface since the active sites were occupied heavily by dye molecules [83, 85, 110,111]. Moreover, the capability of photons to reach the photocatalyst surface is negatively impacted due to the invisible barriers of high concentrations of dye moieties. This concept is mainly relied upon the Beer–Lambert law, which states that the decrease of penetration of photons into the solution occurs by increasing the molecules of the dye, which consequently causes lower photonic absorption by the nano photocatalyst and, thus, reducing the efficiency of electron-hole pair (e^-_{CB}/h^+_{VB}) formation [40].

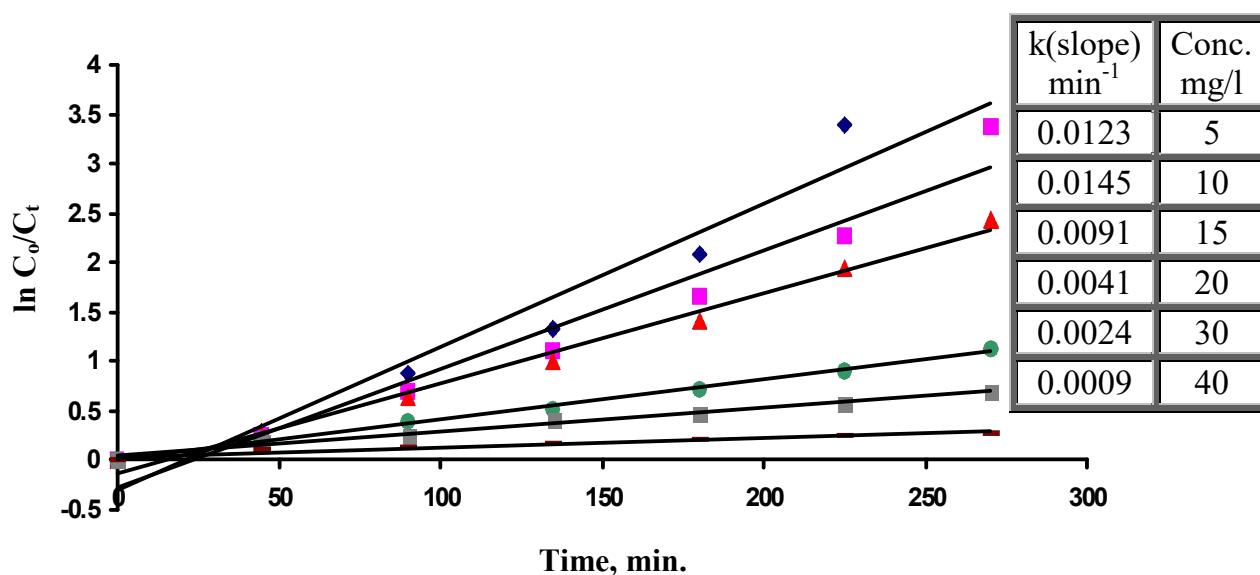


Figure (3-31): Plot of $\ln(C_0/C_t)$ vs. reaction time at different initial concentrations of OG; (2% Au-TiO₂ = 40 mg; pH = 3.0).

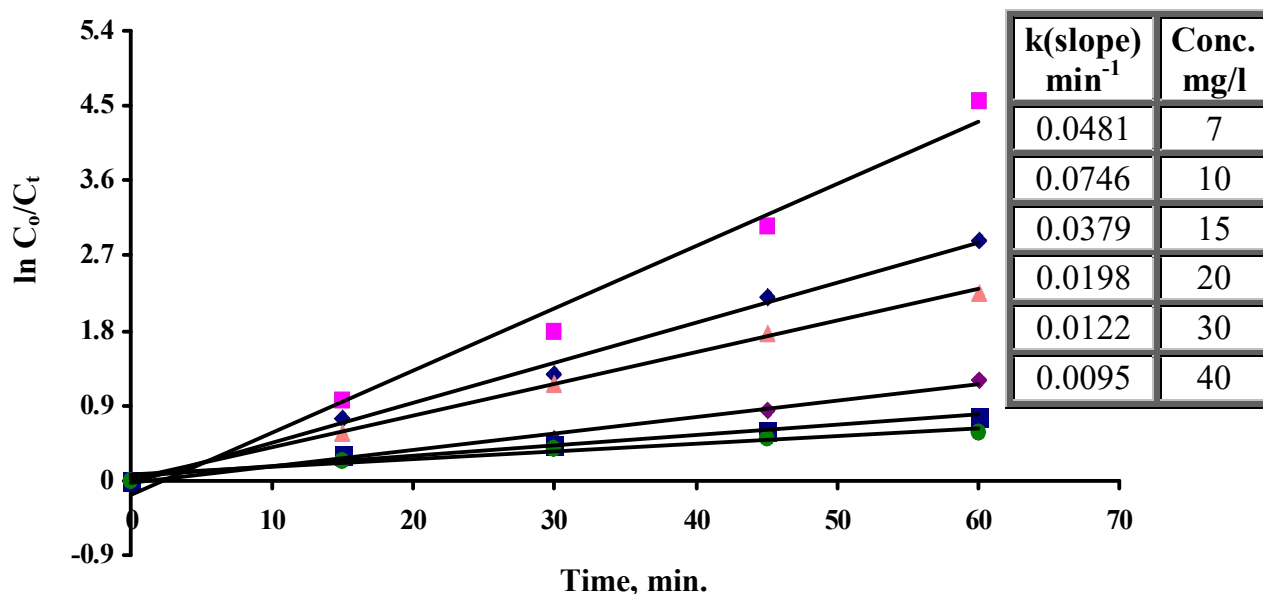


Figure (3-32): Plot of $\ln(C_0/C_t)$ vs. reaction time at different initial concentrations of OG; (4% Pt=TiO₂ = 50 mg/L; pH = 3.0).

3.4.4 Effect of dopants abundance on photocatalytic activity.

The impacts of the dopants, Au and Pt, percent on the photocatalytic degradation of OG dye was investigated for three levels of abundance 1%, 2% and 4% at optimum experimental conditions. Figures (3-33) and (3-34) correlate the process rate constants with dopant's content. While, Figures (3-35) and (3-36) show the relationship between process time and degradation percent of OG for all the three levels of dopants content.

Based on above results, one could observe that the apparent rate constants k_{app} for (1%, 2%, 4%) Au/TiO₂ samples, over 270 min process time, are 0.0083 min⁻¹, 0.0097 min⁻¹ and 0.0084 min⁻¹, respectively, corresponding to OG photodecomposition percents of 90% and 93% and 89%, respectively. Whereas, the apparent rate constants k_{app} for (1%, 2%, 4%) Pt/TiO₂ catalysts, over 120 min process time, have been 0.0138 min⁻¹, 0.0206 min⁻¹ and 0.0222 min⁻¹ respectively, corresponding to OG photodegradation percents of 67%, 85%, and 96%, respectively.

The optimal gold content has been 2 % with a maximal degradation efficiency of OG (93%). It can also be seen that the apparent rate constant of 2 % Au-doped TiO₂ sample is higher than the others. Whereas, the optimal platinum content has been 4 % with a maximal degradation efficiency of OG (96%). It can also be seen that the apparent rate constant of 4 % Pt-doped TiO₂ sample is higher than the others. Niea et al. [112] reported that the catalytic activity often increases with increasing noble metal loading and abundance. However, when the noble metal content exceeds a certain value, the number of surface active centers does not increase with increasing noble metal content due to the growth of larger crystals; i.e, agglomeration.

The major impact of surface deposition of small metal clusters on TiO₂ is ascribed to the acceleration of hydroxyl radical formation and decreasing e⁻/h⁺ pair recombination which enhance the degradation rate of pollutants initiated by h⁺ or OH radical [113]. Qamar, and Ganguli [114] concluded in their work on the self-assembling behavior of Pt nanoparticles onto surface of TiO₂ that when the platinum particles are deposited onto the surface of TiO₂, a Schottky barrier formed at the interface of TiO₂ and Pt metal particles, resulting in an efficient channeling of excited conduction band electrons from the bulk of TiO₂ to the newly formed interface and hence, higher photocatalytic activity was observed. Some researchers [114,115] have rationalized the decrease in the degradation rate of certain dye moieties and the high metal amounts in terms of shadowing of catalysts surface.

Moreover, other authors [99, 108] have reported that when Au/TiO₂ was used to degrade Methyl Orange, the catalyst particles exhibited some sort of agglomeration when the dosage of catalyst exceeded above certain optimum value.

Accordingly, gold nanoparticles would not reveal surface plasmon resonance peak due to the agglomeration of gold nanoparticles, which consequently, the decolorization rate decreased.

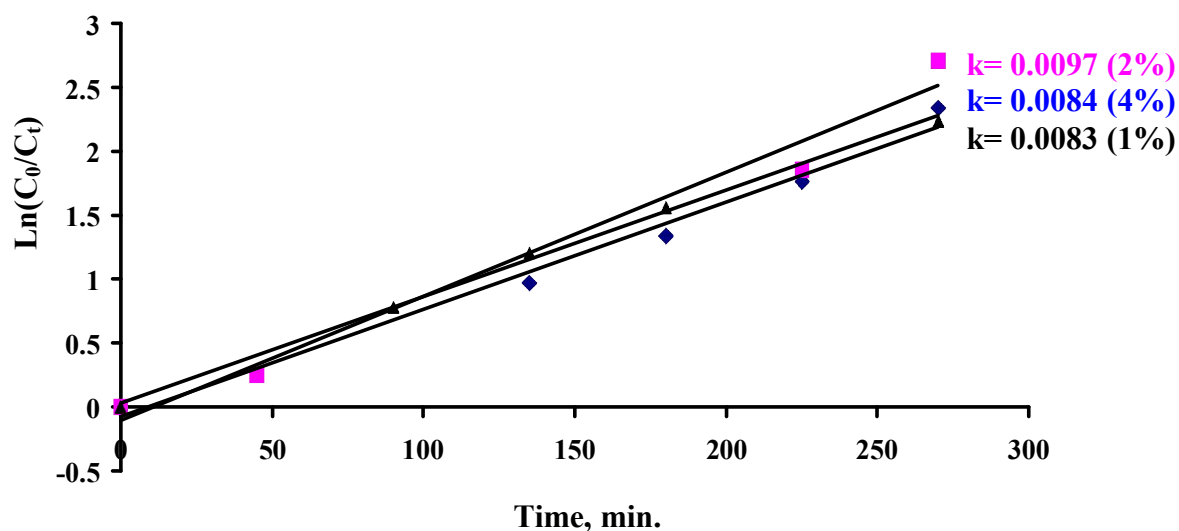


Figure (3-33): Impact of Au doping percent on the rate of photodegradation of OG under visible illumination.

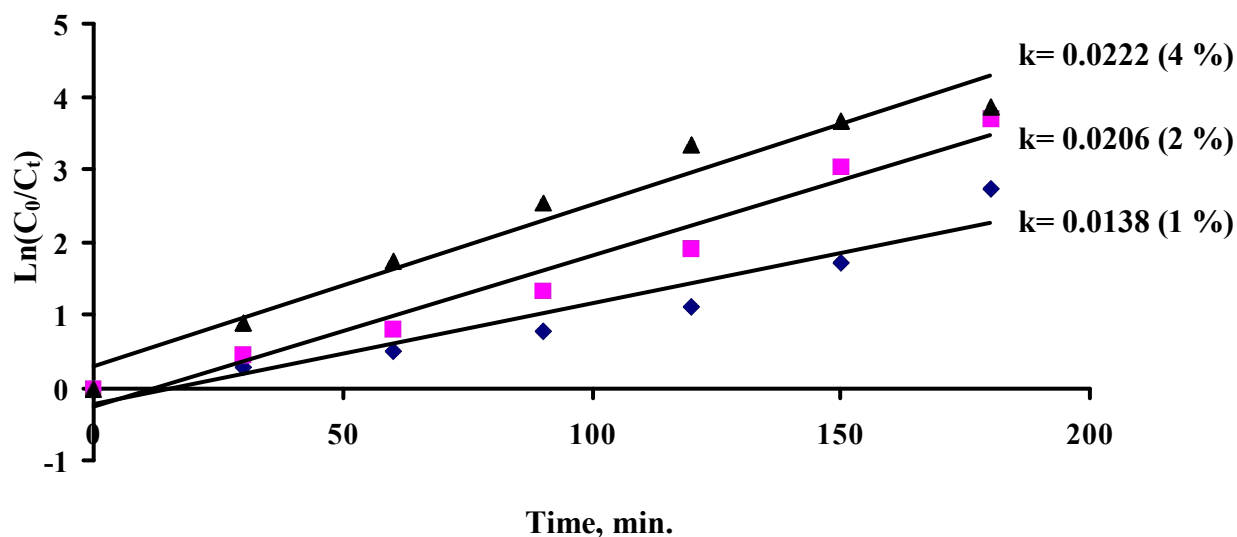


Figure (3-34): Impact of Pt doping percent on the rate of photodegradation of OG under visible illumination.

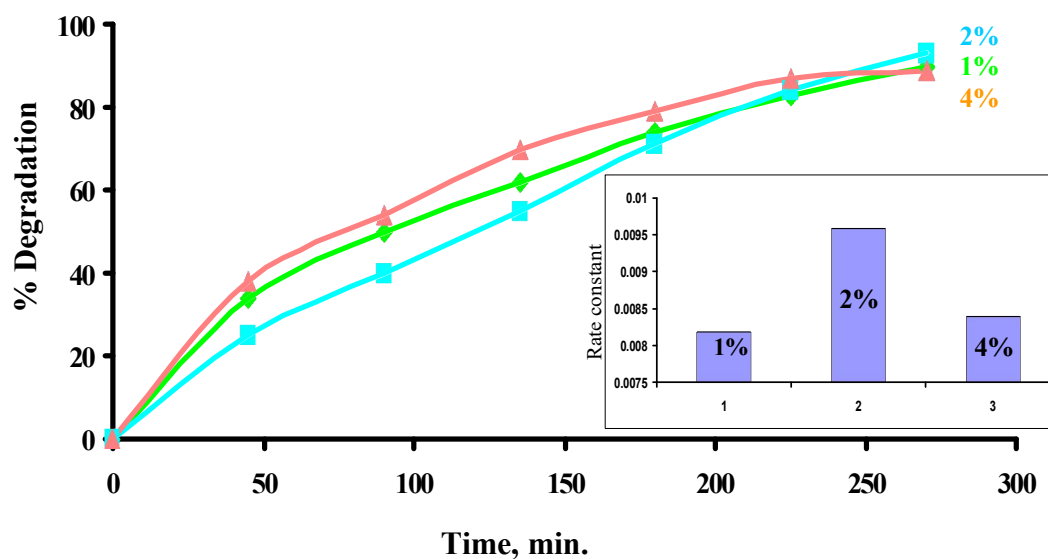


Figure (3-35): Effect of Au doping percent on the degradation percent of OG under visible illumination. Inset represents variation of process rate constant (k) of photodegradation of OG with Au doping percent.

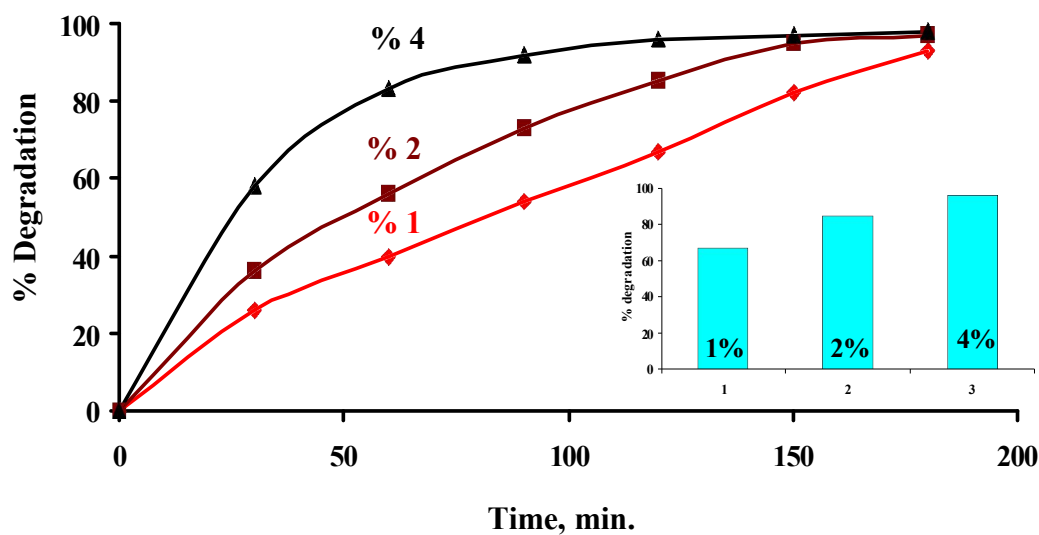


Figure (3-36): Effect of Pt doping percent on the photodegradation percent of OG under visible illumination. Inset represents variation of process rate constant (k) with Pt doping percent.

3.4.5 Effect of radiation dose on the degradation of OG.

Irradiation light intensity plays significant role in the kinetics of the photocatalysis process, where; (i) at low light intensities (0–20 mW/cm²), the rate would increase linearly with increasing light intensity (first order), (ii) at intermediate light intensities beyond a certain value (approximately 25 mW/cm²) the rate would depend on the square root of the light intensity (half order), and (iii) at high light intensities the rate is independent of light intensity [1]. Some researchers [116, 117] reported that, at low light intensity, reactions involving electron–hole formation are predominant, and electron–hole recombination is negligible. On the other hand, at increased light intensity, electron–hole pair separation competes with recombination, thereby causing a lower impact on the rate of reaction.

The influence of visible light intensity on the kinetics and degradation yield of OG degradation during 270 min is presented in Figure (3-37). The degradation rate and degradation yield were appreciably higher under the higher intensity (2.87×10^{-9} mol / L.sec.) of halogen lamp than of intermediate intensity (0.55×10^{-9} mol /L.sec.) and low intensity (0.26×10^{-9} mol /L.sec.) of visible light. This change in rate of degradation of dye molecules by variation in light intensity could be ascribed to the increase in number of photons reaching the active site of catalyst as light intensity increases, so number of excited catalyst molecules increases which enhances the number of hydroxyl radicals and superoxide ions and consequently rate of degradation of dye molecules also increase [17, 118].

For better evaluation of the efficiency of photocatalytic process, we estimated the quantum yield Φ , employing the following expression [18,40];

$$\Phi = \text{rate of reaction} / \text{rate of absorption of radiation}$$

The calculated quantum yield of OG degradation under high, medium, and low intensities of halogen lamp are shown in Table (3-4). We notice that the rates of photodegradation of OG are increasing with increasing light intensity, hence, it is a stand-alone verification for the first order process.

The low quantum yield is one of the features of heterogeneous photocatalysis because the absorbed photons, is experimentally experiencing reflection, scattering and absorption by the suspended particulates [119], accordingly the previously reported quantum yields are in fact apparent quantum yields, i.e. lower limits of the true quantum yields. On the other hand, a number of active sites have often been replaced due to the competition for degradation between the reactant and the intermediate products, thus, this is one of the reasons for the reduced quantum yield in many photo response-extended doped photocatalysts [120].

Table (3-4): Quantum yields of photodegradation of OG obtained at different intensities.

Intensity (Ein/L.sec.) $\times 10^{-7}$	Rate=k[C] (mol/L.sec.) $\times 10^{-9}$	Quantum yield $\Phi = \text{Rate}/\text{Intensity}$
3.39	2.87	0.0085
1.47	0.55	0.0038
0.38	0.26	0.0067

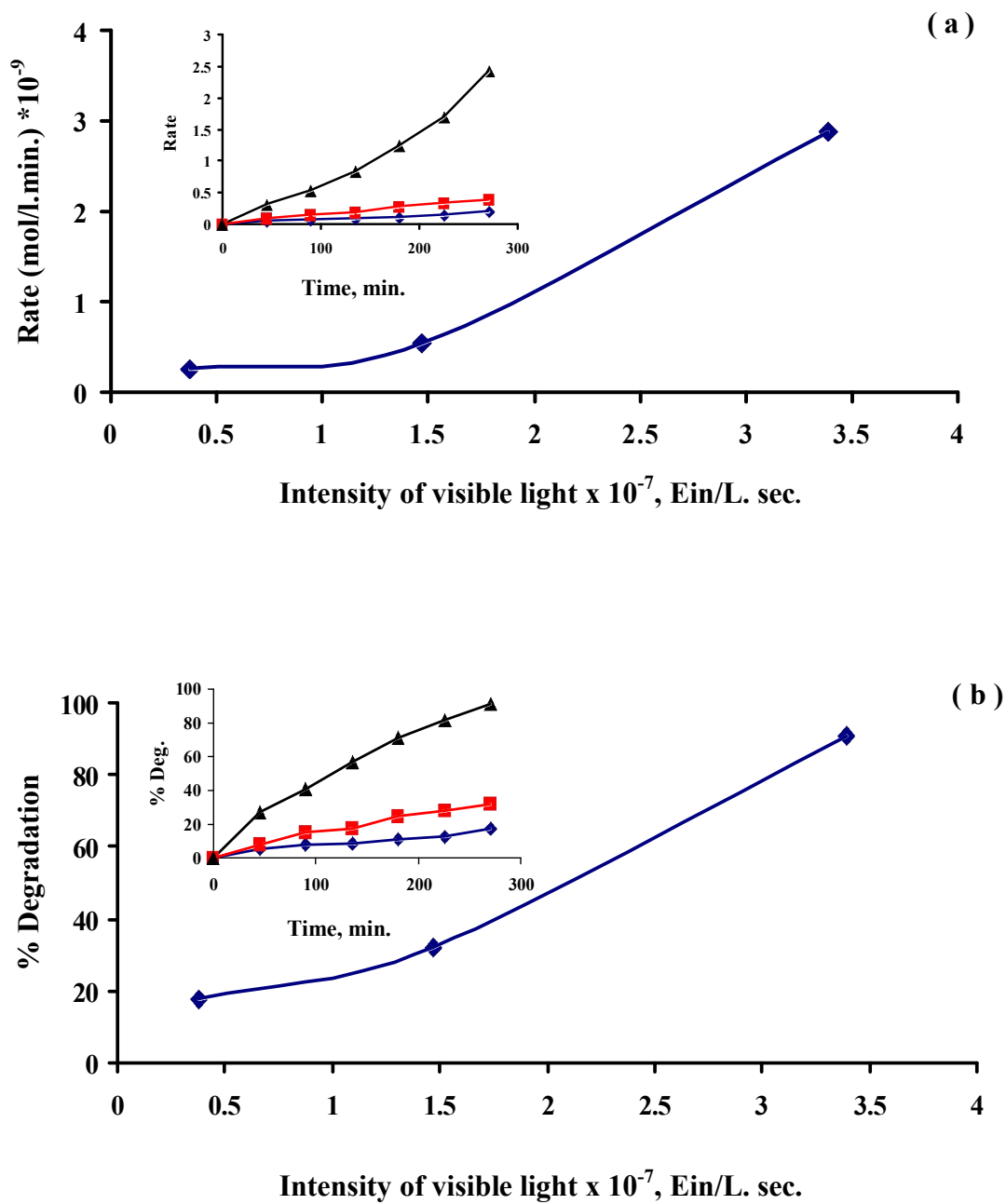


Figure (3-37): Variations of the a) initial rate and b) degradation yield of OG as a function of visible light source intensity.

3.5 Kinetic study

3.5.1 Influence of irradiation time on the reaction kinetics.

Figures (3-38) and (3-39) and related Tables (3-5) and (3-6) reveal quantitative photodegradation for OG over 270 min of irradiation using Au-TiO₂ (96%) and over 60 min of irradiation employing Pt-TiO₂ (99%). It is also evident that the percentage of photodegradation and decolorization increases with increasing irradiation time. The photocatalytic degradation of OG happens on the surface of catalysts, where the O₂ and OH radicals are trapped in the holes of the reactive species, as oxygen and water are fundamental for photocatalytic degradation. At constant light intensity and OG concentration, the quantity of OH and O₂ radicals increases with an increase in the illumination period, and hence, the dye molecules are completely decolorized [121].

Saggiaro et al. [122] reported that azo bonds, nitrogen to nitrogen double bonds, are the most active bonds in azo dye molecules and can be easily oxidized either by OH radicals or positive holes. However, Konstantinou and Albanis [117] stated that the slow kinetics of azo dyes degradation after a long time of illumination emerges from the difficulty in converting the N atoms of the dyes into oxidized nitrogen compounds, and the disappearance of color of azo dye solution was associated with cleavage of the azo linkage in dyes molecules.

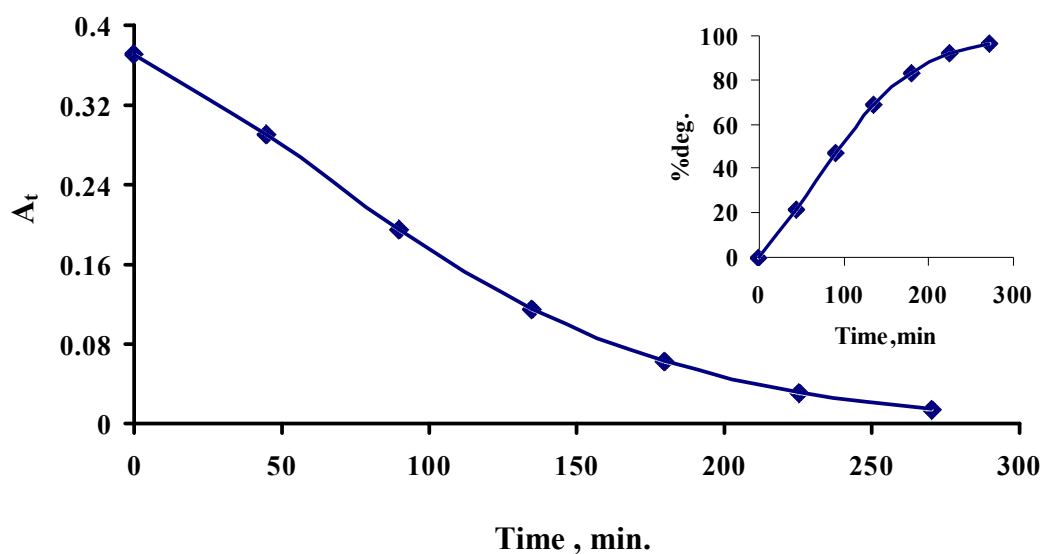


Figure (3-38): Correlation of OG concentration with irradiation time in the presence of Au-TiO₂.

Table (3-5): Variation of concentration and degradation percent of OG in the case of Au-TiO₂.

Time, min.	A_t	% Degradation ($A_0 - A_t / A_0$)*100
0	0.371	0
45	0.291	22
90	0.196	47
135	0.115	69
180	0.063	83
225	0.031	92
270	0.014	96

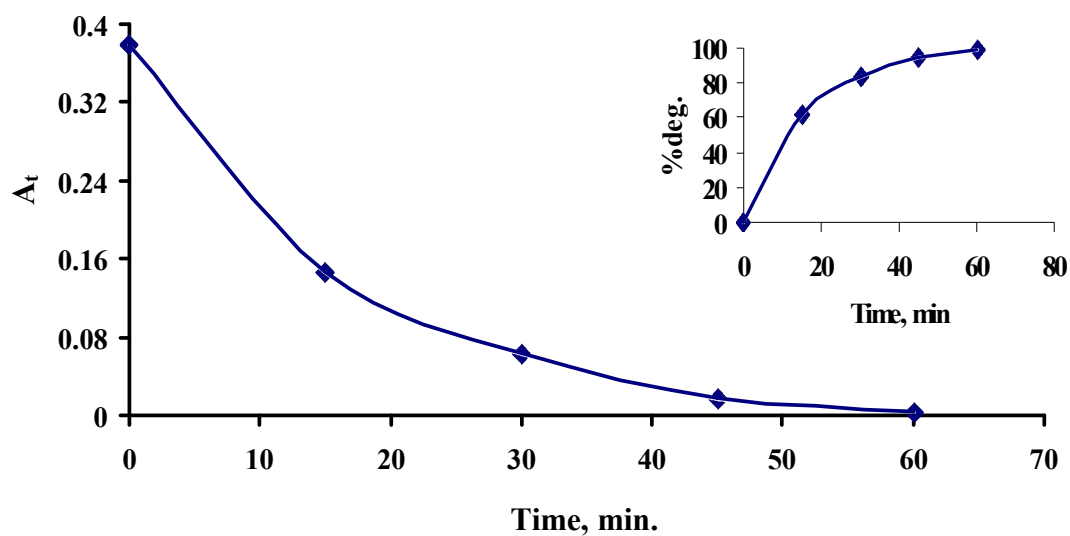


Figure (3-39): Correlation of OG concentration with irradiation time in the case of Pt-TiO₂.

Table (3-6): Variation of concentration and degradation percent of OG in the case of Pt-TiO₂.

Time, min.	A_t	% Degradation ($A_0 - A_t / A_0$) * 100
0	0.379	0
15	0.146	61
30	0.064	83
45	0.018	95
60	0.004	99

For further analysis from kinetics perspectives, the plots of $\ln A_t$ (as first order index) and $1/A_t$ (as second order index) versus time were established in order to devote the R^2 values as one of the methodologies to assign the pseudo-order of the photocatalytic degradation process of OG dye.

Figures (3-40) and (3-41) exhibit the computed values of regression coefficients (R^2) as 0.973 and 0.9849 for $\ln A_t$ vs. time, as pseudo first order evidence for the OG decolorization kinetics, using Au-TiO₂, and Pt-TiO₂, respectively. Whereas, The poor R^2 values of 0.721 and 0.6709 for $1/A_t$ vs. time, as pseudo second order indicator for the OG photodegradation process, reveal explicitly that the Au-TiO₂, and Pt-TiO₂ don't follow pseudo second order mechanism since they did not exhibit a linear behavior during photolysis reaction of OG.

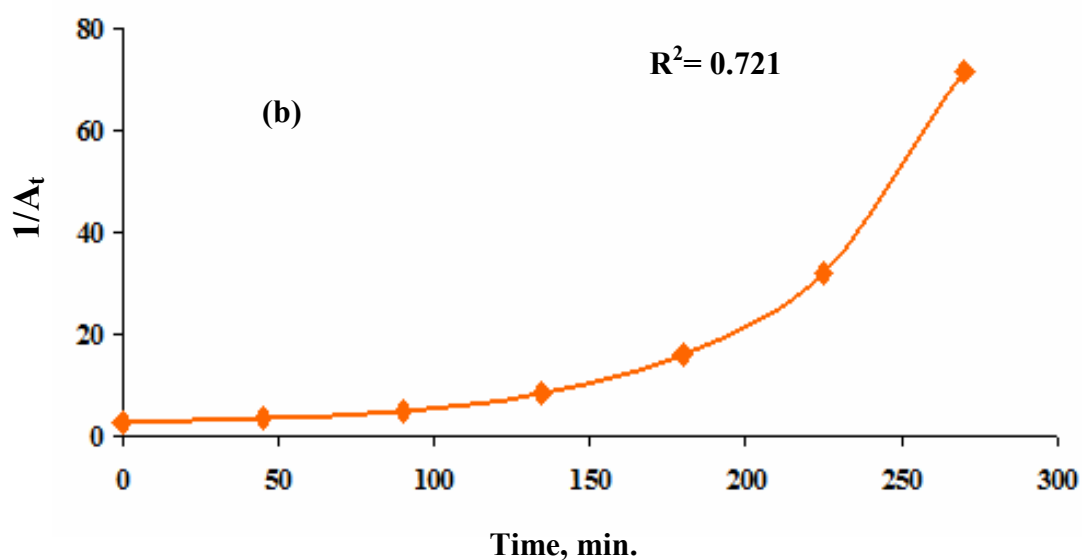
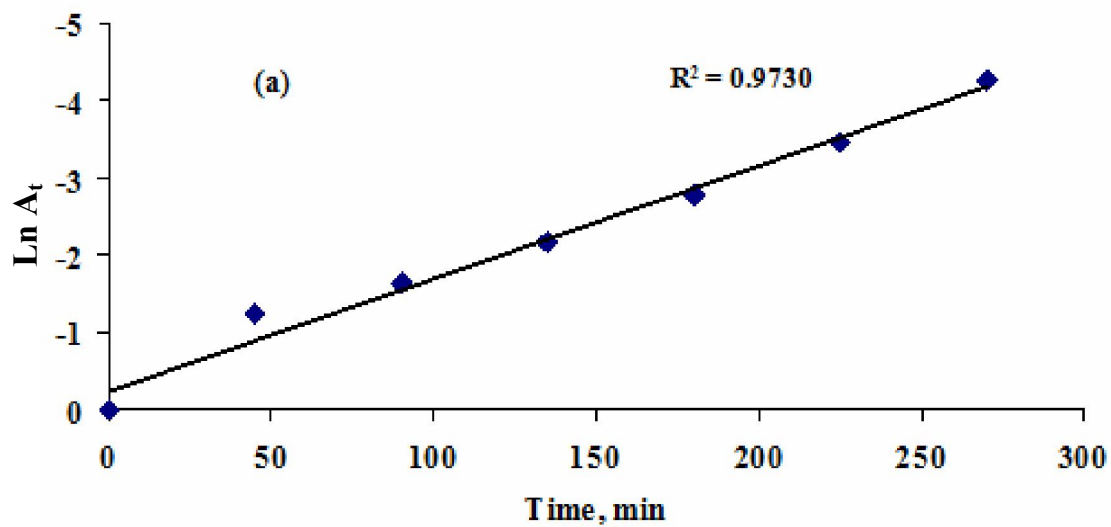


Figure (3-40): (a) first and (b) second pseudo order of Orange G photodegradation at optimum experimental conditions; (A_t : Absorbance at time t and 478 nm) for Au-TiO₂

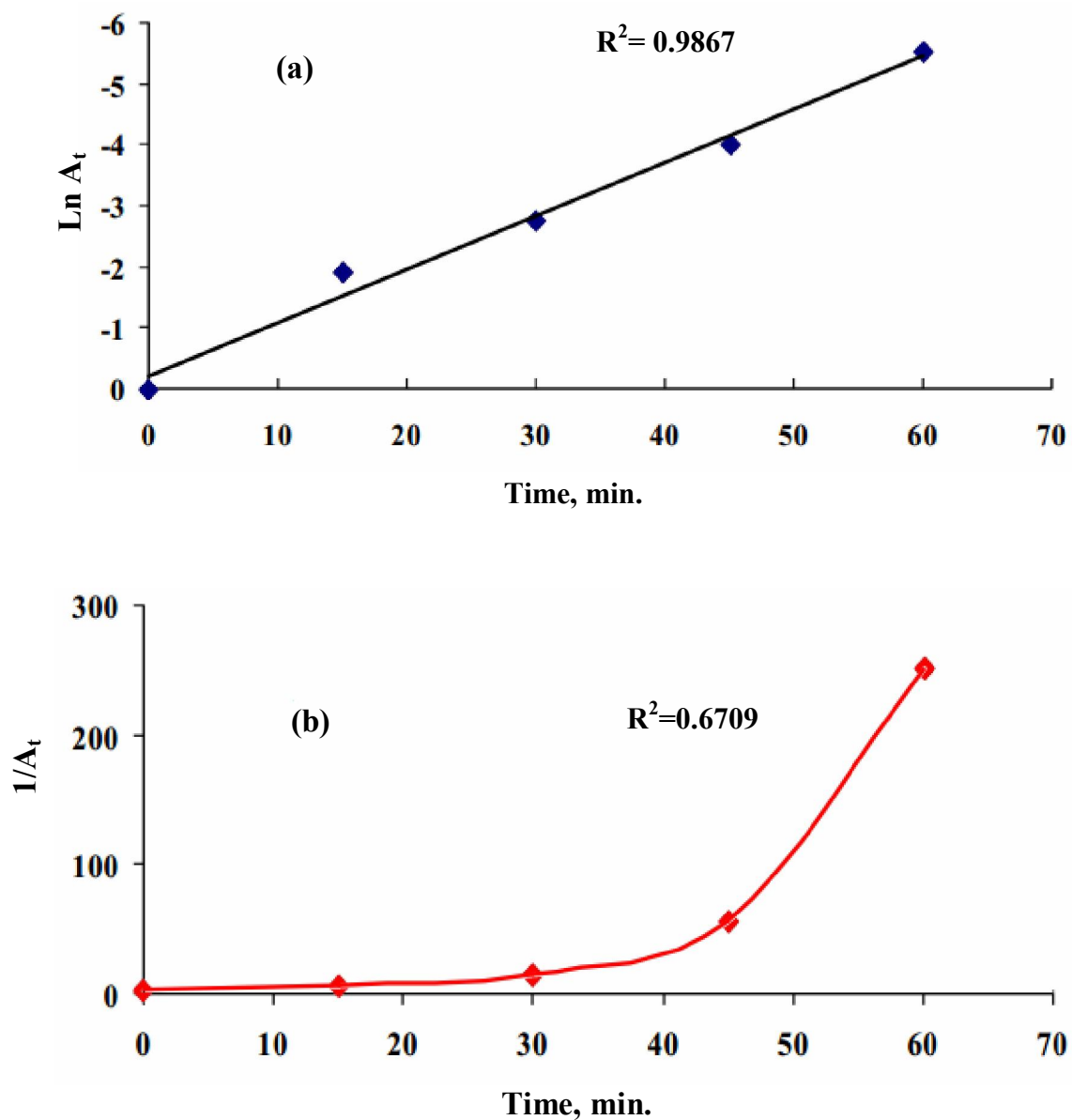


Figure (3-40): (a) first and (b) second pseudo order of Orange G photodegradation at optimum experimental conditions; (A_t : Absorbance at time t and 478 nm) for Au-TiO₂

3.5.2 Kinetics model

Bethi et al. [123] reported that the degradation reactions of numerous organic pollutants in advanced oxidation processes follow the pseudo first order reaction. The calculated rate constant from the slope of OG concentration change (Figures (3-42) and (3-43)) follows the pseudo first order kinetics as per following equation [124].

$$-d[C]/dt = k_{app}[C]$$

Integration of this equation (with the same restriction of $C = C_0$ at $t = 0$, with C_0 being the initial concentration of dye and t the reaction time) will lead to the expected relation:

$$\ln [C_0/C_t] = k_{app} t$$

where C_0 is the initial concentration and C_t is the concentration at any time, k is the apparent first order rate constant and 't' is the time of irradiation.

Kinetic studies were monitored by the change in azo dye concentration at a certain interval of time (C_t). The plots of $\ln(C_0/C_t)$ versus reaction time (t) show straight lines with good correlation coefficients ($R^2 = 0.9726$) for Au-TiO₂ and ($R^2 = 0.9849$) for Pt-TiO₂, see Figures (3-42) and (3-43). The rate constants were found to be 0.0123 min⁻¹ for Au-TiO₂ and 0.0746 min⁻¹ for Pt-TiO₂ under the reaction conditions given in the figure caption.

The half-life of the reaction accordingly computed from the expression $t_{1/2} = 0.693/k_{app}$, which has been equal to 56 min. for Au-TiO₂ and 9 min. for Pt-TiO₂.

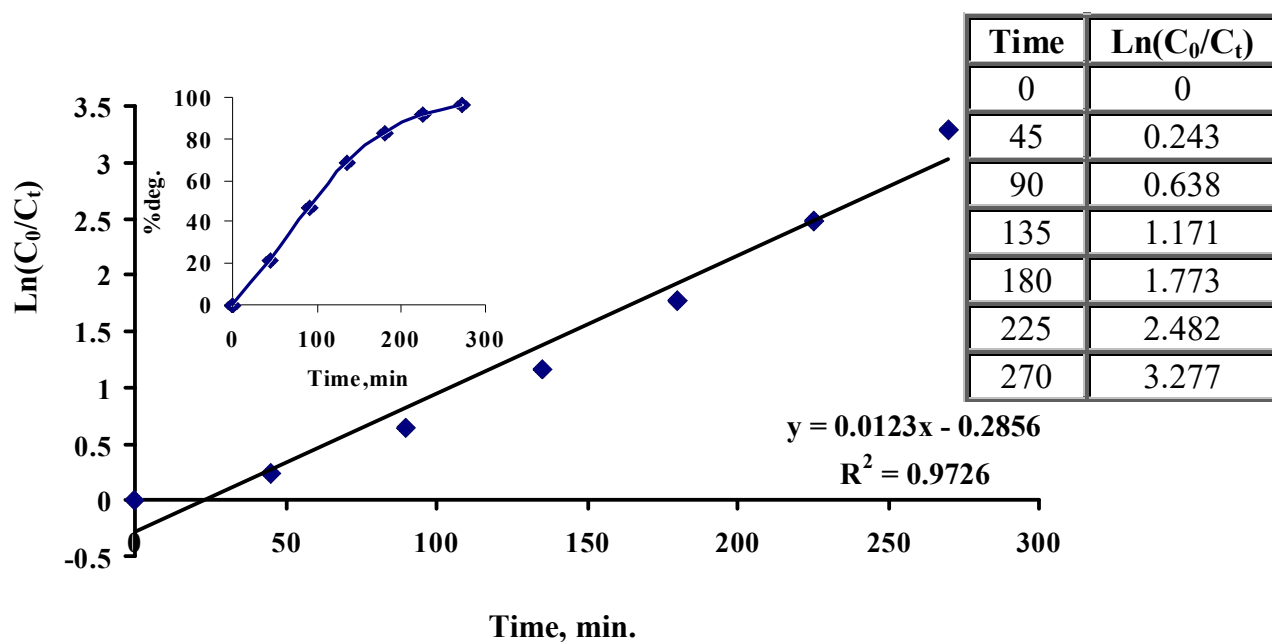


Figure (3-42): Degradation rate of OG at optimum conditions; (Au-TiO₂ = 40 mg/L; pH = 3.0 ; OG=10 ppm).

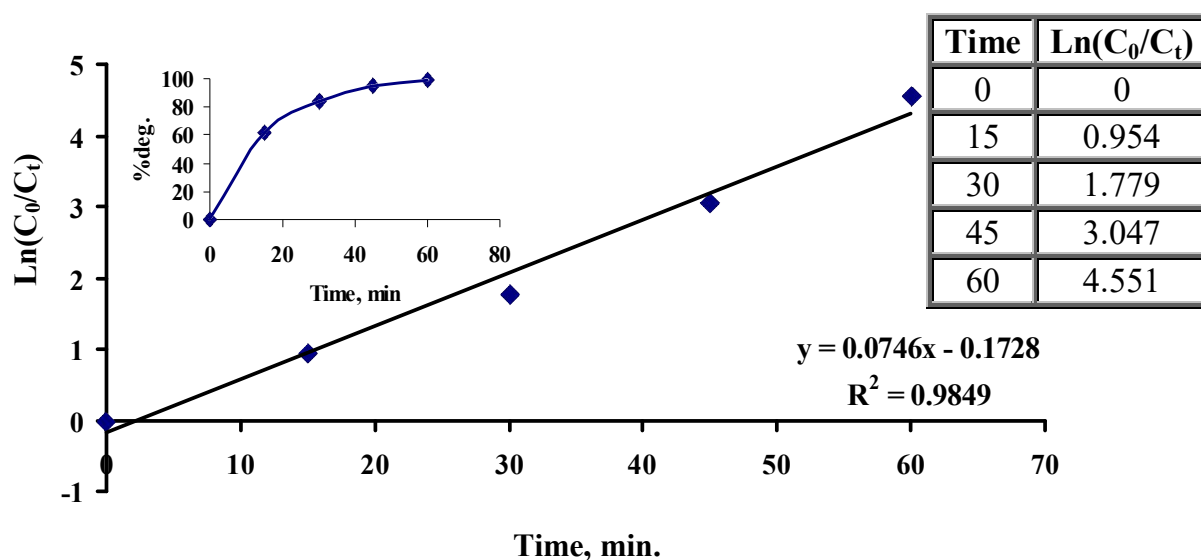


Figure (3-43): Degradation rate of OG at optimum conditions; (Pt-TiO₂ =50 mg/L; pH = 3.0 ; OG=10 ppm).

3.6 Influence of some experimental variables on apparent quantum yield

The heterogeneous photocatalysis literature uses the term quantum yield which is defined as the number of molecules converted relative to the total number of photons incident on the reactor walls. The overall quanta of light absorbed by any photocatalyst or reactant are given by overall quantum yield [18, 125].

$$\Phi_{\text{overall}} = \text{rate of reaction} / \text{rate of absorption of radiation}$$

where the rate of reaction (mol/time) accounts for moles of reactants consumed or product formed in the bulk phase and the rate of absorption of radiation (Einstein/time) relates to the amount (*i.e.*, mol or einstein) of photons at wavelength λ absorbed by the photocatalyst.

The quantum yield is a useful parameter for indicating the efficiency of a photodegradation reaction.

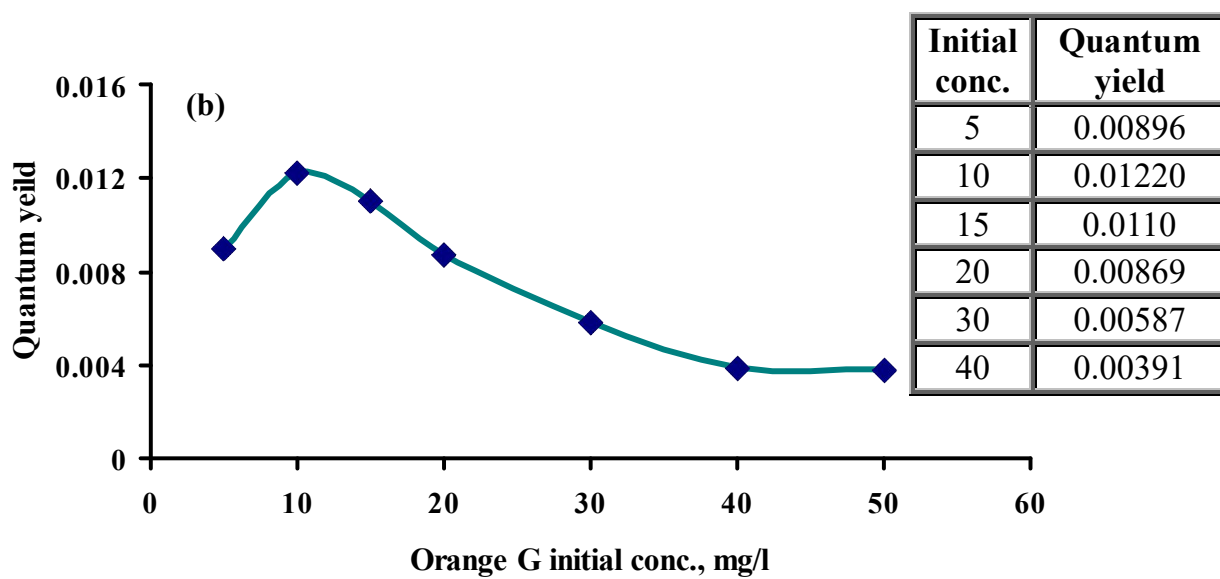
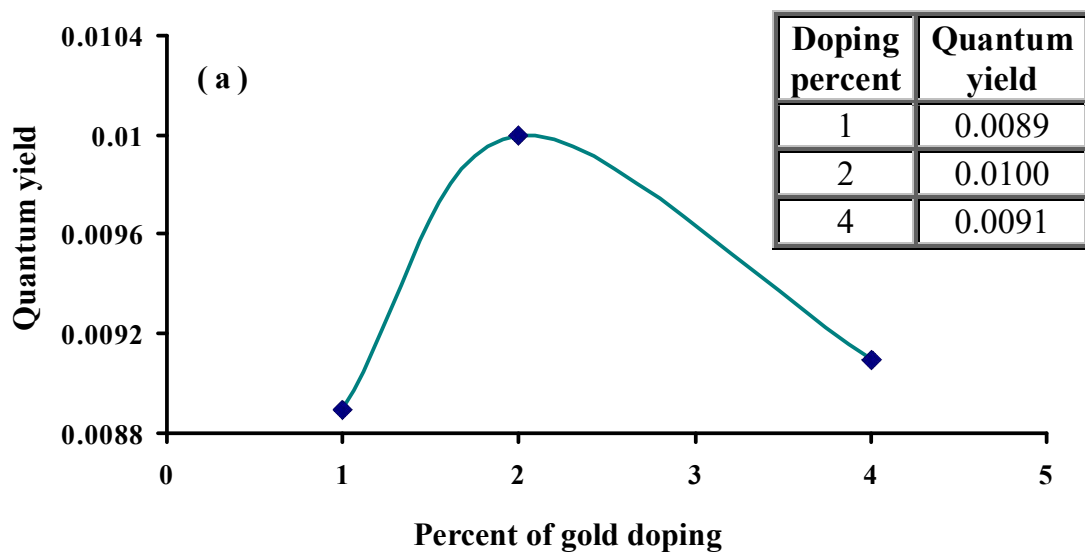
The quantum yield of 2 % Au-TiO₂ is much higher than that of 1% and 4% Au-TiO₂ and also 4% Pt-TiO₂ is greater than that of 1% and 2% Pt-TiO₂. The photocatalytic performance of Au-doped TiO₂ and Pt-doped TiO₂ revealed the dependence of Φ on the Au dopant and Pt dopant amounts as shown in Figures (3- 44 a) and (3-45 a). Observed that the increase of the gold content lowers the quantum yield under illumination after a certain value, whereas, in the case of Pt-doped TiO₂, the quantum yield increases with the platinum content.

The initial dye concentration is another important variable in the evaluation of photocatalytic efficiency. The results which are shown in Figures (3- 44 b) and (3-45 b) elucidate the relation between OG initial concentration and the process quantum yield.

Quantum yield decreases when the concentration of OG increases. This may be due to lowering of the number of reached photons into solution because of screening effect as the concentration of dyes increases and eventually Φ decreases [126].

Figures (3-44 c) and (3-45 c) exhibit quantum yield variation due to different Au-TiO₂ and Pt-TiO₂ loadings for degradation of OG. Upon increasing of the catalyst loading, the flux of absorbed photons increases resulting in an increase in quantum yield. Nevertheless, excess increases of the catalyst concentration would no longer increase the number of active sites generated by light illumination, and instead, Riaz et al. [127] reported that this phenomenon would most likely results in agglomeration of catalyst particles and interception of the light by the suspension; hence, part of the catalyst surface becomes unavailable for photon absorption, then diminishing the quantum yield value.

The initial solution pH is another important variable in the evaluation of photocatalytic efficiency. The relationship between pH and Φ is shown in Figures (3- 44 d) and (3-45 d). Generally, the variations in pH can result in enhancement of the efficiency of photo removal of organic pollutants in presence of photocatalysts [128].



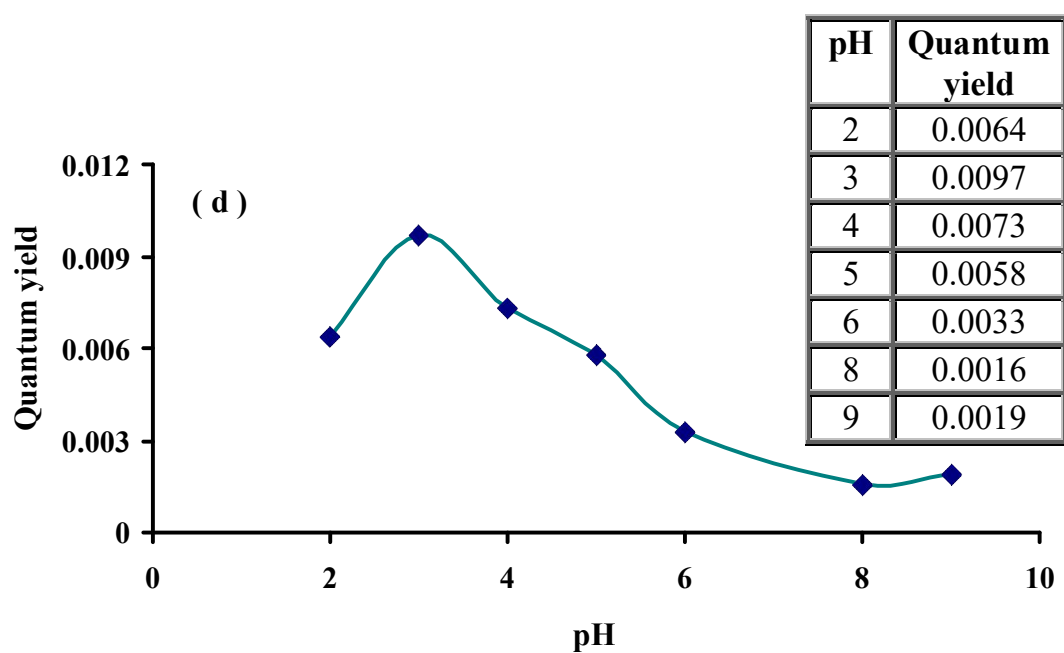
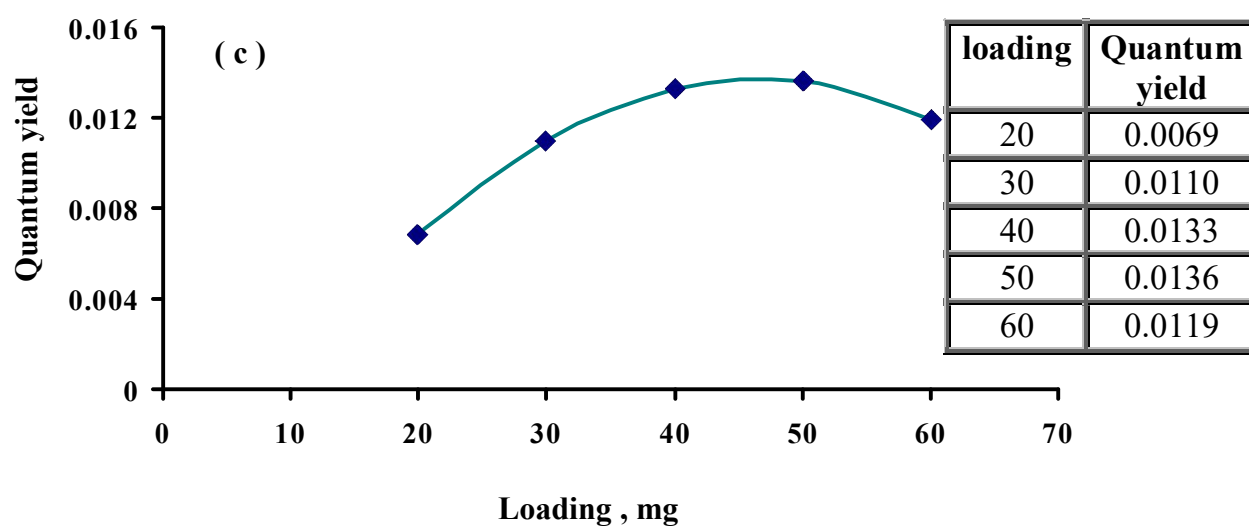
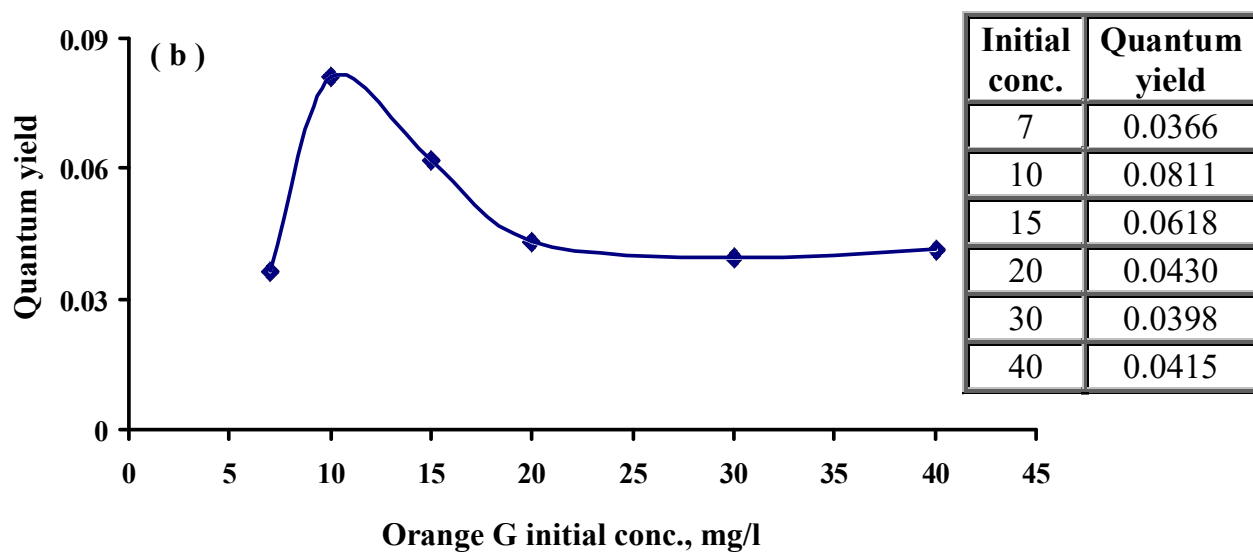
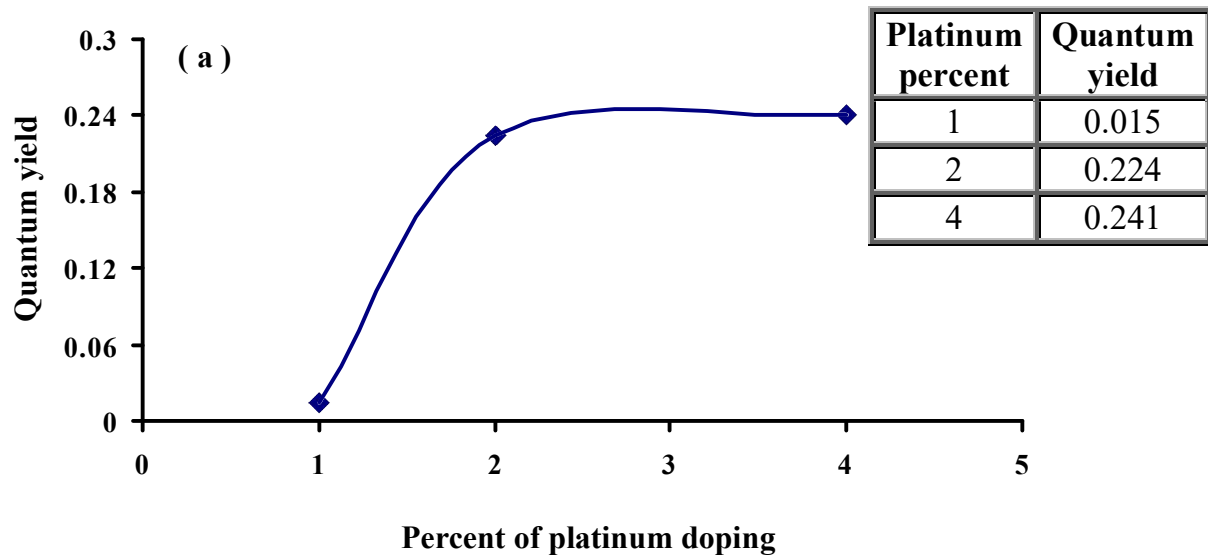


Figure (3-44): Effect of (a) gold percent; (b) OG initial concentration ; (c) Au-TiO₂ loading and (d) pH on the quantum yield of photocatalytic reaction



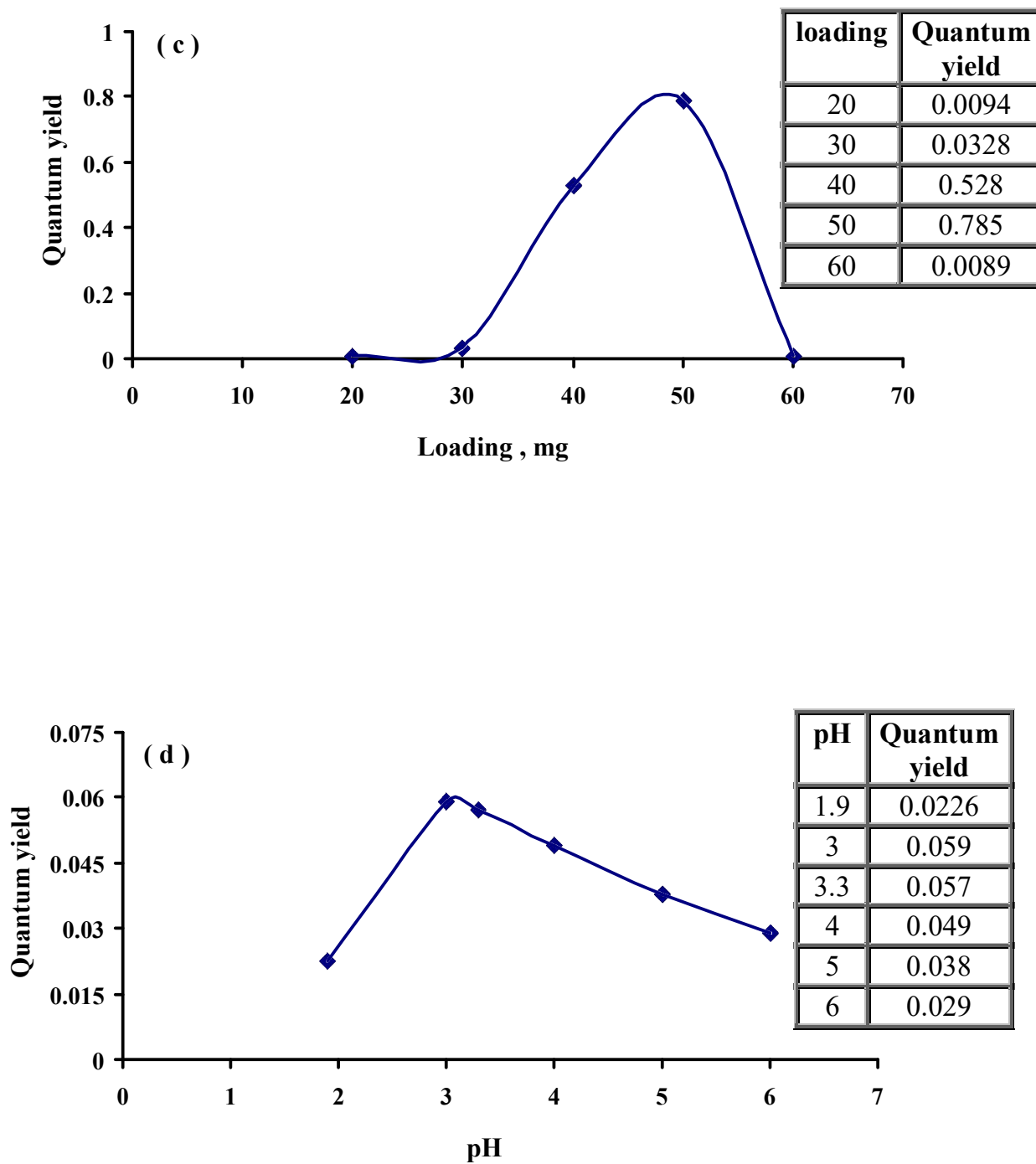


Figure (3-45): Effect of (a) platinum percent; (b) OG initial concentration; (c) Pt-TiO₂ loading and (d) pH on the quantum yield of photocatalytic reaction.

3.7 Effect of temperature and thermodynamic parameters.

The photocatalytic degradation rate of different organic compounds depends on various operational parameters including temperature and corresponding thermodynamic functions [40, 87]. The effect of temperature on the decolorization of OG was studied at different temperatures of 293, 298, 303, 308, and 318 K by keeping other experimental conditions constant at OG concentration of 10 ppm, catalysts dosage 40 mg for Au-TiO₂ and 50 mg for Pt-TiO₂, initial pH of dye solution equals to 3. The results are shown in Figures (3-46) and (3-47). These results indicate that raising the temperature has a positive impact on the decolorization of OG. The apparent rate constant and temperature can be expressed by Arrhenius relation as follows [129]:

$$k_{app} = Ae^{-E_a/RT} \dots\dots\dots (3-3)$$

where k_{app} is the apparent rate constant, A is the frequency factor or pre-exponential factor, E_a is the activation energy of the reaction, R is general gas constant and T is the absolute temperature. The natural logarithm of Eq. (3-3) resulted Eq. (3-4)

$$\ln k_{app} = \ln A - E_a /RT \dots\dots\dots (3-4)$$

The apparent activation energy E_a , obtained from the Arrhenius plot of $\ln k_{app}$ versus $1/T$ is shown in Figures (3-46) and (3-47). It can be seen that a good linear relationship exists in the plots, ($R^2 > 0.9378$) and ($R^2 > 0.973$), for Au-TiO₂ and Pt-TiO₂, respectively. The other thermodynamic parameters for instance free energy of activation ($\Delta G^\#$), enthalpy of activation ($\Delta H^\#$) and entropy of activation ($\Delta S^\#$) were calculated using activation energy and apparent rate constant as follows [130]:

$$k_{app} = k_B T/h e^{(-\Delta G^\ddagger/RT)} \dots\dots\dots (3.5)$$

$$\Delta G^\ddagger = RT \times [\ln (k_B T/h) - \ln k_{app}] \dots\dots\dots (3.6)$$

where h is Planck constant (6.6256×10^{-34} J.s) and k_B is Boltzmann constant (1.3805×10^{-23} J.K⁻¹). The introduction of the constant values, leads to:

$$\Delta G^\ddagger = RT \times (23.76 + \ln T - \ln k_{app}) \dots\dots\dots (3.7)$$

The entropy (ΔS^\ddagger) and enthalpy (ΔH^\ddagger) of activation are derived from equations 3.4, 3.5 and 3.6, leading to the final relations;

$$d(\ln k_{app}) / dT = E_a / RT^2 \dots\dots\dots (3.9)$$

likewise, equation (3.5) is rewritten as:

$$\ln k_{app} = \ln (k_B T/h) - \Delta H^\ddagger / RT + \Delta S^\ddagger / R \dots\dots\dots (3.10)$$

$$d(\ln k_{app}) / dT = 1 / T + \Delta H^\ddagger / RT^2 = (\Delta H^\ddagger + RT) / RT^2 \dots\dots (3.11)$$

Solving equations 3.9 and 3.11 for the activation enthalpy gives

$$\Delta H^\ddagger = E_a - RT \dots\dots\dots (3.12)$$

finally giving access to the entropy of activation

$$\Delta S^\ddagger = (\Delta H^\ddagger - \Delta G^\ddagger) / T \dots\dots\dots (3.13)$$

From Tables (3-7) and (3-8), it can be concluded that with increasing temperature, the rate of reaction increases which is due to the reason that increases in temperature helps to speed up the velocity of both the hydroxyl radicals and the dye molecules to interact with each other thus the reaction competes more efficiently with the electron-hole recombination [131]. On the other hand, Chen and Ray [132] stated that the increase in rate constant was most likely due to the increasing collision frequency of molecules in solution that increases with increasing temperature.

The positive ΔG^\ddagger obtained indicate that the reaction is non-spontaneous . This positive ΔG^\ddagger could be ascribed to activated state being a well solvated structure formed between the dye molecules and the reaction intermediates that is hydroxyl radicals which are also supported by the negative entropy of activation [133]. The process was endothermic due to positive values of ΔH^\ddagger i.e., that higher temperatures are favored for enhanced removal of organic pollutant. The negative values of ΔS^\ddagger suggest the decreased randomness at the solid/ solution interface during the adsorption of azo dye on catalyst and further ratification for the non spontaneous process [134]

Tables (3-7) and (3-8) exhibit the activation energies for photodegradation of OG using Au-TiO₂ and Pt-TiO₂ catalysts in the temperature range 293-318 K which equal to 14.66, and 36.29 kJ.mol⁻¹ , respectively. Despite the higher activation energy required in case of Pt-TiO₂, our experimental results revealed better rates for Pt-TiO₂ powders in comparison to Au-TiO₂ suspension. Hence, this is stand-alone verification for independence of photocatalysis on the thermodynamic properties of the photocatalysts.

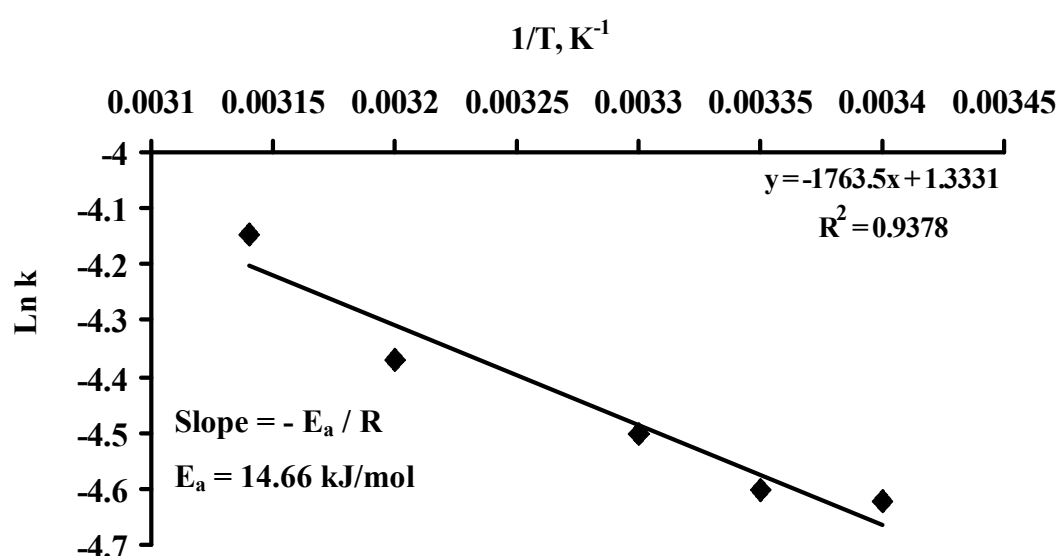


Figure (3-46): Arrhenius plot of rate constant versus reciprocal of reaction temperature for degradation of OG using Au-TiO₂.

Table (3-7): Thermodynamic parameters for the photocatalytic degradation of Orange G using Au-TiO₂.

T (K)	E _a (kJ.mol ⁻¹)	ΔG* (kJ.mol ⁻¹)	ΔH* (kJ.mol ⁻¹)	ΔS* (J.K ⁻¹ .mol ⁻¹)
293	14.66	82.99	12.22	-241.54
298		84.40	12.18	-242.35
303		85.62	12.14	-242.51
308		86.72	12.09	-242.31
318		89.03	12.02	-242.17

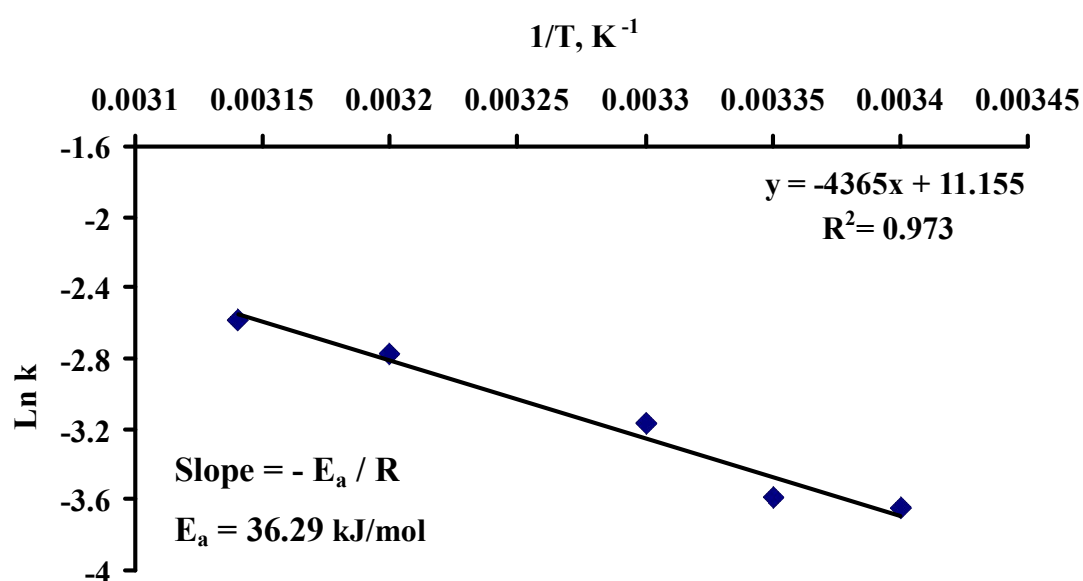


Figure (3-47): Arrhenius plot of rate constant versus reciprocal of reaction temperature for degradation of OG using Pt-TiO₂.

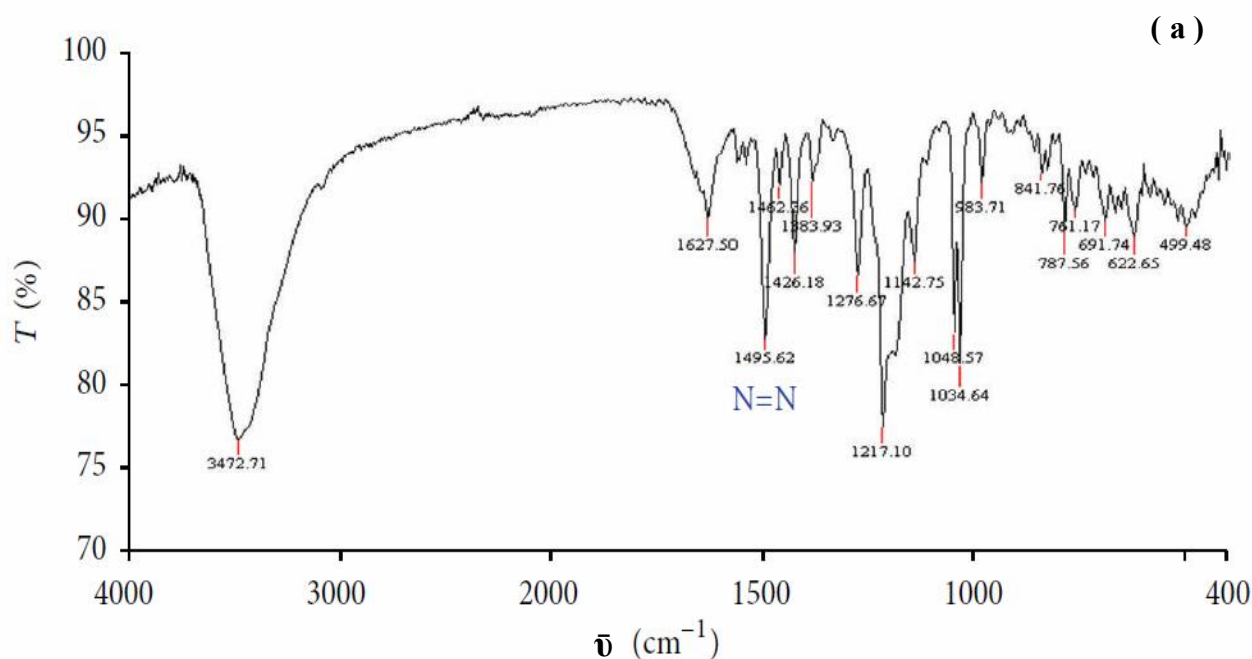
Table (3-8): Thermodynamic parameters for the photocatalytic degradation of Orange G using Pt-TiO₂.

T (K)	E _a (kJ.mol ⁻¹)	ΔG* (kJ.mol ⁻¹)	ΔH* (kJ.mol ⁻¹)	ΔS* (J.K ⁻¹ .mol ⁻¹)
293	36.29	80.61	33.85	-159.59
298		81.88	33.81	-161.31
303		82.25	33.77	-160.00
308		82.63	33.73	-158.77
318		84.89	33.65	-161.13

3.8 FTIR characterization of Orange G / Pt-TiO₂ system.

The change of functional groups of azo dye after photocatalytic treatment was surveyed. The initial OG concentration of 10 mg L⁻¹ was treated using 50 mg Pt-TiO₂ for 60 min of photocatalysis period.

Figure (3-48 a) presents the referenced frequency values for pure OG [135], where 1050 cm⁻¹ is assigned for S=O stretch in SO₃Na group, 1426, 1462 and 1492 cm⁻¹ for N=N, 3437-3464 cm⁻¹ for O-H and N-H, 1627.9 cm⁻¹ for C=C and 1203.6 cm⁻¹ for C-N. These frequencies are in a good agreement with the values measured in our research work shown in Figure (3-48b). Figure (3-48 c) presents the FTIR spectrum for the OG degraded solution, where the bands located at 1426, 1463, and 1496 cm⁻¹ for N=N and the band located at 1050 cm⁻¹ disappeared. Moreover, a broadband appeared at 2831.50 cm⁻¹ which is likely attributed to asymmetric vibrations of the methylene and methyl groups [136]. Accordingly, it is possible to report here that the disappearance of such functional groups and additionally appearance of a new band at 3402.4 cm⁻¹ which is mainly assigned for phenolic and amines groups [137] ought to be ratification for the photodegradation of the model dye OG.



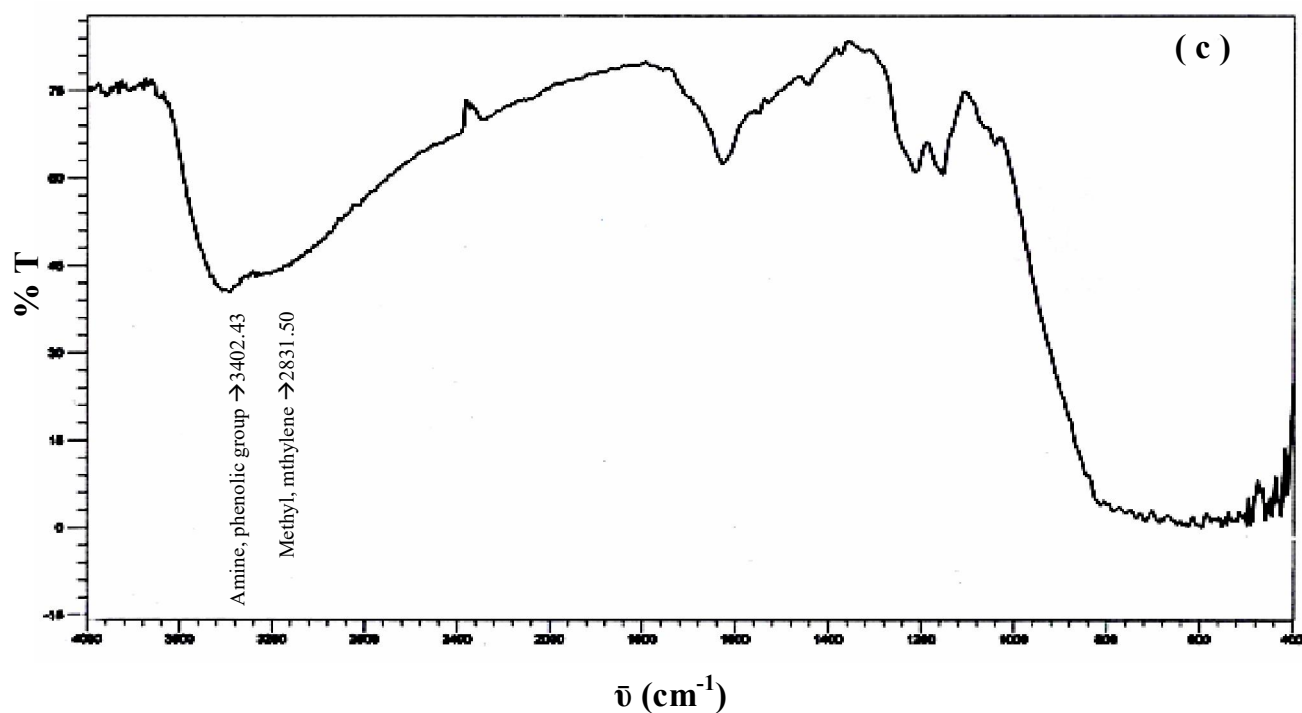
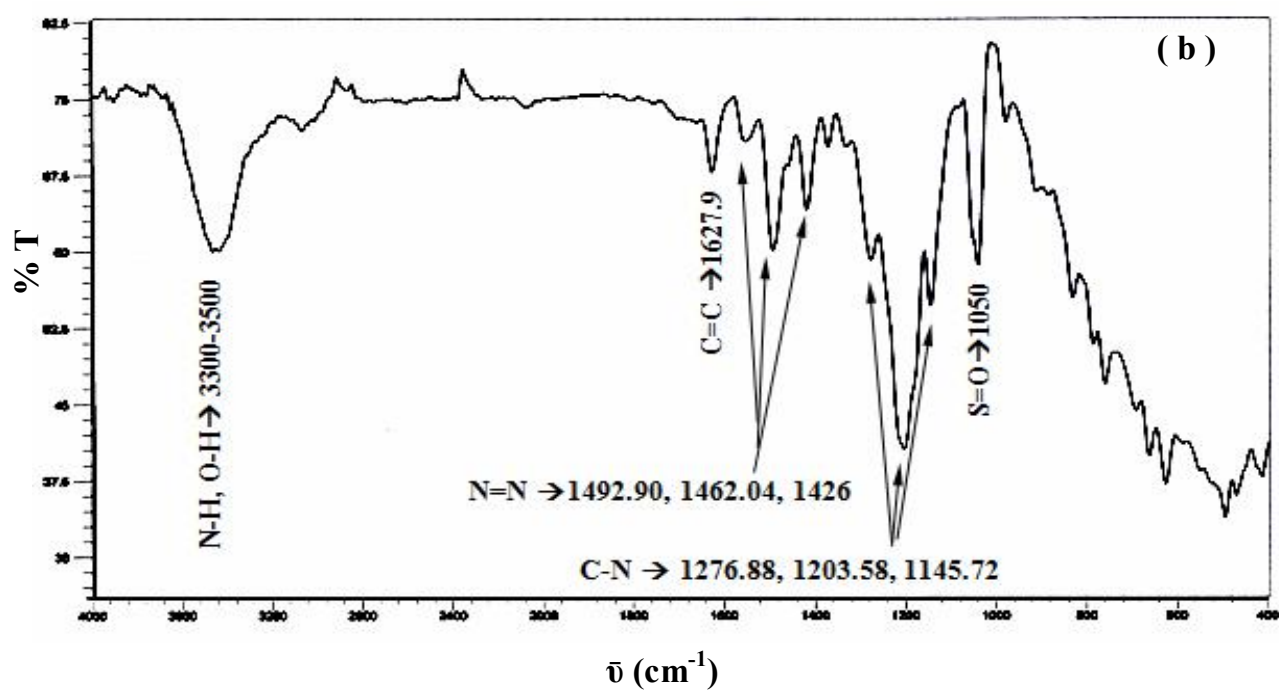


Figure (3-48): FTIR spectra for OG: (a) reference; (b) before and (c) after Pt/TiO₂ photocatalytic degradation.

3.9 photocatalytic activity of Au-TiO₂ and Pt-TiO₂ catalysts under solar light irradiation.

The photocatalytic activity of Au-TiO₂ and Pt-TiO₂ catalysts were estimated by measuring the decomposition rate and degradation percent of OG under sunlight illumination. All the experiments were carried out when the intensity of sunlight was relatively high during the period between 10:15 am to 12:15 pm for Au-TiO₂ and between 10:15 am to 10:40 am for Pt-TiO₂ on the 15 and 20 June (summer season). It was noticed that 2% Au-TiO₂ and 4% Pt-TiO₂ achieved 94.5% and 91.1% degradation, respectively, for OG within 2 hours for Au-TiO₂ and 25 min for Pt-TiO₂.

Photodegradation rate of OG under solar light and in presence of 2 % Au-doped TiO₂ and 4 %Pt- doped TiO₂ are illustrated in Figures (3-49) and (3-50), respectively. This enhanced degradation rate of OG under sunlight irradiation using Au-doped TiO₂ and Pt-TiO₂ is attributed mainly to the existence of about 5% UV light within the solar light .

The high photocatalytic efficiency which is exhibited by the laboratory synthesized doped catalysts under sun light might be ascribed to their capability to absorb both visible and UV radiations of solar light where in terms of energy, sunlight at Earth's surface is around 52 to 55 percent infrared (above 700 nm), 42 to 43 percent visible (400 to 700 nm), and 3 to 5 percent ultraviolet (below 400 nm) [138, 139]. Under the high intensity of light irradiation, the enhancement was considerably higher because of the electron-hole formation is predominant and, hence, electron-hole recombination is negligible [140].

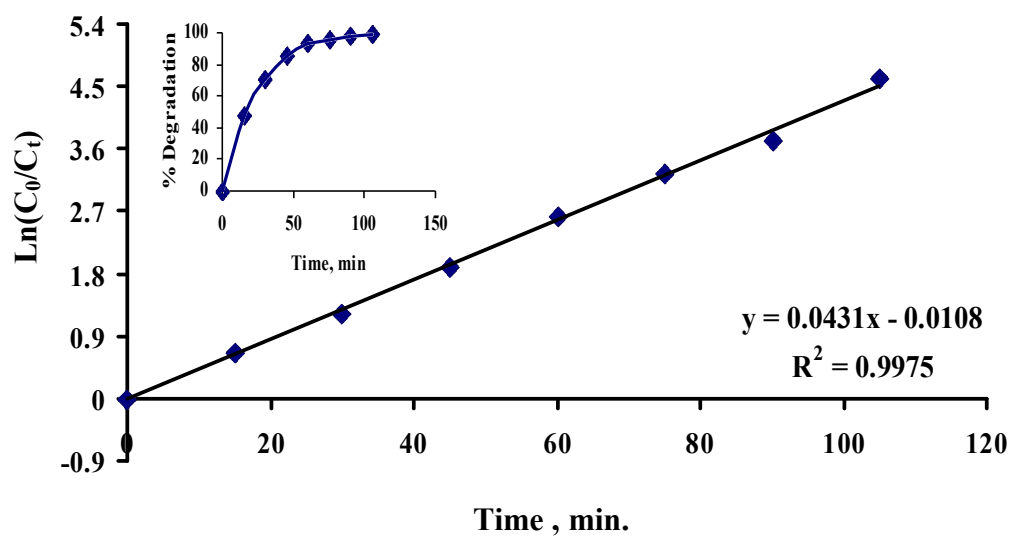


Figure 3-49: Rate of OG photodegradation onto 2% Au-TiO₂ surface under solar illumination; inset shows degradation percent.

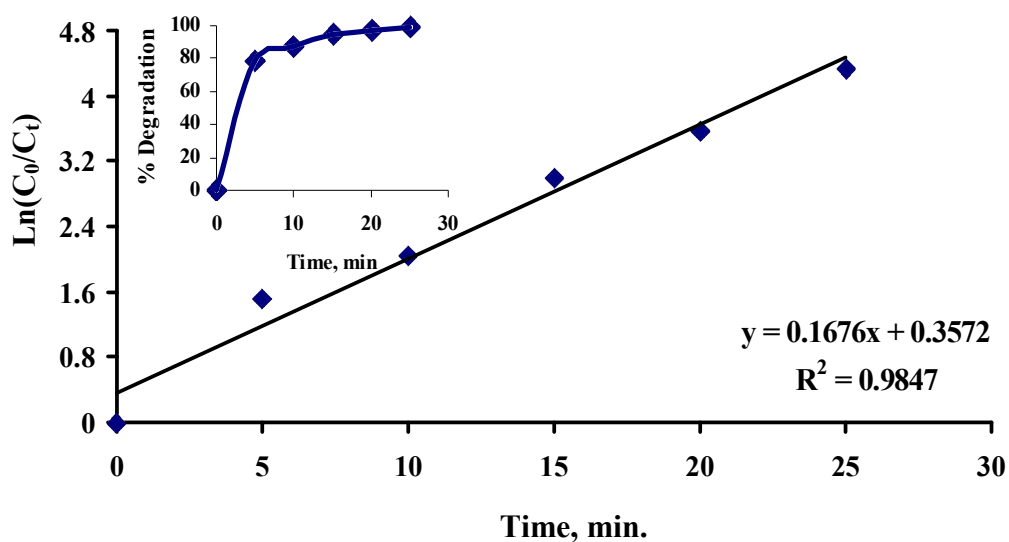


Figure (3-50): Rate of OG photodegradation onto 4% Pt-TiO₂ surface under solar illumination; inset shows degradation percent.

3.10 Comparison of reductive methodologies for Au and Pt onto nano TiO₂ slurry particles

Figures (3-51) and (3-52) depict a comparison between Au–TiO₂ and Pt–TiO₂ prepared by the chemical reduction methods (CR) employing 2-Oxoglutaric acid, Sodium borohydride and Citric acid and also UV-illumination (UVR), respectively. Upon reaction results, the chemical reduction method for Au–TiO₂ synthesis especially prepared by 2-Oxoglutaric acid, demonstrated the highest degradation rate for OG dye in comparison with other chemical and illumination methods of preparation. These results point to clearly that only when Au was gradually reduced from Au^{III} to Au⁰ the activity of the gold catalysts was significantly enhanced [141]. Whereas, UVR illumination method for Pt–TiO₂ preparation revealed the best photodegradation for OG among the other chemical and irradiation techniques. Samples modified by using UV light source for PtCl₆²⁻ anions reduction had a higher photocatalytic activity than samples modified using other reducing agents [142].

As for any redox reaction, the values of the standard reduction potentials (E^0) determine the pairs of reactants required for successful chemical conversion. This means that the free energy change in the reaction, ΔG^0 , must be negative, or what is equivalent to $\Delta E^0 > 0$ [143]. Thus, in the case of gold, the relatively large electropositive reduction potential of $[\text{AuCl}_4]^- + 3e^- \rightarrow \text{Au}_{(s)} + 4\text{Cl}^-$ $E^0 = +0.93$ V, $\text{PtCl}_6^{2-} + 2e^- \rightarrow \text{PtCl}_4^{2-} + 2\text{Cl}^-$ $E^0 = +0.726$ V, permits the use of several reducing agents, for example sodium citrate $E^0 = -0.180$ V and sodium borohydride $E^0 = -0.481$ V.

On the basis of the above findings, we may report here that gold could be doped (reduced) onto TiO₂ quantitatively using chemical reduction route rather than UV irradiation method, whereas, platinum behaves differently where UV irradiation technique exhibited superior doping over the chemical reduction route.

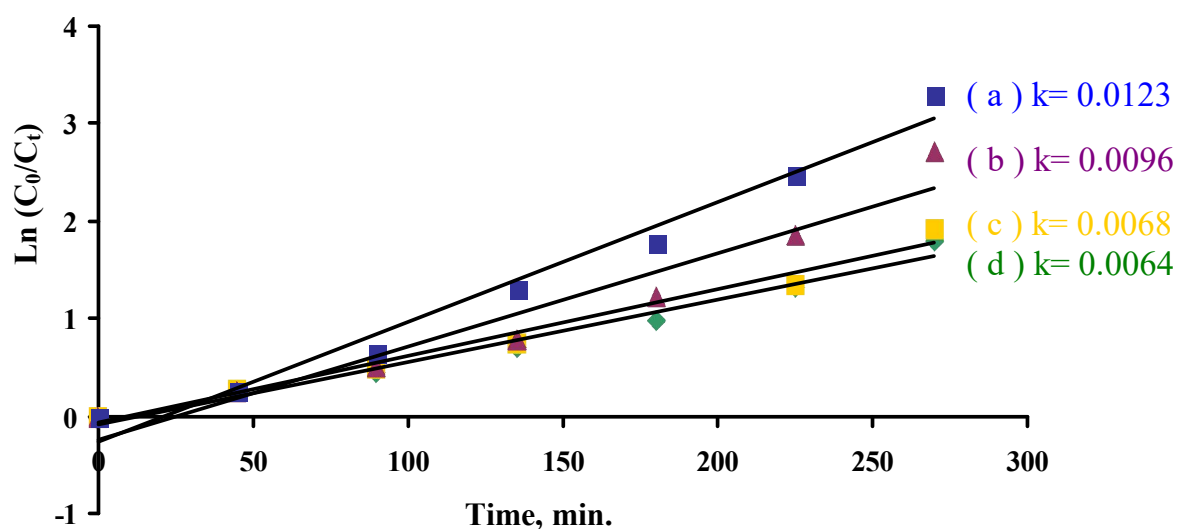


Figure (3-51): Effect of UVR and CR methods on the rate of OG degradation under visible illumination employing 2% Au-TiO₂: (a) 2-Oxoglutaric acid; (b) UV; (c) Sodium borohydride; (d) Citric acid .

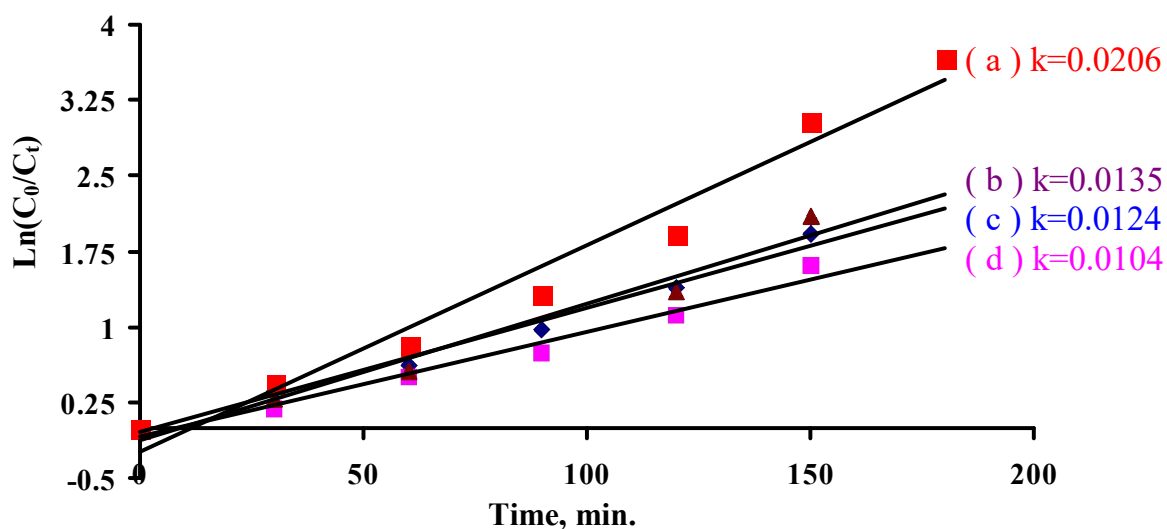


Figure (3-52): Effect of UVR and CR methods on the rate of OG degradation under visible illumination employing 2% Pt-TiO₂: (a) UV; (b) Sodium borohydride; (c) 2-Oxoglutaric acid; (d) Citric acid.

3.11 Predicted mechanism for Orange G degradation

The mechanism of the degradation of azo dyes by visible light is very complex because of different reaction possibilities. Hydroxyl radical is a strong oxidizing agent and thus oxidizes dye molecules and leads to its complete mineralization [144]. The mechanism of OG azo dye degradation may be expected as it is illustrated in Figure (3-53).

The degradation of the OG appears to involve primarily oxidative steps; the cleavage of the C–N bond resulting in aniline and 1-hydroxylamine-2-naphthol-6,8-disulfonic acid intermediate (1), indicating different generation rate of hydroxyl radical between the photolysis and catalysts (Au-TiO₂ and Pt-TiO₂). The hydroxyl products of 7-hydroxy-8-(hydroxyamino) naphthalene-1,3-disulfonic acid as the consequence of OH hydroxyl radical attack including 2, 3, 4 and 5 steps were detected by Cai et al. [145].

The another possible degradation pathway of the dye is the reactions of hydroxyl radicals with the N=N bond with a generation of benzene and 2-naphthol-6,8-disulfonic acid (6) and its hydroxy products (2).

The third probable pathway is shown in Figure (3-54). This reaction involves intermolecular dehydration forms 7,8 epoxyazonaphthalene-1,3 disulfonic acid (8), which was also reported by Muruganandham et al. [146] in the degradation process of Reactive Orange 4 using TiO₂-P25. The detected 7-hydroxy-8- azophenyl-naphthalene-1-sulfonic acid (9) and 7-oxy-8-azonaphthalene-(1'-oxy-2'-azo-phenyl)-1-sulfonic acid (10) also indicated the reactions of desulfonation of sulfuric acid and the intermolecular dehydration [147]. Mostly, the photocatalytic degradation processes for organic moieties lead finally to carbon dioxide and water post successive photoreactions.

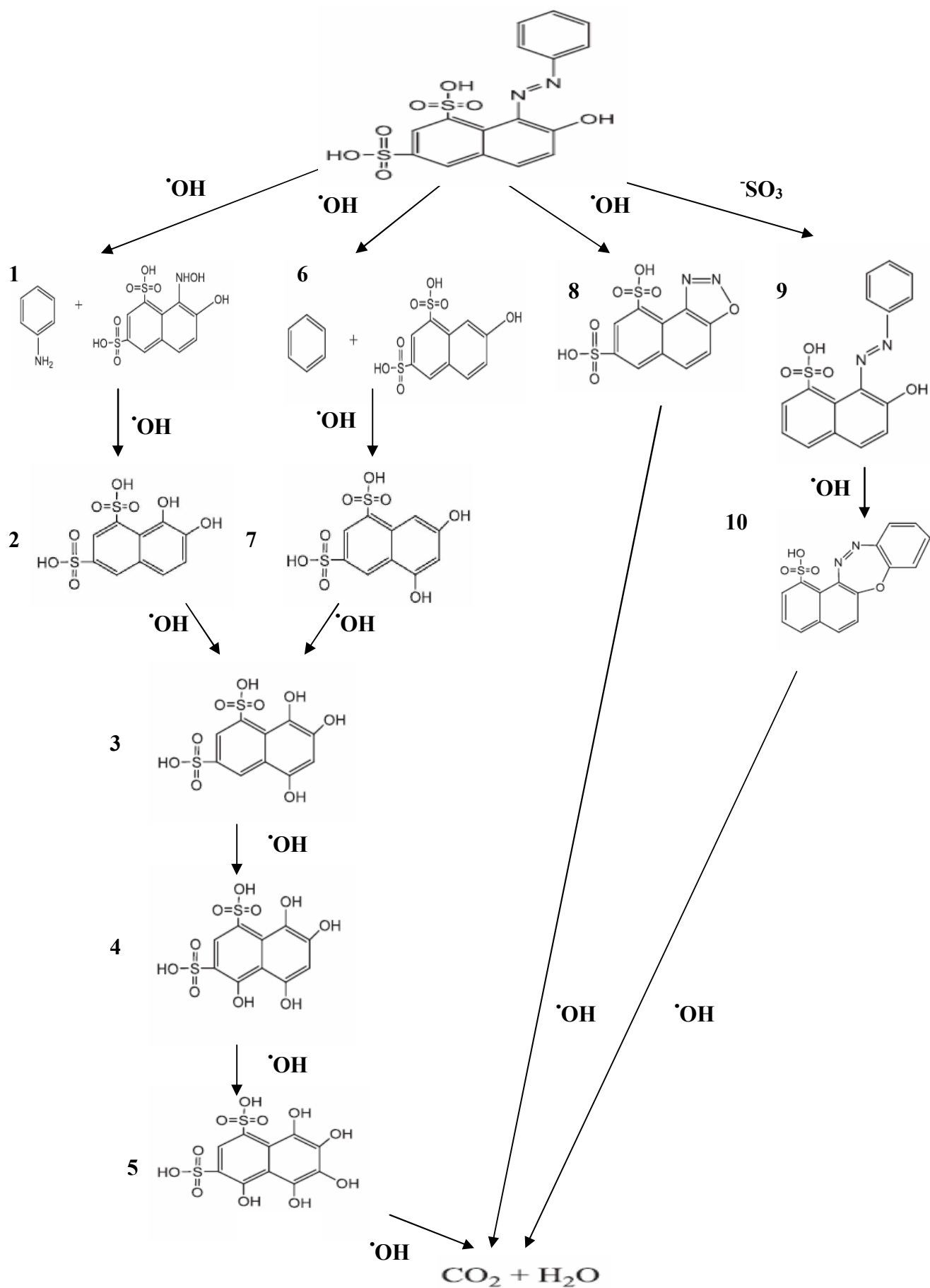


Figure (3-53): Schematic diagram of degradation pathways of Orange G.

3.12 Comparison and evaluation of photocatalytic degradation of OG azo dye using Au-TiO₂ and Pt-TiO₂

The comparison of photodegradation of OG employing Au-TiO₂ and Pt-TiO₂ under optimum experimental conditions, revealed that both photocatalysts responded positively under visible light and further, operated optimally at acidic media (pH = 3), despite slight differences in their points of zero charges; 6.0, for Au-doped TiO₂ and 6.2, for Pt-doped TiO₂ particles. Nevertheless, the experimental results exhibited lower rate constant and longer half-life for Au-TiO₂ (0.0123 min⁻¹, 56 min.) but higher rate constant and shorter half-life for Pt-TiO₂ (0.0746 min⁻¹, 9 min.). Also from thermodynamic aspect and despite the higher activation energy required in case of Pt-TiO₂, our experimental results revealed better rates for Pt-TiO₂ powders in comparison to Au-TiO₂ suspension. Hence, this is stand-alone verification for an independence of photocatalysis on the thermodynamic properties of the photocatalysts.

Several explanations [62,148-149] have been appeared in the literature concerning the increased photocatalytic activity of Pt/TiO₂ over Au/TiO₂; Schmickler and Santos [148] reported that the increased photocatalytic activity of Pt/TiO₂ over Au/TiO₂ could be attributed to the density of states in the vicinity of the Fermi level of Pt which is higher and consists mainly of contributions from d electrons. In contrast, the d band in Au lies much lower, and the density of states at the Fermi level is consequently lower.

A second explanation for the higher photocatalytic activity of Pt/TiO₂ may be probably due to the size of the Au and Pt particles. The higher size (Au) might block the active sites for the OG oxidation and/or reduce the number of active sites on which the oxygen reduction can proceed.

Furthermore, Ismail et al. [149] also expected that the kinetics of the oxygen reduction would also be determined by the oxophilicity of the Pt nanoparticles.

Additionally, under visible irradiation, the incident photons are absorbed by Au particles (SPR peak wavelength: ~520 nm in a visible light region) through SPR excitation. Then, electrons transfer from the plasmon-excited Au to the conduction band of TiO₂ [62]. This is generally believed to be one of the reasons why the OG photodegradation is kinetically hindered on Au.

Other than these explanations, Sato et al. [150] stated that the increase in photoconversion of H₂O to H₂ upon a Pt–TiO₂ catalyst system employment is due to the creation of a Schottky barrier at the interface of the metal–semiconductor, which was also confirmed by Chen et al. [151]. Whereas, Au, Ag and Cu follow Surface Plasmon Resonance phenomenon which is based on three mechanisms [152, 153]; photon scattering, hot electron transfer and Plasmon Resonance Energy Transfer (PRET).

3.13 Conclusions and Suggestions

3.13.1 Concluding remarks

The photodegradation of Orange G (OG) as anionic model dye in aqueous media was investigated employing laboratory synthesized nano Au-TiO₂ and Pt-TiO₂ semiconductor photocatalysts under visible light illumination. Several spectroscopic advanced machines, namely; SEM, TEM, EDX, XRD and BET have been utilized for the characterization of the prepared Au and Pt doped nano TiO₂ powders.

SEM and TEM images illustrated smooth surfaces with high dispersion of Au and Pt metal atoms. EDXS measurements revealed the content of the precious metal doped powders which were resulted from the doping

process. BET measurements verified the mesoporosity of the impregnated photocatalyst powders and the adsorption-desorption isotherm plots resulted in surface areas of 130, 121 and 109 m²/g for TiO₂, Au-TiO₂ and Pt-TiO₂ specimen, respectively. XRD patterns confirmed the existence of Au and Pt diffraction signals within the photocatalyst pattern and revealed an average crystalline size of 15.3, 14.2 and 12.4 nm for TiO₂, Au-TiO₂ and Pt-TiO₂ specimen, respectively.

The impacts of several operational parameters namely; initial pH, OG initial concentration, Au and Pt abundance, Au-TiO₂ and Pt-TiO₂ loadings and visible light intensity on the photodegradation of Orange G dye has been investigated. The photocatalytic process is favored at solution pH of 3 for both photocatalysts, 40 mg/l loading for 2% Au-TiO₂ and 50 mg/l loading for 4% Pt-TiO₂ and 10 mg/l of initial dye concentration.

Furthermore, the apparent quantum yield was also explicitly influenced by photocatalysis solution pH, Au-TiO₂ and Pt-TiO₂ loadings and initial dye concentration.

The kinetics and thermodynamics of the photodegradation of OG employing both Au-TiO₂ and Pt-TiO₂ photocatalysts have also been explored. The kinetics of the photocatalytic oxidation follows the pseudo first order. Moreover, an increase of the photocatalysis process temperature has revealed positive impacts on the kinetics of the process following the Arrhenius relation. The activation energies of the degradation for OG using Au-TiO₂ and Pt-TiO₂ were found to be 14.66 and 36.29 kJ mol⁻¹, respectively.

Gold has been doped onto TiO₂ quantitatively using chemical reduction route rather than UV irradiation method, whereas, platinum behaves differently where UV irradiation technique exhibited superior doping over the chemical reduction route. The experimental results exhibited

lower rate constant and longer half life for OG degradation using Au-TiO₂ but higher rate constant and shorter half life employing Pt-TiO₂, i.e; better photocatalytic activity of Pt/TiO₂ over Au/TiO₂.

Under optimum experimental conditions, the solar photodegradation of OG attained better process rate and yield in comparison to the laboratory outcomes for both Au-TiO₂ and Pt-TiO₂ photocatalysts.

3.13.2 Suggestions

In the light of the present research work, several suggestions for the future research activities can be reported:

- 1- Since the solar photocatalytic process has exhibited interesting and green chemistry friendly results, we would suggest employing immobilized nano Au-TiO₂ and Pt-TiO₂ prototype systems for the photodetoxification of the photomineralization of persisting organic moieties like poly aromatic hydrocarbons (PAH) and azo pollutants under solar irradiation.
- 2- The study of the photocatalytic decontamination of the persisting organic pollutants in aqueous media together with computational authentication could be an interesting extension of this work.
- 3- Adoption of semiconductor sensitization by means of dyes and coupling via other low band gap photocatalyst based on 2D and 3D structural materials could also be a good progressive pace for future work research.



References

- [1] M. A . Rauf , M . A . Meetani, S. Hisaindee, " An overview on the photocatalytic degradation of azo dyes in the presence of TiO₂ doped with selective transition metals", *Desalination* 276 (2011) 13-27.
- [2] A. Giwa, P. O. Nkeonye, K. A. Bello, K. A. Kolawole, " Photocatalytic decolourization and degradation of C. I. Basic Blue 41 using TiO₂ nanoparticles ", *J. Environ. Prot. Ecol.* 3 (2012) 1063-1069.
- [3]. R. Munter, " Advanced oxidation processes: current status and prospects ", *Proc. Estonian Acad. Sci. Chem.* 50 (2001) 59-80.
- [4]. Y. A. Mustafa, R. R. Omran, " Treatment of furfural wastewater by (AOPs) photo-fenton method ", *J. Eng.* 21(2015) 129-141.
- [5] M. Fathinia, A. R. Khataee, M. Zarei, S. Aber, " Comparative photocatalytic degradation of two dyes on immobilized TiO₂ nanoparticles: effect of dye molecular structure and response surface approach ", *J. Mol. Catal. A: Chem.* 333 (2010) 73-84.
- [6] A. AL-Kdasi, A. Idris, K. Saed, C. T. Guna, " Treatment of textile wastewater by advanced oxidation processes –a review " *Global Nest J.* 6 (2004) 222-230.
- [7] E. Guivarch, S. Trevin, C. Lahitte, M. A. Oturan, " Degradation of azo dyes in water by electro-fenton process ", *Environ Chem. Lett.* 1 (2003) 38-44.
- [8] M. I. Litter, N. Quici, " Photochemical advanced oxidation processes for water and wastewater treatment ", *Recent Patents on Engineering* 4 (2010) 217-241 .
- [9] A. Goi, " Advanced oxidation processes for water purification and soil remediation ", M.Sc. Thesis, Tallinn University of Technology, 2005.
- [10] C. C. A. Loures, M. A. K. Alcântara, H. J. I. Filho, A. C. S. C. Teixeira, F. T. Silva, T. C. B. Paiva, G. R. L. Samanamud, " Advanced oxidative degradation processes: fundamentals and applications", *Int. Rev. Chem. Eng.* 5 (2013) 102-120.

- [11] B. Grote, " Application of advanced oxidation processes (AOP) in water treatment " 37th Annual old Water Industry Operations Workshop Parklands, Gold Coast. (2012) 17-23.
- [12] M. L. Satuf, M. J. Pierrestegui, L. Rossini, R. J. Brandi, O. M. Alfano, " Kinetic modeling of azo dyes photocatalytic degradation in aqueous TiO₂ suspensions. toxicity and biodegradability evaluation " *Catal. Today* 161 (2011) 121–126.
- [13] S. Sharma, J. P. Ruparelia, M. L. Patel, " A general review on advanced oxidation processes for waste water treatment " Nirma University International Conference, Ahmedabad (2011).
- [14] F. Olalla, M. & J. P. Pérez., " Combination of advanced oxidation processes with biological treatment for the remediation of water polluted with herbicides " *Universitat Autònoma de Barcelona* (2007).
- [15] A. L. N. Mota, L. F. Albuquerque, L. T. C. Beltrame, O. Chiavone-Filho, A. M. Junior, C. A. O. Nascimento, " Advance oxidation processes and their application in the petroleum industry :a review " *Braz. J. Petrol. Gas* 2 (2008) 122-142.
- [16] M. Termtanun, " Photocatalytic degradation of pesticides using TiO₂ nanoparticles " Ph.D. Thesis, University of Nottingham, 2013.
- [17] K. M. Mezughi, " Heterogeneous photocatalytic degradation of organic pollutants in water over nanoscale powdered titanium dioxide " Ph.D. Thesis, University of Bradford, 2010.
- [18] U. I. Gaya, A. H. Abdullah, " Heterogeneous photocatalytic degradation of organic contaminants over titanium dioxide: a review of fundamentals, progress and problems " *J. Photochem. Photobiol. C* 9 (2008) 1-12.

- [19] S. Alahiane, S. Qourzal, M. El Ouardi, A. Abaamrane, A. Assabbane, " Factors influencing the photocatalytic degradation of reactive yellow 145 by TiO₂-coated non-woven fibers " *Am. J. Anal. Chem.* 5 (2014) 445-454.
- [20] F. X. Xiao, J. Miao , H. B. Tao, S. F. Hung, H. Y. Wang, H. B. Yang, J. Chen, R. hen, B. Liu, " One-dimensional hybrid nanostructures for heterogeneous photocatalysis and photoelectrocatalysis " *Small* 11 (2015) 2115-2131.
- [21] H. Li, " Synthesis of titanium dioxide photocatalyst with the aid of supercritical fluids " Ph.D. Thesis, University of South Florida, 2013.
- [22] X. Hu, " Synthesis and characterization of graphene oxide-modified Bi₂WO₆ and its use as photocatalyst " Ph.D. Thesis, University of Ottawa, 2014.
- [23] Z. Jinkai, " Modified titanium dioxide (TiO₂) photocatalysts for the degradation of organic pollutants in wastewater " Ph.D. Thesis, National University of Singapore, 2007.
- [24] P. Pattanaik, " TiO₂ photocatalysis: design and biomedical applications " *Appl. Sci. Adv. Mater. Int.* 6 (2015) 192–202.
- [25] S.M. M. Fonseca, " Development of scanning electrochemical microscopy for the investigation of photocatalysis at semiconductor surfaces " Ph.D. Thesis, University of Warwick, 2002.
- [26] V. Diesen " Heterogeneous TiO₂ photocatalysis: fundamental chemical aspects and effects of solid phase alterations" Doctoral Thesis in Chemistry, ISBN 978-91-7501-930-7, University of Paris, 2013.
- [27] X. Chen, " Synthesis and investigation of novel nanomaterials for improved photocatalysis " Ph.D. Thesis, Case Western Reserve University, 2015.

- [28] N. M. Nursam, X. Wang, R. A. Caruso, " High-throughput synthesis and screening of titania-based photocatalysts " *ACS Comb. Sci.* 17 (2015) 548–569.
- [29] S. E. Salas, " Photocatalytic water splitting using a modified Pt-TiO₂. kinetic modeling and hydrogen production efficiency " *Doctoral dissertation, University of Western Ontario, 2013.*
- [30] S. Mondal, C. G. Bhagchandani, " Novel effluent treatment technique in textile industry " *Int. J. Adv. Innov. Ideas educ.* 2 (2016) 2395-4396.
- [31] C. H. Wu, C. L. Chang, " Decolorization of reactive red 2 by advanced oxidation processes: comparative studies of homogeneous and heterogeneous systems " *J. Hazar. Mater.* , 128 (2006) 265–272.
- [32] I. T. Peternel, N. Koprivanac, A. M. L. Božić, H. M. Kušić, " Comparative study of UV/TiO₂, UV/ZnO and photo-fenton processes for the organic reactive dye degradation in aqueous solution " *J. Hazar. Mater.* 148 (2007) 477–484.
- [33] K. R. Reddy, B. V. Rao, C. Sarala, " Proceeding of 4th international conference on hydrology and watershed management ", center for water resources, Telangana state, India , 2014.
- [34] R. S. Juang, S. H. Lin, P. Y. Hsueh, " Removal of binary azo dyes from water by UV-irradiated degradation in TiO₂ suspensions " *J. Hazar. Mater.*, 182 (2010) 820–826.
- [35] A. K. Gupta, A. Pal, C. Sahoo, " Photocatalytic degradation of a mixture of Crystal Violet (basic violet 3) and methyl red dye in aqueous suspensions using Ag⁺ doped TiO₂ " *Dyes Pigm.* 69 (2006) 224-232.
- [36] C. G. Niu, Y. Wang, X. G. Zhang, G. M. Zeng, D. W. Huang, M. Ruan, X. W. Li, " Decolorization of an azo dye Orange G in microbial fuel cells using Fe(II)-EDTA catalyzed persulfate " *Bioresour. Technol.* 126 (2012) 101–106.

- [37] S. Brosillon, H. Djelal, N. Merienne, A. Amrane, " Innovative integrated process for the treatment of azo dyes: coupling of photocatalysis and biological treatment " *Desalination* 222 (2008) 331–339.
- [38] M. A. M. Salleh, D. K. Mahmoud, W. A.W. A. Karim, A. Idris, " Cationic and anionic dye adsorption by agricultural solid wastes: a comprehensive review " *Desalination* 280 (2011) 1–13.
- [39] C. S. Keng, Z. Zainal, A. H. Abdullah, " Removal of cationic and anionic dyes by immobilized titanium dioxide loaded activated carbon " *Malays. J. Anal. Sci.* 12 (2008) 451 – 457.
- [40] I. N. Ismaeel, " Photobleaching of dye pollutants onto immobilized TiO₂ anatase nanocatalyst " M.Sc. Thesis, AL-Nahrain University, 2016.
- [41] M. Ali, W. Bux, " Application of bioenzymatic soil stabilization in comparison to macadam in the construction of transport infrastructure " *J. Clean WAS* 1 (2017) 1-4.
- [42] O.O. Ajani, O.E. Akinremi, A.O. Ajani, A.E. Osoh, W.U. Anake, " Synthesis and spectroscopic study of naphtholic and phenolic azo dyes " *Phys. Rev. Res. Int.* 3 (2013) 28-41.
- [43] N. J. Ara, " Development of dyes removal method from textile waste water " Ph.D. Thesis, University of Dhaka, 2015.
- [44] M. M. A. Unis, " Peroxide reactions of environmental relevance in aqueous solution " Ph.D. Thesis, University of Northumbria, 2010.
- [45] Y. Zhang, G. P. Berman, S. Kais, " The radical pair mechanism and the avian chemical compass: quantum coherence and entanglement " *Int. J. Quantum Chem.* 115 (2015) 1327-1341.
- [46] S. Gligorovski, R. Streckowski, S. Barbati, D. Vione, " Environmental Implications of Hydroxyl Radicals ($\cdot\text{OH}$) " *Chem. Rev.* 115 (2015) 13051-13092.

- [47] J. Zhang, Y. Nosaka, " Mechanism of the OH radical generation in photocatalysis with TiO₂ of different crystalline types " *J. Phys. Chem.* 118 (2014) 10824–10832.
- [48] A. Buthiyappan, A. R. A. Aziz, W. M. A. W. Daud, " Recent advances and prospects of catalytic advanced oxidation process in treating textile effluents " *Rev. Chem. Eng.* 32 (2016) 1–47.
- [49] Solarchem Environmental Systems, " The Uv/Oxidation handbook " Markham, Ontario, Canada ; Las Vegas 1994.
- [50] A. Heponiemi, U. Lassi, " Advanced oxidation processes in food industry wastewater treatment-a review " INTECH Open Access Publisher, 2012.
- [51] M. Rodríguez, " Fenton and UV-vis based advanced oxidation processes in wastewater treatment: degradation, mineralization and biodegradability enhancement " Universitat de Barcelona, 2003.
- [52] K. Ikehata, N. J. Naghashkar, M. G. El-Din, " Degradation of aqueous pharmaceuticals by ozonation and advanced oxidation processes: a review " *Ozone Sci. Eng.* 28 (2006) 353-414.
- [53] M. A. Lazar, S. Varghese, S. S. Nair, " Photocatalytic water treatment by titanium dioxide: recent updates " *Cat.* 2(2012) 572-601.
- [54] K. M. Mayer, J. H. Hafner, "Localized surface plasmon resonance sensors" *Chem. Rev.* 111(2011) 3828-3857.
- [55] X. M. Zhang, Y. L. Chen, R. S. Liu and D. P. Tsai, " Plasmonic photocatalysis " *Rep. Prog. Phys.* 76 (2013).
- [56] C. Wang, D. Astruc, " Nanogold plasmonic photocatalysis for organic synthesis and clean energy conversion " *Chem. Soc. Rev.* 43 (2014) 7188-7216.
- [57] E. Petryayeva, U. J. Krull, " Localized surface plasmon resonance: nanostructures, bioassays and biosensing - a review " *Anal. Chim. Acta* 706 (2011) 8-24.

- [58] K. L. Kelly, E. Coronado, L. L. Zhao, G. C. Schatz, " The optical properties of metal nanoparticles: the influence of size, shape, and dielectric environment " *J. Phys. Chem. B* 107 (2003) 668-677.
- [59] S. Eustis, M. A. El-Sayed, " Why gold nanoparticles are more precious than pretty gold: noble metal surface plasmon resonance and its enhancement of the radiative and nonradiative properties of nanocrystals of different shapes " *Chem. Soc. Rev.* 35 (2006) 209-217.
- [60] X. Zhou, G. Liu, J. Yu, W. Fan, " Surface plasmon resonance-mediated photocatalysis by noble metal-based composites under visible light " *J. Mater. Chem.* 22 (2012) 21337-21354.
- [61] Y. Liua, H. Yub, X. Quanc, " Fabrication and visible response of Au-TiO₂ (P25) composite photocatalyst with obvious surface plasmon resonance effect " *Adv. Mater. Res.* 465 (2012) 215-219.
- [62] J. Yan, G. Wu, N. Guan, L. Li, " Synergetic promotion of the photocatalytic activity of TiO₂ by gold deposition under UV-visible light irradiation " *Chem. Commun.* 49 (2013) 11767-11769.
- [63] C. Fu, M. Li, H. Li, C. Li, X. .G. Wu, B. Yang, " Fabrication of Au nanoparticle/TiO₂ hybrid films for photoelectrocatalytic degradation of methyl orange" *J. Alloys Compd.* 692 (2017) 727-733.
- [64] V. Subramanian, E. E. Wolf, P. V. Kamat, " Catalysis with TiO₂/Gold nanocomposites. Effect of metal particle size on the Fermi level equilibration " *J. Am. Chem. Soc.* 126 (2004) 4943-4950.
- [65] Á. Kmetykó, K. Mogyorósi, V. Gerse, Z. Kónya, P. Pusztai, A. Dombi, K. Hernádi, " Photocatalytic H₂ production using Pt-TiO₂ in the presence of oxalic acid: influence of the noble metal size and the carrier gas flow rate " *Mater.* 7 (2014) 7022-7038.

- [66] W. Choi, A. Termin, M. R. Hoffmann, " The role of metal ion dopants in quantum-sized TiO₂: correlation between photoreactivity and charge carrier recombination dynamics " *J. Phys. Chem.* 98 (1994) 13669-13679.
- [67] A. Matsuda, S. Sreekantan, W. Krengvirat, " Well-aligned TiO₂ nanotube arrays for energy-related applications under solar irradiation " *J. Asian Cer. Soc.* 1 (2013) 203-219.
- [68] A. Mahmood, S. M. Ramay, Y. S. Al-Zaghayer, S. Atiq, S. H. Ansari, " Thermal/plasma treatment effect on photocatalytic degradation of aqueous solution of methylene blue using Au-doped Fe/TiO₂ photocatalyst " *Desalin. Water Treat.* 57 (2016) 5183-5192.
- [69] Z. He, J. Fu, B. Cheng, J. Yu, S. Cao, "Cu₂(OH)₂CO₃ clusters: Novel noble-metal-free cocatalysts for efficient photocatalytic hydrogen production from water splitting " *Appl. Catal. B: Environ.* 205 (2017) 104–111.
- [70] M. J. H. Rodríguez, E. P. Meliána, D. G. Santiagoa, O. G. Díaz, J.A. Navíoc, J.M. D. Rodríguez, "NO photooxidation with TiO₂ photocatalysts modified with gold and platinum " *Appl. Catal. B: Environ.* 205 (2017) 148–157.
- [71] B. Liu, S. Su, W. Zhou, Y. Wang, D. Wei, L. Yao, Y. Ni, M. Cao, C. Hu, " Photo-reduction assisted synthesis of W-doped TiO₂ coupled with Au nanoparticles for highly efficient photocatalytic hydrogen evolution " *Cryst Eng. Comm.* (2017) 1-8.
- [72] F.B. Li, X.Z. Li, " The enhancement of photodegradation efficiency using Pt–TiO₂ catalyst " *Chemosphere* 48 (2002) 1103-1111.
- [73] H. Chen, Y. Ku, Y. Kuo, " Effect of Pt/TiO₂ characteristics on temporal behavior of o-cresol decomposition by visible light-induced photocatalysis " *Water Res.* 41 (2007) 2069-2078.

- [74] B. Kraeutler, A. J. Bard, " Heterogeneous photocatalytic preparation of supported catalysts. Photodeposition of platinum on titanium dioxide powder and other substrates " *J. Am. Chem. Soc.* 100 (1978) 4317- 4318.
- [75] J. Ohyama, A. Yamamoto, K. Teramura, T. Shishido, T. Tanaka, " Modification of metal nanoparticles with TiO₂ and metal-support interaction in photodeposition " *ACS Catal.* 1 (2011) 187-192.
- [76] K. Wenderich, " photodeposition of platinum nanoparticles on well-defined tungsten oxide " Ph.D Thesis, universiteit Twente, 2016.
- [77] M.C. Hidalgo, J.J. Murcia, J.A. Navio, G. Colon, " Photodeposition of gold on titanium dioxide for photocatalytic phenol oxidation " *Appl. Catal. A* 397 (2011) 112-120.
- [78] A. Tanaka, A. Ogino, M. Iwaki, K. Hashimoto, A. Ohnuma, F. Amano, B. Ohtani, H. Kominami, " Gold–Titanium (IV) Oxide plasmonic photocatalysts prepared by a colloid-photodeposition method: correlation between physical properties and photocatalytic activities " *Langmuir* 28 (2012) 13105-13111.
- [79] Á. Kmetykó, K. Mogyorósi, P. Pusztai, T. Radu, Z. Kónya, A. Dombi, K. Hernádi, " Photocatalytic H₂ evolution using different commercial TiO₂ catalysts deposited with finely size-tailored Au nanoparticles: critical dependence on Au particle size " *Materials* 7 (2014) 7615-7633.
- [80] K. Tanabe, T. Sumiyoshi, K. Shibata, T. Kiyoura, J. Kitagawa, " New hypothesis regarding surface acidity of binary metal-oxides " *Bull. Chem. Soc. Japan* 47 (1974) 1064-1066.
- [81] M. Zhou, J. Zhang, B. Cheng, H. Yu, " Enhancement of visible light photocatalytic activity of mesoporous Au-TiO₂ nanocomposites by surface plasmon resonance " *int. J. Photoenergy* (2012) 1-10.

- [82] A. Masakazu, M. Takeuchi, " The design and development of highly reactive titanium oxide photocatalysts operating under visible light irradiation " *J. Catal.* 216 (2003) 505-516.
- [83] Z. Barzgari, A. Ghazizadeh, S. Z. Askari, " Preparation of Mn-doped ZnO nanostructured for photocatalytic degradation of Orange G under solar light " *Res. Chem. Intermed.* 42 (2016) 4303-4315.
- [84] A. Roy, S. Chakraborty, S. P. Kundu, B. Adhikari, S. B. Majumder, " Lignocellulosic jute fiber as a bioadsorbent for the removal of azo dye from its aqueous solution: Batch and column studies " *J. Appl. Poly. Sci.* 129 (2013) 15-27.
- [85] G. Thennarasu, S. Kavithaa, A. Sivasamy, (2012). " Photocatalytic degradation of Orange G dye under solar light using nanocrystalline semiconductor metal oxide" *Environ. Sci. Pollut. Res.* 19 (2012) 2755-2765.
- [86] C. G. Hatchard, C. A. Parker, "A new sensitive chemical actinometer. II . potassium ferrioxalate as a standard chemical actinometer" *Math. Phys. Sci.* 235 (1956) 518-536.
- [87] A. A. Hussain, " Photocatalytic oxidation of phenol red on nanocrystalline TiO₂ particles" M.Sc. thesis, AL-Nahrain university , 2014 pp.14 ,27, 78.
- [88] R. Asahi, T. Morikawa, T. Ohwaki, K. Aoki, Y. Taga, " Visible-light photocatalysis in nitrogen-doped titanium oxides " *Sci.* 293 (2001) 269-271.
- [89] S. Mahshid, M. S. Ghamsari, M. Askari, N. Afshar, S. Lahuti, " Synthesis of TiO₂ nanoparticles by hydrolysis and peptization of titanium isopropoxide solution " *Semicond. Phys. Quantum Electron. Optoelectron.* 9 (2006) 65-68.

- [90] M. A. Meetani, M. A. Rauf, S. Hisaindee, A. Khaleel, A. AlZamly, A. Ahmad, " Mechanistic studies of photoinduced degradation of Orange G using LC/MS " *Rsc. Adv.* 1 (2011) 490-497.
- [91] G. Zhang, Y. Hong, W. He , " Experimental study of factors affecting Pt-TiO₂ thermal catalytic oxidation of formaldehyde " *Indoor Built Environ.* 24 (2015)138–144.
- [92] J. Jiu, S. Isoda, M. Adachi, F. Wang, " Preparation of TiO₂ nanocrystalline with 3–5 nm and application for dye-sensitized solar cell " *J. of Photochem. Photobiol. A: Chemistry* 189 (2007) 314–321.
- [93] L.E. Brus, "Electron–electron and electronhole interactions in small semiconductor crystallites: The size dependence of the lowest excited electronic state" *J. Chem. Phys.* 80 (1984) 4403-4409.
- [94] A. A. Hussain, H. S. Wahab " Synthesis and spectroscopic characterization of anatase TiO₂ nanoparticles " *Int. J. Nanotechnol. Nanosci.* 2 (2014) 1- 6.
- [95] M. M. Khan, J. Lee, M. H. Cho, " Au@TiO₂ nanocomposites for the catalytic degradation of methyl orange and methylene blue: An electron relay effect " *J. Ind. Eng. Chem.* 20 (2014)1584-1590.
- [96] A. Ofiarska, A. Pieczynska, A. F. Borzyszkowska, P. Stepnowski, E. M. Siedlecka, " Pt–TiO₂-assisted photocatalytic degradation of the cytostatic drugs ifosfamide and cyclophosphamide under artificial sunlight " *Chem. Eng. J.* 285 (2016) 417-427.
- [97] J. Sun, L. Qiao, S. Sun, G. Wang, " Photocatalytic degradation of Orange G on nitrogen-doped TiO₂ catalysts under visible light and sunlight irradiation" *J. Hazar. Mater.* 155 (2008) 312-319.
- [98] J. Sun, X. Wang , J. Sun, R. Sun, S. Sun, L. Qiao, " Photocatalytic degradation and kinetics of Orange G using nano-sized Sn(IV)/TiO₂/AC photocatalyst " *J. Mol. Catal. A: Chem.* 260 (2006) 241-246.

- [99] G. K. Naik, P. M. Mishra, K. Parida, " Green synthesis of Au/TiO₂ for effective dye degradation in aqueous system " *Chem. Eng. J.* 229 (2013) 492-497.
- [100] W. W. Dunn, Y. Aikawa, A. J. Bard, " Characterization of particulate titanium dioxide photocatalysts by photoelectroretic and electrochemical measurements" *J. Am. Chem. Soc.* 100(1981) 3456-3459.
- [101] Y. S. Ma, C. N. Chang, Y. P. Chiang, H. F. Sung , A. C. Chao, " Photocatalytic degradation of lignin using Pt/TiO₂ as the catalyst " *Chemosphere* 71 (2008) 998-1004.
- [102] K. H. Wang, Y. H. Hsieh, L. J. Chen, " The heterogeneous photocatalytic degradation, intermediates and mineralization for the aqueous solution of cresols and nitrophenols " *J. Hazar. Mater.* 59 (1998) 251-260.
- [103] J. Madhavan, F. Grieser, M. Ashokkumar, " Degradation of Orange-G by advanced oxidation processes" *Ultrason. Sonochem.* 17 (2010) 338-343.
- [104] H. S. Wahab, T. Bredow, S. M. Aliwi " Computational investigation of water and oxygen adsorption on the anatase TiO₂ (100) surface " *J. Molec. Struct.:Theochem.* 868 (2008) 101-108.
- [105] H. S. Wahab, A. D. Koutselos " A Computational study on the adsorption and ·OH initiated photochemical and photocatalytic primary oxidation of aniline " *Chem. Phys.* 358 (2009) 171-176.
- [106] M. Huang, C. Xu, Z. Wu, Y. Huang, J. Lin, J. Wu, " Photocatalytic discolorization of methyl orange solution by Pt modified TiO₂ loaded on natural zeolite " *Dyes and Pigs.* 77 (2008) 327-334.
- [107] R. Camarillo, J. Rincón, " Photocatalytic discoloration of dyes: relation between effect of operating parameters and dye structure " *Chem. Eng. Technol.* 34 (2011) 1675-1684.

- [108] A. Jodat, M. A. Nikjoo, M. Ghamkhari, " Comparison of photocatalytic activities of two different dyes using Pt-modified TiO₂ nanoparticles under visible light " *J. Appl. Chem. Res.* 8 (2014) 85-103.
- [109] K. E. O'shea,, I. Garcia, M. Aguilar, " TiO₂ photocatalytic degradation of dimethyl-and diethyl-methylphosphonate, effects of catalyst and environmental factors " *Res. Chem.. Intermed.* 23 (1997) 325-339.
- [110] J. Grzechulska, A. W. Morawski, " Photocatalytic decomposition of azo-dye acid black 1 in water over modified titanium dioxide " *Appl. Catal. B: Environ.* 36 (2002) 45–51.
- [111] D. Ghime, J. Mahajan, P. Ghosh, " Decoloration of orange g by mineral hematite catalyzed Fenton-like process " *Environ. Eng. Sci.* (2016) 1-11.
- [112] L. Niewa, J. Yua, M. Jaroniec, F. Tao, " Room-temperature catalytic oxidation of formaldehyde on catalysts " *Catal. Sci. Technol.* 6 (2016) 3649-3669.
- [113] S. Sakthivel, M. V. Shankar, M. Palanichamy, B. Arabindoo, D. W. Bahnemann, V. Murugesan, " Enhancement of photocatalytic activity by metal deposition: characterisation and photonic efficiency of Pt, Au and Pd deposited on TiO₂ catalyst " *Water Res.* 38 (2004) 3001-3008.
- [114] M. Qamar, A. K. Ganguli, " Self-assembling behaviour of Pt nanoparticles onto surface of TiO₂ and their resulting photocatalytic activity " *Bull. Mater. Sci.* 36 (2013) 945-951.
- [115] R. C. Hsiao, L. S. Roselin, H. L. Hsu, R. Selvin, R. S. Juang, " Photocatalytic degradation of reactive orange 16 dye over Au-doped TiO₂ in aqueous suspension " *Int. J. Mater. Eng. Innovation* 2 (2011) 96-108.

- [116] H. S. Wahab, A. A. Hussain, " Photocatalytic oxidation of phenol red onto nanocrystalline TiO₂ particles " *J. Nanostruct. Chem.* 6 (2016) 261-274.
- [117] I. K. Konstantinou, T. A. Albanis, " TiO₂-assisted photocatalytic degradation of azo dyes in aqueous solution: kinetic and mechanistic investigations a review " *Appl. Catal. B: Environ.* 49 (2004) 1-14.
- [118] M. Swati, R. C. Meena, " Photocatalytic degradation of textile dye through an alternative photocatalyst methylene blue immobilized resin dowex 11 in presence of solar light " *Arch. Appl. Sci. Res.* 4 (2012) 472-479.
- [119] N. Serpone, A. Salinaro, " Terminology, relative photonic efficiencies and quantum yields in heterogeneous photocatalysis" *Pure Appl. Chem.*, 71 (1999) 303–320.
- [120] A. O. Ibhaddon, P. Fitzpatrick, " Heterogeneous Photocatalysis: Recent Advances and Applications " *Catalysts* 3 (2013) 189-218.
- [121] C. Mathivathana, V. Balasubramanian, K. Pandian, " The influence of the oxidizing agents on the rates of degradation of rose bengal using titanium oxide nanoparticles " *Elixir Dye Chem.* 56 (2013) 13510-13518.
- [122] E. M. Saggioro, A. S. Oliveira, T. Pavesi, C. G. Maia, L. F. V. Ferreira, J. C. Moreira, " Use of titanium dioxide photocatalysis on the remediation of model textile wastewaters containing azo dyes " *Molecules* 16 (2011) 10370-10386;
- [123] B. Bethi, S.H. Sonawane, G.S. Rohit, C.R. Holkar, D.V. Pinjari, B.A. Bhanvase, A.B. Pandit, " Investigation of TiO₂ photocatalyst performance for decolorization in the presence of hydrodynamic cavitation as hybrid AOP " *Ultrason. Sonochem.* 28 (2016) 150–160
- [124] R. A. Rather, S. Singh, B. Pal, " Photocatalytic degradation of methylene blue by plasmonic metal-TiO₂ nanocatalysts under visible light irradiation " *J. Nanosci. Nanotechnol.* 16 (2016) 1-7.

- [125] N. Serpone, G. Sauv, R. Koch, H. Tahiri, P. Pichat, P. Piccinini, E. Pelizzetti, H. Hidaka, " Standardization protocol of process efficiencies and activation parameters in heterogeneous photocatalysis: relative photonic efficiencies " *J. Photochem. Photobio. A: Chem.* 94 (1996) 191-203.
- [126] D. M. Fouad, M. B. Mohamed, " Comparative study of the photocatalytic activity of semiconductor nanostructures and their hybridMetal nanocomposites on the photodegradation of malathion " *J. Nano mater.* 2 (2012)1-8.
- [127] N. Riaz, M. A. Bustam, A. M. Shariff, " Iron doped TiO₂ photocatalysts for environmental applications: fundamentals and progress " *Adv. Mater. Res.* 925 (2014) 689-693.
- [128] J. C. Colmenares, R. Luque, J. M. Campelo, F. Colmenares, Z. Karpinski, A. A. Romero, " Nanostructured photocatalysts and their applications in the photocatalytic transformation of lignocellulosic biomass: an overview " *Mater.* 2 (2009) 2228-2258.
- [129] K. Naeem, P. Weiqian, F. Ouyang, " Thermodynamic parameters of activation for photodegradation of phenolics " *Chem. Eng. J.* 156 (2010) 505-509.
- [130] T. Lonhienne, C. Gerday, G. Feller, " Psychrophilic enzymes: revisiting the thermodynamic parameters of activation may explain local flexibility " *Biochim. Biophys. Acta* 1543 (2000) 1-10.
- [131] S. B. Gajbhiye, " Photocatalytic degradation study of methylene blue solutions and its application to dye industry effluent " *Int. J. Mod. Eng. Res.* 2 (2012) 1204-1208
- [132] D. Chen, A. K. Ray, " Photodegradation kinetics of 4-nitrophenol in TiO₂ suspension " *Water Res.* 32 (1998) 3223-3234.

- [133] D. H. Mohsin , A. M. Juda, M. S. Mashkour, " Thermodynamic and kinetic study for aromatic rings effect on the photooxidation rate " *Inter. J. Eng. Technol.* 13 (2013) 34-41.
- [134] H. M. Hadi, " Photocatalysis of azo compounds on doped titanium dioxide " M.Sc. thesis, AL-Nahrain university , 2015.
- [135] M. C. Chang, H. Y. Shu, T. H. Tseng, H. W. Hsu, " Supported zinc oxide photocatalyst for decolorization and mineralization of Orange G dye wastewater under UV365 irradiation " *Int. J. Photoenergy* (2013) 1-12.
- [136] M. C. Chang, C. P. Huang, H. Y. Shu, Y. C. Chang, " A new photocatalytic system using steel mesh and cold cathode fluorescent light for the decolorization of azo dye Orange G " *Int. J. Photoenergy* (2012) 1-9.
- [137] A. Christiane, M. Steeve, S. Tchinda J. Bosco, N. M. Kor, I. Brama1, G. Eric, G. Philippe, " Biodegradation of reactive blue 4 and Orange G by pycnopus sanguineus strain isolated in gabon " *J. Bioremed. Biodeg.* 4 (2013) 1-7.
- [138] J. Lim, D. M. Satoca, J. S. Jang, S. Lee, W. Choi, " Visible light photocatalysis of fullerol-complexed TiO₂enhanced by Nb doping " *Appl. Catal. B: Environ.* 152–153 (2014) 233–240
- [139] Bird, R.E. and R.L. Hulstrom, L.J. Lewis," Terrestrial Solar Spectral Data Sets ", *Solar Energy*, 30 (1983) 563.
- [140] B. Neppolian, H. C. Choi, S. Sakthive, B. Arabindoo, V. Murugesan, " Solar/UV-induced photocatalytic degradation of three commercial textile dyes " *J. Hazard. Mater.* B89 (2002) 303–317.
- [141] N. Dimitratos, A. Villa, C. L. Bianchi, L. Prati, M. Makkee, " Gold on titania: effect of preparation method in the liquid phase oxidation " *Appl. Catal. A: General* 311 (2006) 185–192.

- [142] R. Drunka, J. Grabis, D. Jankovica, A. Krumina, D. Rasmane, " Microwave-assisted synthesis and photocatalytic properties of sulphur and platinum modified TiO₂ nanofibers " *Mater. Sci. Eng.* 77 (2015) 1-5.
- [143] N. L. Pacioni, C. D. Borsarelli, V. Rey, A. V. Veglia, " Synthetic routes for the preparation of silver nanoparticles " Springer International Publishing, (2015) 13-46.
- [144] J. Kaur, S. Singhal, " Facile synthesis of ZnO and transition metal doped ZnO nanoparticles for the photocatalytic degradation of Methyl Orange " *Ceram. Int.* 40 (2014) 7417-7424.
- [145] M. Cai, J. Su, Y. Zhu, X. Wei, M. Jin, H. Zhang , C. Dong, Z. Wei, " Decolorization of azo dyes Orange G using hydrodynamic cavitation coupled with heterogeneous fenton process " *Ultrason. Sonochem.* 28 (2016) 302–310.
- [146] M. Muruganandham, M. Swaminathan, " Photochemical oxidation of reactive azo dye with UV–H₂O₂ process " *Dyes Pigm.* 68 (2006) 133–142.
- [147] M. Cai, M. Jin , L. K. Weavers, " Analysis of sonolytic degradation products of azo dye Orange G using liquid chromatography–diode array detection-mass spectrometry " *Ultrason. Sonochem.* 18 (2011) 1068-1076.
- [148] W. Schmickler, E. Santos, " Interfacial electrochemistry " 2nd ed. , Springer-Verlag Germany, Heidelberg 2010.
- [149] A. A. Ismail, S. A. Al-Sayari, D.W. Bahnemann, " Photodeposition of precious metals onto mesoporous TiO₂ nanocrystals with enhanced their photocatalytic activity for methanol oxidation " *Catal. Today* 209 (2013) 2– 7.
- [150] S. Sato, J. M. White, " Photodecomposition of water over Pt-TiO₂ catalysis " *Chem. Phys. Lett.*, 72 (1980) 83–86.

- [151] X. Chen, S. Shen, L. Guo, S. S. Mao, " Semiconductor-based photocatalytic hydrogen generation " *Chem. Rev.* 110 (2010) 6503–6570.
- [152] S. C. Warren, E. Thimsen, " Plasmonic solar water splitting " *Energy Environ. Sci.* 5 (2012) 5133–5146.
- [153] Y. Tian, T. Tatsuma, " Mechanisms and applications of plasmon-induced charge separation at TiO₂ films loaded with gold nanoparticles " *J. Am. Chem. Soc.* 127 (2005) 7632–7637.

المخلص

تم تحضير ثنائي اوكسيد التيتانيوم النانوي المطعم بالذهب والبلاطين باعتماد طريقة السائل الهلامي (صول-جل) والاختزال الضوئي للمعادن من خلال ضوء الأشعة فوق البنفسجية والاختزال الكيميائي باستخدام مختزلات معينة. تم دراسة طبيعة السطح و المحتوى والحجم البلوري والمسامية والمساحة السطحية للمساحيق المحضرة باستخدام تقنيات عديدة ومنها المجهر الماسح والمجهر النافذ وحيود اشعة اكس. أظهرت مساحيق 2% من الذهب- ثنائي اوكسيد التيتانيوم و4% من البلاطين-ثنائي اوكسيد التيتانيوم أفضل تحطيم لصبغة G البرتقالية تحت الضوء المرئي وعند الظروف التجريبية الملائمة.

وتم كذلك دراسة تأثير بعض المتغيرات التجريبية للتفكك الضوئي للصبغة مثل الدالة الحامضية الابتدائية ، التركيز الابتدائي للصبغة، كميته المحفز ثنائي اوكسيد التيتانيوم المشوب بالبلاطين وثنائي اوكسيد التيتانيوم المشوب بالذهب وشده الضوء المرئي.

تحققت الظروف التجريبية المثلى لعملية التفكك الضوئي لصبغة G البرتقالية عند الدالة الحامضية المساوية إلى 3 وكمية المحفز المساوية إلى 40 ملغم في حالة استخدام ثنائي اوكسيد التيتانيوم المشوب بالذهب وبوجود 10 مول/لتر من الصبغة كانت قيمه ثابت السرعة 0.0123 لكل دقيقة وعمر نصف العملية مساوي الى 56 دقيقة. وحين استخدام ثنائي اوكسيد التيتانيوم المشوب بالبلاطين كانت قيمه ثابت السرعة 0.0746 لكل دقيقة وعمر نصف العملية مساوي الى 9 دقيقة أي كفاءة تحطيم أفضل للصبغة.

بينت الدراسة الحركية لعملية التحطم الضوئي ان العملية تتبع قانون المرتبة الاولى الكاذب وبغض النظر عن ظروف التفاعل. وتم كذلك احتساب الدوال الثرموديناميكية الأساسية لعملية التفكك الضوئي مثل طاقه التنشيط وطاقه جبس والانثالبي والانثروبي .



جمهورية العراق
وزارة التعليم العالي والبحث العلمي
كلية العلوم / جامعة النهرين
قسم الكيمياء

التفكك الضوئي المحفز لصبغة G البرتقالية على سطحي ثنائي اوكسيد التيتانيوم المشوب بالذهب والبلاتين النانوية

رسالة مقدمة إلى مجلس كلية العلوم / جامعة النهرين
كجزء من متطلبات نيل شهادة الماجستير في علوم الكيمياء

من قبل

آلاء رزاق شاكر
بكالوريوس 2013

أشرف
الأستاذ الدكتور
هلال شهاب وهاب

كانون الثاني 2017

جمادي الأول 1438